An Investigation into Nonlinear Random Vibrations based on Wiener Series Theory

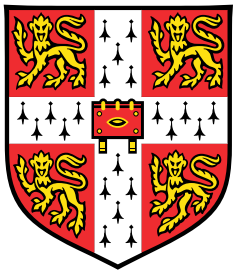

Demetris Demetriou

Supervisor: Prof. Robin S. Langley

Advisor: Prof. Jim Woodhouse

Department of Engineering
University of Cambridge

This dissertation is submitted for the degree of
Doctor of Philosophy

Jesus College December 2018

Abstract

In support of society's technological evolution, the study of nonlinear systems in engineering and sciences has become a vital research area. Aiming to contribute in this field, this thesis investigates the behaviour of nonlinear systems using the 'Wiener theories'. As a useful example the Duffing oscillator is investigated in this work. In many real-life applications, nonlinear systems are excited randomly so this work examines systems under white-noise excitation using the Wiener series.

Equivalent Linearisation (EL) is a well-known and simple method that approximates a nonlinear system by an equivalent linear system. However, it has deficiencies which this thesis attempts to improve. Initially, the performance of EL for different types of nonlinearities will be assessed and an alternative method to enhance it is suggested. This requires the calculation of the first Wiener kernel of various system defined quantities. The first Wiener kernel, as it will be shown, is the foundation of this research and a central element of the Wiener theory. In this thesis, an analytical proof to explain the interesting behaviour of the first Wiener kernel for a system with nonlinear stiffness is included using an energy transfer approach.

Furthermore, the method mentioned above to enhance EL known as the Single-Pole Fit method (SPF) is to be tested for different kinds of systems to prove its robustness and validity. Its direct application to systems with nonlinear stiffness and nonlinear damping is shown as well as its ability to perform for systems with two degrees of freedom where an extension of the SPF method is required to achieve the desired solution.

Finally, an investigation to understand and replicate the complex behaviour observed by the first Wiener kernel in the early chapters is carried out. The groundwork for this investigation is done by modelling an isolated nonlinear spring with a series of linear filters and certain nonlinear operations. Subsequently, an attempt is made to relate the principles governing the successful spring model presented to the original nonlinear system. An iterative procedure is used to demonstrate the application of this method, which also enables this new modelling approach to be related to the SPF method.

Thesis: An Investigation into Nonlinear Random Vibrations based on Wiener Series Theory, Demetris Demetriou.

To family: mum, dad, Evdokia, Stelios, Minas, Thekla and Pantelis.

Declaration

I hereby declare that except where specific reference is made to the work of others, the contents of this dissertation are original and have not been submitted in whole or in part for consideration for any other degree or qualification in this, or any other university. This dissertation is my own work and contains nothing which is the outcome of work done in collaboration with others, except as specified in the text and Acknowledgements. This dissertation contains fewer than 65,000 words including appendices, bibliography, footnotes, tables and equations and has fewer than 150 figures.

Demetris Demetriou
December 2018

Acknowledgements

"I am indebted to my father for living, but to my teacher for living well", Alexander the Great. On this note I would like to thank my supervisor Prof. Langley for his guidance and support all this time I have been working towards this thesis. I would also like to thank him for the fact that he was more than just an academic advisor to me but someone with who I could share thoughts and experiences and discuss about politics, poetry and philosophy.

Furthermore, I would like to acknowledge my funding body EPSRC for the Doctoral Training Award without which this specific research could not have taken place. In addition, I would like to acknowledge IKYK for the additional funding during the last two years of my research.

Finally, I would like to thank all the people surrounded me these past four years in Cambridge as well as my long term friends from home who composed the right environment and social life for me in order to go forward with my PhD. These include all the friends from Jesus College and all my departmental friends as well as the house-mates in Little Trinity, the Jesus College football teams and MCR committees and all my Cypriot and Greek friends.

Table of contents

List of figures

List of tables

Chapter 1

Introduction, Literature Review and Theoretical Background

1.1 Why study Nonlinear Random vibrations?

An interest in the study of vibrational systems has been shown since ancient times. Examples of shock absorbers were found on chariots and other ancient structures, indicating the awareness of the problem of undesired vibrations and the various attempts to find solutions. However, not until Newton was the study of vibrations put into a mathematical context which made it a very popular research area among scientists and engineers.

In the last centuries, the models used to study vibrational systems were mostly based on linear[1] representations of the problems. To build further on these foundations and develop a more complete grasp of the problem though, humanity's quest to understand and tame nonlinear vibrational systems was necessitated. This has opened up new challenges for the field.

One of the most popular ways to visualise the response of a dynamical nonlinear system is to plot it in the phase plane. This illustrates the trajectories of the system also know as the phase portrait between two states of the system, usually the velocity and displacement. The trajectories reveal information such as whether an attractor, a repellor or a limit cycle is present in the solution for a certain set of parameters. Additionally, the topological changes over the attractors, repellors or limit cycles of a system can be studied for a range of a specific parameter to see its effect on them; this is a very well known technique known as bifurcation analysis. More about phase plots and bifurcations can be found in [66].

[1] it satisfies the superposition principles; additivity and homogeneity.

Onto the solution seeking, the fact that we can not get analytical solutions for nonlinear problems which makes the study of such systems much more complicated and at the same more challenging. Classical methods such as the Perturbation method [32], the Describing function [43] and Harmonic balance [47] have being used for the last decades to give good approximate solutions to these problems. However, these methods have many limitations which usually emerge from the increasing analytical work required as a compromise for a better approximated solution. Another important limitation of these methods is the fact that they do not support the case where the input in the nonlinear system is random which is something this research investigates.

Firstly, it must be realised that the input to many mechanical and structural systems such as bridges, off-shore structures, energy harvesters and others is random. This can be caused by wave motion in the ocean, the earth's vibrations in an earthquake or the wind. Therefore, engineers want to ensure that these random conditions of excitation on a structure will not cause any fatigue or high stresses which could eventually lead to a failure. This is where random vibration theory comes in to give a lot of information about the system response under a random excitation input to help engineers design safer and longer-lasting structures.

Thanks to the work of the American mathematician Norbert Wiener in the 1950's the two important concepts of nonlinear and random vibration were able to merge and be studied as one unified problem. This project aims to build on the work of Wiener with the ambition that a better understanding of nonlinear random vibrations will be achieved. Potential findings could result in methodologies which can help with the prediction of the response at the design stage of a mechanical or a structural system and the identification of the nonlinear characteristics such as stiffness and damping properties of said system.

A few examples of a real life applications of the problem under investigation which brings together nonlinear and random theory is to be presented. The first one is a floating offshore structure in the ocean depicted in Fig.1.1. The structure is excited by the waves in the ocean bringing in the random aspect of the problem. Nonlinear effects in the system arise from the reaction of the mooring lines of the platform turning the study of the system response into a nonlinear random vibration problem. The literature about this problem is vast, but some interesting work to summarise it can be found in [48] and [14].

The second example is that of a vibration energy harvester. An energy harvester provides very small amount of power for low-energy electronics such as processors, microchips and microcontrollers. The energy source used by these components is found in ambient background and usually is random. In energy harvesters, nonlinearities are often incorporated in order to allow for a wider resonant response [24][4]. These can be introduced by electromag-

netic effects, configurations of the magnets or geometrical nonlinearities in the structure. An example of a vibrational energy harvester is shown in Fig.1.2.

Another example is a wind turbine as shown in Fig.1.3. Wind turbines exhibit nonlinear behaviour from structural nonlinearities in the blades and the tower. The random excitation from the wind together with the nonlinearities can result in high amplitude vibrations that can cause fatigue in the structure.

In all three of the above examples a very useful feature characterising the system is the response spectrum. From this, useful information can be extracted to advise over the fatigue tests for the wind turbine and the stresses in the mooring lines of the off-shore structure as well as for the response statics of the energy harvester in order to improve its performance. In industry, a popular method to work out the response spectrum is the Equivalent Linearisation (EL) technique[10][45][64]. In this thesis, the limitations of EL are illustrated and a new method to improve EL is proposed and implemented. The theory developed in this thesis, is not applied to any specific industrial examples like those mentioned above but provided a general methodology for analysing nonlinear random systems.

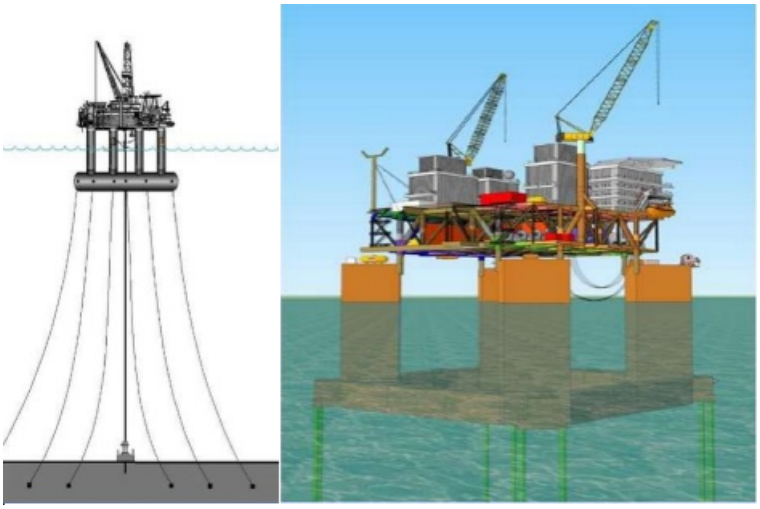

Fig. 1.1 A floating offshore platform. The mooring lines give rise to the nonlinear behaviour of the structure which is excited by the random waves of the ocean. (Photo Source: Semi submersible presentation, Indian Maritime University, Visakhapatnam, https://www.slideshare.net/ABHISHEKKUMAR790/semi-submersible/4)

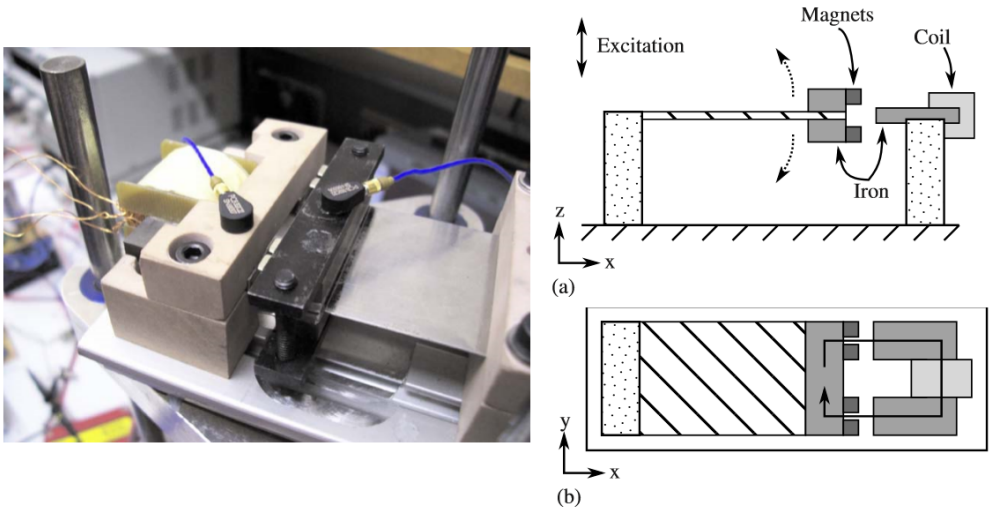

Fig. 1.2 A photograph and a schematic diagram of an energy harvester. The harvester consists of a cantilever beam with a tip mass and the nonlinearity is generated by a particular arrangement of magnets in conjunction with an iron-cored stator [4].

Fig. 1.3 A wind turbine. The nonlinearities originate from the structure itself which is under random excitation from the wind. (Photo source: http://wonderfulengin eering.com/38-high-def-wind-turbine-pictures-from-around-the-world/)

1.2 Theoretical background and Literature Review

This literature review outlines the major and most important publications related to the research. Precisely, it includes theoretical papers related to Volterra and Wiener theories as well as to Random Vibration theory. In addition, some publications on the applications of Volterra and Wiener theories in engineering and elsewhere are mentioned.

1.2.1 Random Vibrations

In this subsection some important concepts and theories related to random vibrations theory are explored.

- **Random process:**

The waves in the ocean have already been mentioned as an example of random behaviour. In general terms random or stochastic vibrations is a type of *non-deterministic* motion arising in many physical systems and engineering applications. The nature of this motion makes it impossible to exactly predict the response of a system that behaves in this way. So, what is of interest in this case is a probabilistic way to describe the response of such systems. For example, from experimental or simulated data the distribution of the response known as the Probability Density Function (PDF) can be found. From this, we can infer and calculate quantities like the mean, root mean square (RMS), standard deviation of the system response. The PDF is the derivative of the Cumulative Probability Function (CPF) which for a random variable x is defined as $P(x)$ where $P(y) =$ probability that $x \leqslant y$. In what follows, a number of definitions related to a random process are summarised. A more detailed guide for these is the book by Newland on Random vibrations, [51].

To begin with, when a random process is a function of time and its statistical properties do not vary with time, it is known as a *stationary process*. A process where this is not true is known as a non-stationary process. In this project we will be looking at a stationary random process. More examples of this kind of a process is the ocean and a rough road while a non-stationary process example is an earthquake.

Random processes can also be separated into two main categories; *narrowband and wideband*. These two terms are widely used in the field of random vibrations. A narrowband process involve a smaller range of frequencies (bandwidth) compared to a wideband process. In a wideband process there is a similar contribution from a wider range of frequencies whereas in a narrowband process some frequencies are significantly more dominant than others. This project will be dealing with wideband vibrations since we will be investigating

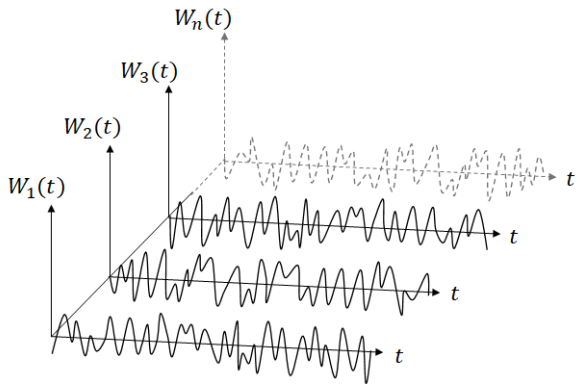

Fig. 1.4 A illustration of the ensemble of a random process. The average value at each time steps is used to calculate the ensemble average of the random process.

systems under white-noise input which itself is a wideband process. More on white-noise follows in this section.

A useful concept for random processes is the *ensemble average*. This is analogous to the expected value in the sense that given a large number of trials or realisations the ensemble average is the 'average process' that would result from averaging the whole set of realisations of a random process. The ensemble average of a stationary random process $W(t)$ is denoted by $\mathrm{E}[W(t)]$ over a set of time history responses also known an the *ensemble* (Fig.1.4) of the random process. This is formulated by,

$$\mathrm{E}[W(t)] = \frac{1}{n}\sum_{n} W_n(t) \tag{1.1}$$

if $W_n(t)$ is the time history of the n^{th} realisation.

Finally, a random process is known as *Gaussian* when the pdf of its response has a Gaussian distribution. This occurs frequently due to the central limit theorem [44]. It is mathematically simple as it is defined by only two parameters; the mean and the standard deviation. A very useful property emerging from this is that a Gaussian input to a linear system producess a Gaussian output. As it will be demonstrated later in this project for most of non-linear systems the output is described by a *non-Gaussian process* and the PDF takes a different form.

A thorough introduction into random processes is given by Newland in [51] where all these definitions are explored and illustrated by various examples. The same book can also be used for the next definitions following.

- **Power spectrum:**

A term to be widely used in this report is the 'power spectrum' also known as Power Spectral Density (PSD). This is a function that shows the frequency distribution in a signal.

The power spectrum is defined as the Fourier transform of the autocorrelation function[2] $R_{yy}(\tau)$ such that,

$$S_{yy}(\omega) = \frac{1}{2\pi}\int_{-\infty}^{\infty} R_{yy}(\tau)\exp^{-i\omega\tau}\,\mathrm{d}\tau \tag{1.2}$$

A key property of the power spectrum is the fact that the area under the spectrum is equal to the mean square value of the random process,

$$\int_{-\infty}^{\infty} S_{yy}(\omega)\mathrm{d}\omega = R_{yy}(0) = \sigma_y^2 \tag{1.3}$$

In more details the power spectrum is just a special case of a more general family of functions known as 'polyspectra'. An introductory paper on polyspectra is found in [9]. The power spectrum (or first order polyspectrum) as well as the bispectrum (second order polyspectrum; spectrum between two quantities or a set of signals) fall in the category of polyspectra and their relation for calculating the Wiener kernels and the coherence function will be explored in later chapters. Generally, the power spectrum and the bispectrum are defined as the discrete Fourier transform of the second and third order cumulant respectively, and a fast calculation of these can be achieved by using the convolution integral between the data sets of interest. Cumulants are the coefficients, κ_n, of $t^n/n!$ in the Taylor series of the natural logarithm of the moment generating function[3], $M_X(t)$, of a random variable. It is well-known that κ_1 represents the mean and κ_2 the variance of a process [13]. More details on cumulants are discussed in Section 3.2.2. Applications of polyspectra can be found in seismology for making bispectral estimates of seismic waves, in characterising the differences between families of musical instruments [20] and for nonlinear interaction between propagating waves [28].

An example of the power spectrum of a signal is presented in Fig.1.5. The three lines in the power spectrum suggest that the signal at the top is mainly made of three harmonic waves whose contribution is reflected by the magnitude of their corresponding lines in the spectrum.

[2]For a stationary random process y, the auto-correlation function is defined as $R_{yy}(\tau) = E[y(t)y(t+\tau)] = \int_{-\infty}^{\infty} y(t)y(t+\tau)dt$

[3]The expected value of $e^{t^T X}$, usually written $M_X(t)$, where X is a given n-dimensional random vector. The r^{th} moment about the origin of a single random variable X is $M_X^{(r)}(0)$, where $M_X^{(r)}(0)$ is the r^{th} derivative of the m.g.f. evaluated at zero; [13].

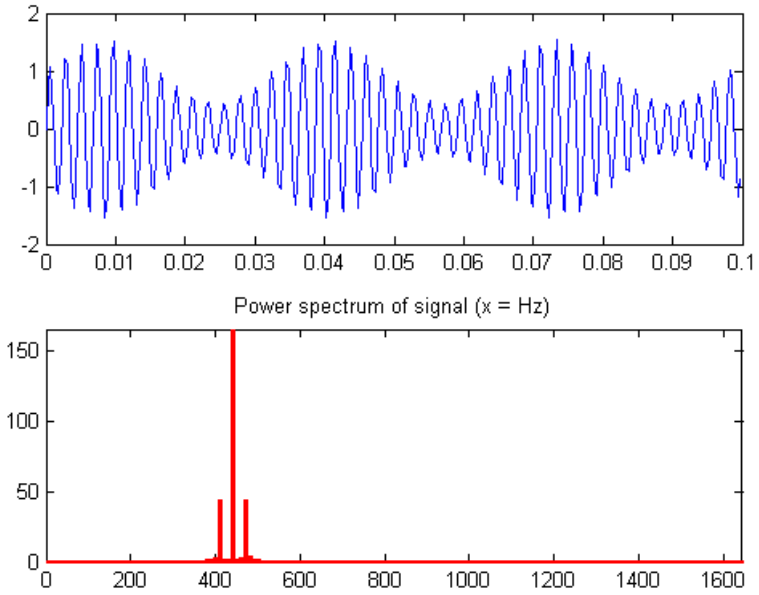

Fig. 1.5 The power spectrum (bottom) of a signal (top). Reference website: "A Pragmatic Introduction to Signal Processing", created and maintained by Prof. Tom O'Haver, Department of Chemistry and Biochemistry, The University of Maryland at College Park. Last updated September, 2017.

- **White-noise:**

White-noise with flat spectrum and $\delta(\tau)$ auto-correlation function is the most commonly used random signal despite the fact that it is not physical. The non-physicality arises from the fact that it has an infinitely long bandwidth meaning that all frequencies have an equal contribution to the signal; hence, its mean square value is infinity by Eq.(1.3). Despite the non-physicality, white-noise signals are a very good approximation for the cases where the range of the excitation signal's frequencies relevant to a system's frequency response range have a flat spectrum. White-noise is the only excitation signal used in this work and a short summary on how it is generated is described in section 2.2.1. More on white-noise theory and applications can be found in [39].

- **Random response:**

So far, a small introduction into random processes and the power spectrum has been presented. Now, a step towards the basis of random vibrations is to be demonstrated. In linear theory, every linear system can be described by its Impulse Response Function (IRF) which describes the reaction of the system as a function of time upon an impulse or the Frequency Response Function (FRF) which describes the frequency content of the response of the system upon an

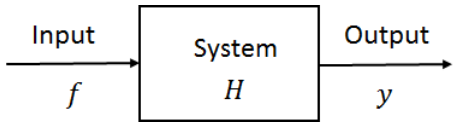

Fig. 1.6 Input-Output relationship for a linear system.

impulse. FRF is the Fourier transform of the IRF; more details on these function follow in the next chapters. Fig.1.6 shows a linear system whose IRF is given by function $h(t)$ and FRF by $H(\omega)$. If the input to the system is a signal $f(t)$ and the output is signal $y(t)$ then the relationship relating the input and the output of the system in time and frequency domain respectively,

$$y(t) = \int_{-\infty}^{\infty} h(t-\tau)f(\tau)\mathrm{d}\tau \Leftrightarrow Y(\omega) = H(\omega)F(\omega) \tag{1.4}$$

Based on the equation above, the following very helpful equation can be derived relating the power spectrum of the input and output signal of a linear system,

$$S_{yy}(\omega) = |H(\omega)|^2 S_{ff}(\omega) \tag{1.5}$$

This relationship will be widely used throughout this report.

- **The Fokker-Planck equation:**

The Fokker-Planck (F-P) equation is a powerful second-order partial differential equation which calculates the time evolution of the probability density function of a nonlinear system under a white noise input. This is the type of input applied to the nonlinear systems we will be studying in this project using the Wiener series theory introduced in the next section, which is itself defined for systems with white noise input. Knowing the transition pdf from one time to another, the equilibrium distribution of the process can be found for nonlinear systems with white-noise excitation. From the equilibrium distribution, useful quantities characterising the process such as the mean and variance can be found. In this project these quantities will primarily be found through the power spectrum of the nonlinear process. The main limitation of this method is the fact that exact solutions to the F-P equation exist only for certain types of nonlinear systems, particularly those with linear damping and nonlinear stiffness, like the Duffing oscillator described in Section 2.2. A useful example comes from the solution of F-P equation for a Wiener process[4] to give the expected Gaussian shaped pdf

[4] A stochastic process that models Brownian motion. A family of real-valued random variables $X_t(t \geq 0)$ with $X_0 = 0$, such that each $X_{t+s} - X_t(s,t \geq 0)$ has Normal distribution with mean zero and variance s, while for $0 \leq t_0 < t_1 < \ldots < t_n$, the random variables $X_{t_{i+1}} - X_{t_i}$ are independent for $0 \leq i < n$; [13].

using the delta function around the mean as the initial pdf. In contrast to the F-P equation, solutions to the Wiener series-based theory presented in this project may be found for any kind of system with polynomial nonlinearity, both damping and stiffening. More information on the F-P equation and its applications can be found in [44].

- **Equivalent Linearisation:**

In the introduction, the EL method was mentioned as a tool to solve nonlinear random vibrations problems. The general idea of EL is to replace a nonlinear system by an equivalent linear system [10][45] that minimises the error between the two systems. A good overview on EL for stochastic dynamic systems is given in the textbook by Socha in [64]. EL will be thoroughly explored in later chapters, but here, a few examples of how it is applied in industry are presented.

EL was used by Esmaeilzadeh [21] on nonlinear soil-structure systems in order to consider the simultaneous effects of soil-structure interaction and inelastic behaviour of the structure. The outcomes from this work can help with understanding the consequences of using improper pairs of EL parameters for interacting systems in the framework of performance-based design of structures.

Another practical application of EL is illustrated by Park et al in [54] during the nonlinear analysis performed in the seismic design of piping systems with Energy Absorber (EA) supports. The practicality of the presented EL analysis is demonstrated in two application examples for piping systems with EA supports. Also, an EL approach based on the direct solution of response covariance matrix is illustrated and new algorithms to convert response spectra to the equivalent power spectral density functions are presented.

In the area of electronics, the overvoltage and overcurrent generated by a resonance can damage voltage transformers (VT) or other components, and lower the power quality in the system; this phenomenon is known as ferroresonance. EL is used by Bo et al [6] to construct an algorithm which can can avoid the damaging resonance and efficiently protect the VTs from it.

NASA researchers looked at the problem of random vibration of geometrically nonlinear MDOF structures and solutions obtained by application of two different versions of a stochastic linearisation method [59]. Using their new methodology they can demonstrate a way to determined the values of the nonlinear stiffness coefficients of a MDOF structure and obtain results for the root-mean-square (RMS) displacements for the system. They demonstrate the validity of their method on two examples of beam-like structures. Two of these researchers, Rizzi and Muravyov, extend the validation of this work using a numerical integration technique in physical coordinates using the case of a clamped-clamped beam

under an extensive load range to establish the limits of validity of the EL approach [56]. In addition, they developed a software tool to implement the analysis mentioned in the two previous papers [57].

Luca *et al* [25] extend a special EL technique knows as the Tail-Equivalent Linearization Method (TELM) to the frequency domain with the aim to extract the frequency response function (FRF) of the equivalent linear system. The frequency-response function of the Tail-Equivalent Linear System offers insights into the geometry of random vibrations discretised in the frequency domain and into the physical nature of the response process. A simplified jack-up rig model is used to test the proposed approach.

As it can be seen, EL usage and application can be found in all kinds of engineering applications. However, it is not limited in engineering only; its application can be found in other fields like economics. An example of this is demonstrated by Bothwell [7] who uses EL for the analysis of oscillatory economic systems which possess large nonlinearities. More specifically, the paper performs some analysis on market oscillations using Goodwin's nonlinear model of the business cycle[26]. This model contains nonlinear terms describing the induced investment function defined by the first order derivative of the dependent variable, which represents the present income of a business.

In most of the above applications, the EL method was used to linearise systems with weak nonlinearities or predict various statistical quantities such as the mean and variance of a process, which as we will see in the next chapter EL performs sufficiently well.

Despite all these applications and uses EL has certain significant limitations especially for systems with nonlinear stiffness. In section 2.4, it is shown that for nonlinear stiffness EL cannot capture the true shape of the power spectrum and consequentially that of the autocorrelation function of a process. This brings to the surface a few of the limitations of EL. One of them is demonstrated in section 2.4.1. For weak nonlinear stiffness EL performs well in predicting the natural frequency of the system. However, as the strength of the nonlinearity increases, EL fails or gets worse in predicting the natural frequency. This is anticipated since the approximation of the power spectrum gets worse at the same time. The fact that EL cannot capture the true shape of the power spectrum also makes the calculation of quantities such as the half power bandwidth and the individual frequency power contribution impossible.

To improve on all these limitations, this project will make use of the Wiener series theory introduced in the next section to try and find a better approach than EL in predicting the power spectrum of a nonlinear process.

- **Wiener series:**

A different way to study nonlinear random vibrations is based on the Wiener theory. This theory forms the backbone of this research, therefore an extensive introduction to it including the history of its derivation, its main properties along with the advantages and disadvantages as well as an extensive literature review on the theoretical and applied aspects of it follows.

1.2.2 Introduction to Wiener series

1.2.2.1 A bit of history: From Linear to Nonlinear theory

The story begins in the 1830s when the British mathematician George Green came up with the idea of what is known today as the 'Green's function'. In vibrational systems this function is the impulse response of a linear system described by,

$$a\ddot{y}(t) + b\dot{y}(t) + cy(t) = f(t) \tag{1.6}$$

where a, b and c are constants. The solution of such a system can be expressed by,

$$y(t) = \int_{-\infty}^{\infty} G(s,t) f(s) \mathrm{d}s \tag{1.7}$$

where $G(s,t)$ is the Green's function and $f(t)$ is the input to the system. The above result is based on the superposition principle[5] which holds for all linear systems. This allows the overall response $y(t)$, subject to a complex input function $f(t)$ to be evaluated as the sum of the responses of many simpler inputs which compose the initial complex input. This result is very important in the fields of sciences and engineering and is mainly used for solving different kinds of linear differential equations.

A differential equation becomes nonlinear if at least one of the terms involving the dependent -usually time dependent- variable is a power, product or a function (i.e. $\sin(y)$, e^y, $\dot{y}y$, y^3) of the variable (page 6, [66]). In this case the principle of superposition does not hold and hence, the response of the function can not be represented in the form given by Eq.(1.7) because no Green functions (or impulse response functions) exist for such systems.

In order to find solutions of nonlinear differential equations researchers usually use numerical techniques such as Monte Carlo, Numerical Shooting and Collocation methods[6].

[5]The principle that any linear combination of solutions to a homogeneous linear differential equation is also a solution [13].

[6]Finds the solution which satisfies the given equation (i.e. ODE or PDE) at a number of points in the domain known as collocation points. These points form the domain of a finite-dimensional space where candidate solutions of polynomials of a certain degree are evaluated to satisfy the equation of interest.

Another option is to find approximate analytical solutions to a nonlinear problem using techniques like the Harmonic Balance[47], the Describing Function[43] and the method of Perturbation[46].

In this project, an alternative approach for studying nonlinear systems is suggested. It originates from the work of the Italian mathematician Vito Volterra firstly introduced in his 1887 paper, '*Sopra le funzioni che dipendono de altre funzioni*' (Translation: '*Above you can find functions that depend upon other functions*') and his book '*Theory of functionals and of Integral and Integro-Differential Equations*' (1930) [74]. Volterra suggested an interesting way of expressing the response of nonlinear system in a similar way Green did for the linear systems. In mathematical terms, the response of a nonlinear system,

$$p\ddot{y} + qQ(y,\dot{y}) = f(t) \tag{1.8}$$

where p and q are constants and Q is a nonlinear term can be expressed by a Volterra series described by,

$$y(t) = \sum_{n=0}^{N} \mathbf{H}_n[h_n; f(t)] \tag{1.9}$$

where each term in the series also known as a Volterra functional[7] is defined as,

$$\mathbf{H}_n[h_n; f(t)] = \int_{-\infty}^{t} \dots \int_{-\infty}^{t} h_n(\tau_1, ..., \tau_n) f(\tau_1) ... f(\tau_n)\, d\tau_1 ... d\tau_n. \tag{1.10}$$

with h_n being the Volterra kernel of order n. In other words, the above expression suggests that the response of a nonlinear system can be represented as the sum of the integrals between the input function $f(t)$ and the Volterra kernels $h_n(\tau_1, ..., \tau_n)$. This functional representation is based on Fréchet's theorem described fully in [23] and summarized by Schetzen [62] as, "*any continuous functional can be represented by a series of functionals of integer order whose convergence is uniform in all compact sets if continuous functions*".

In his 1958 book '*Nonlinear problems in random theory*' [77] the American mathematician Norbert Wiener came to improve Volterra's work on nonlinear systems by suggesting a more accurate representation of the response of a nonlinear system to white-noise excitation. This new approach represents the response of a nonlinear system by the so called Wiener series,

$$y(t) = \sum_{n=0}^{\infty} \mathbf{G}_n[k_n; f(t)] \tag{1.11}$$

[7] A function whose domain is itself a set of functions, and whose range is another set of functions that maybe numerical constants, [13].

where $\mathbf{G}_n[k_n; f(t)]$ is the Wiener functional of order n, characterised by the nth order Wiener kernel k_n and the input force $f(t)$. In addition, it is known that any Wiener functional is the sum of all the lower order Volterra functionals such as,

$$\mathbf{G}_N[k_N; f(t)] = \sum_{n=0}^{N} \mathbf{H}_n[h_n; f(t)]. \tag{1.12}$$

Specifically, the first terms of the series are expressed as,

$$\mathbf{G}_0[k_0; f(t)] = k_0 \tag{1.13a}$$

$$\mathbf{G}_1[k_1; f(t)] = \int_{-\infty}^{\infty} k_1(\tau_1) f(t-\tau_1) d\tau_1 \tag{1.13b}$$

$$\mathbf{G}_2[k_2; f(t)] = \int_{-\infty}^{\infty}\int_{-\infty}^{\infty} k_2(\tau_1,\tau_2) f(t-t_1) f(t-t_2) d\tau_1 d\tau_2 - \pi S_0 \int_{-\infty}^{\infty} k_2(\tau_1,\tau_1) d\tau_1. \tag{1.13c}$$

where S_0 is the constant power spectrum of the white-noise input.

Another way the response of a nonlinear system $y(t)$ based on Wiener theory looks at the individual response components $y_1(t)$ to $y_n(t)$ such as,

$$y(t) = y_0(t) + y_1(t) + y_2(t) + ...y_n(t) \text{ for } n = 0...N. \tag{1.14}$$

where every component is described by the equivalent Wiener functional given in Eq.(1.13). This representation will be used for some further analysis in the next chapter. Just like with the Volterra series, for a linear system the contribution of the functionals of an order greater than one is zero such as $y(t) = y_1^{lin}(t)$. Finally, the zero order component and thus the zero order functional are not included in any of the expressions since k_0 is just a constant value equal to the mean response of the process which is always zero for the system used in this thesis and which is described in more details in the next chapter.

The derivation of Wiener series is based on a rearrangement of the Volterra functionals to make the new series into an orthogonal one. This requires that any Wiener functional is orthogonal to all the Volterra functionals of lower order such that,

$$\mathrm{E}[\mathbf{G}_n[k_n; f(t)]\mathbf{H}_m[h_m; f(t)]] = 0, \quad m < n. \tag{1.15}$$

From this rearrangement arises the key feature of the Wiener series that the G-functionals are statistically uncorrelated meaning the cross-correlation between any two of them is zero,

$$\mathrm{E}[\mathbf{G}_n[k_n; f(t)]\mathbf{G}_m[k_m; f(t)]] = 0, \quad m \neq n \tag{1.16}$$

More details on Volterra and Wiener series are given in the next section when discussing the differences between the two representations mainly due to the orthogonality relationship mentioned above. It should be noted that the above representations of the two series is the same as given in Schetzen's book, 'The Volterra & Wiener Theories of Nonlinear Systems' [63].

Finally, it should be noted that the general example presented in this section is a single-input-single-output system. However, the Wiener series representation is not limited to these systems, but it can efficiently be generalised to represent multiple-input-multiple-output systems. An example of a two degrees of freedom system and its relation to the Wiener kernel representation is found in [40].

1.2.2.2 A comparison of Volterra and Wiener theories

The main differences between the Volterra and Wiener series are discussed and some of the most important properties and limitations of the two series are summarised in this section. The main points of this comparison are also tabulated in Table 1.1. For more information and analytic explanations on this subject refer to Chapters 1.3 and 9 of Schetzen's book, [63].

To begin with, it must be stated that the representation of these series is valid for time-invariant[8] and continuous systems. It means that the output of the system does not depend explicitly on time; thus, allowing the output to be expressed as a sum of convolution integrals between the input and the Volterra kernels or Wiener kernels. This representation is given by equations Eq.(1.9) to Eq.(1.13) in the previous section. The fact that each functional in the series is a convolution integral means that the series have memory since all the points prior to the evaluation point are taken into account for the calculation of each integral. As a result, it can be thought that the response of the system is dependent on the previous states of the system.

Two of the main limitations of the Volterra series which are resolved with the Wiener series are:

a) Problem of convergence: This problem emerges from the fact that the Volterra series is also a power series just like the Taylor series. Specifically, the Volterra series is just a Taylor series with some delay. The power series characteristic results in the series converging only within a bounded range of the system input. This restriction automatically restrains the cases where the Volterra series representation can be used to only low amplitude inputs.

To overcome this problem, Wiener constructed the functionals given in Eq.(1.13) to be orthogonal to each other when the input is a stochastic process. The orthogonalisation does

[8] For an output system $y(t)$ due to an input $x(t)$, $y(t)$ is said to be time-invariant system if a delay to the input $x(t+\delta)$ causes the same delay to the output, $y(t+\delta)$.

not only set the error between the actual response and the series representation to zero but also removes the derivative of the error, allowing for a bigger radius of convergence for the Wiener series. As a result, for any amplitude of a Gaussian process input the Wiener series is a good approximation for a nonlinear system.

b) Measurement of Volterra kernels: There is not a simple way we can measure an individual Volterra kernel in the same way we can do for the Wiener kernels as we will show in a later chapter. This is due to the fact that it is hard to isolate an individual Volterra functional given by Eq.(1.10) from the total system response. A different perspective to express this limitation comes from the fact that any one of the Volterra kernels is dependant on the other kernels in the series. The calculation of a single Volterra kernel can be achieved only for a finite-order system by isolating the highest-order Volterra functionals. The method for this special case is demonstrated in chapter 4.5 of the Schetzen's book, [63]. Another way to calculate the Volterra kernels is Harmonic probing demonstrated in chapter 8 of [78]. This method makes use of the response of a dynamical nonlinear system under an input with known harmonics. The number of harmonics in the input increases every time and together with the results for lower order kernels, the new higher order kernel can be calculated. The drawback for this method is the fact that the complexity increases when calculating higher order Volterra kernels. Unlike Volterra kernels, the direct extraction of the Wiener kernels by cross-correlation can be implemented due to the orthogonalisation properties of the Wiener functionals as shown in Eq(1.16). The way to do that will be demonstrated later in chapter 2.3.

1.2.3 The Literature on Wiener series

The original work of Vito Volterra investigating functionals and how they can be used to express the response of a nonlinear process using the well recognised Volterra series was firstly introduced in [72] and [73]. In these books Volterra gives the definitions and properties of functionals and describes the operations on them. In addition, he introduces the so called Volterra kernels and investigates their application in integral equations. The term kernels is used in different ways by engineers, computers scientists and mathematicians. In this case, they are functions used in convolution integrals in the place of the nucleus of the integrals. In the case of a linear system the first and only non-zero kernel takes the place of the impulse response function in the convolution integral characterising the input-output relationship of the system. Most importantly, Volterra uses the theory behind the functionals and the kernels to come up with the Volterra series and explores its application. A modern version of this work is found in [74].

Table 1.1 Differences between Volterra and Wiener series

Feature/Property		Volterra	Wiener
Kernels	Excitation dependence	Independent of the excitation	Dependent on the excitation
	Kernel computation	Hard to compute individual kernels	Easy to compute individual kernels
Terms	Terms' dependence	Terms are dependent on all the other terms	Terms are dependent on the lower order terms only
	Terms correlation	Terms in the series are correlated; $E[y_m y_n] \neq 0, m \neq n$.	Terms in the series are uncorrelated; $E[y_m y_n] = 0, m \neq n$.
System	Convergence	No general proof of convergence. Uniform convergence. May diverge for particular types of input; high amplitude input.	Convergence in the mean square sense[9].
	Input type	Square integrable functions over a finite interval[10].	Random process type input; mainly for white noise.

[9] $y = \sum_{n=0}^{N} y_n \quad \Rightarrow \quad \mathcal{E}\{(y_{N+1} - y_N)^2\} \leq \mathcal{E}\{(y_N - y_{N-1})^2\}$

[10] A function $f(x)$ is said to be square integrable if $\int_{-\infty}^{\infty} |f(x)|^2 dx$ is finite, [61].

On the other hand, Norbert Wiener's work for the eponymous series is firstly found in [77] which forms a selection of some lecture notes Wiener had presented at MIT during his time there as a professor in the Department of Electrical Engineering. These explore random functions and most importantly orthogonal functions which form the basis for obtaining the Wiener series based on the orthogonalisation of the Volterra series as it has already been mentioned in the previous section. In the same book, Wiener investigates the application of these functions to the study of random time, coupled oscillators and even tries to make a reference to quantum theory. The book begins by exploring random functions in time and phase forming the basis of the type of forcing used for exciting a nonlinear system.

The whole of Volterra and Wiener theories are presented in detail and clear structure by Schetzen in [63] which begins with a general introduction on Time-Invariant and Time-Varying systems. These are systems whose characteristics such as the impulse response function explicitly depend on time. This is followed by a briefing into linear systems and a detailed exploration of second and higher order Volterra systems. In these later chapters an extensive work on the Volterra functionals and Volterra kernels is included. Then, some analysis over the averages of system responses and particularly of those with Gaussian Random Variables is included which is required for the understanding and implementation of the work in the next chapter where the measurement of the Volterra kernels and the Power Spectrum of a nonlinear system are extracted by cross-correlation techniques. Before moving to Wiener theory, Schetzen explains the disadvantages of Volterra series and highlights the main differences between the two theories. On Wiener's work, he includes a section on Wiener functionals and the determination of Wiener kernels by cross-correlation in a similar manner as in the Volterra case. In addition, he explores the identification of a nonlinear system using the Wiener series and investigates the orthogonal development of the Wiener functionals.

One of the most important chapters of the book mentioned in the previous paragraph covers the measurement of Wiener kernels by cross-correlation methods and is presented in more detail by a paper from Schetzen and Lee [42]. The way they approach the problem is through a multi-dimensional-delay representation of the Wiener functionals for systems with white-noise input. Using a black-box representation they define the delays in a multi-dimensional circuit. They also take advantage of the fact that any functional is orthogonal to any other functional of lower order in order to get an expression of the n^{th} order Wiener kernel in terms of the cross-correlation between the output and the white-noise input.

An extension of this work which was later also included in Schetzen's book is a paper published in 1981 [62] about nonlinear system modeling based on the Wiener theory. This includes a section about the Volterra kernel measurement which forms the basis and the

motivation along with a chapter on orthogonal polynomials to describe the nonlinear system identification through cross-correlation for system with Gaussian and non-Gaussian inputs.

A rather interesting paper on identification methods for nonlinear systems based on an extension of Wiener theory is presented by Palm and Poggio in [53]. They provide conditions and theorems for the Wiener functionals in the cases where the input to the system is a stochastic process including Brownian motion which related to white-noise as being its derivative.

Along with the publications in the previous paragraphs, another paper on the identification of nonlinearities in vibrational systems is [55]. In this paper they relate the nonlinearities in a system with the second Wiener kernel. This is done by measuring the first and second Wiener kernels in the time domain for linear and nonlinear systems and then, comparing the kernels by direct inspection.

While the papers presented so far deal with Volterra and Wiener series in the time domain. A paper by Langley [40] investigates the role of the first Wiener kernel in the frequency domain and comes up with a very interesting relationship between the kernel and the velocity power spectrum of a system with nonlinear stiffness. An expression for finding the first kernel in the frequency domain by cross-correlation is also given and numerical extractions for measuring the first Wiener kernel for a single and two degrees of freedom system are presented.

In his PhD thesis, Hawes [30] used Wiener theory to investigate nonlinear systems under white-noise and non-white excitation inputs. His primary task was to apply the work on nonlinear energy harvesters in order to find upper bounds for the maximum power that can be harvested. One of his main results was the extension of Wiener theory for non-white excitation inputs. In addition, he went on to investigate some other properties of the first Wiener kernel related to the power dissipation of a nonlinear MDOF system. Specifically, he proved that for an unconstrained system the integral over the frequency domain first Wiener kernel is proportional to the total oscillating mass. Hawes illustrated the validity of his results by some experimental work involving a base-excited cantilever beam with magnets generating a nonlinear restoring force on a tip mass. This part of the thesis work has also been published in [31].

On a different direction from the work mentioned already, Chatterjee and Vyas published a paper [12] on the stiffness nonlinearity classification using Volterra series. They use response component analysis to identify the form of nonlinearity in the system which is limited to polynomial form. What mostly interests us from this paper is the investigation done over the symmetry of the polynomial form of nonlinearity and how this is related to the Volterra kernels. In accordance to this, they came up with a proof that for a symmetric

nonlinearity all the Volterra kernels of even order are zero; this is of great use when measuring the second order Wiener kernel.

1.2.4 Applications of Volterra and Wiener theories

To begin with, an application of Wiener series on a structural system is demonstrated by Da Silva in [15]. A method to replace Linear Finite Element (FE) for model updating is suggested for structures which contain local nonlinearities. Local nonlinearities can arise by the asymmetric geometry or by local elements such as joints, bolts and gaps in the structure. The proposed method makes use of the first and second order Wiener kernels to define multiple convolutions of objective functions which are used for the updating procedure. The proposed method is then applied to updating a three-dimensional portal frame, and used to identify the nonlinear parameters of the structure. This is implemented in three different cases of nonlinear stiffness; cubic stiffness, bilinear stiffness and general nonlinear stiffness.

The above paper is a follow up on a paper [16] by Da Silva *et al* one year before. This first paper includes most of the theory behind the nonlinear identification process included in [15] which is based on Wiener series and Kautz filters[33]. These are fixed-pole traversal filters which can be used to represent the second-order dynamics of a system and are very effective in representing orthogonal kernels (i.e. Wiener kernels). The main objective is the identification of local nonlinearities in the structure using the vibration response of the system, which is done by considering the first two orders of Volterra kernels. However, an orthogonal expansion of the Volterra kernels to form the Wiener kernels which are used instead is performed in order to improve the nonlinear coefficient identification. The orthogonal expansion is based on a Kautz filter, which enables Wiener kernels to be described on a discrete-time series and allows high-order kernels to be taken into account in the model update procedure. This results in a faster convergence of the optimization procedure explained in the paper, as well as an improvement in the accuracy of the results. The validation of the method is done on a nonlinear cantilever beam.

Volterra and Wiener theories are frequently used in electronics. A good paper to show their use in this area is given in [68] where Volterra and Wiener spline series are used for analyzing nonlinear electric circuits. The phase portrait of the integro-differential equation characterizing the nonlinear electric circuit is divided into various local charts. Each function in these charts is then approximated by a low degree polynomial using a spline method and the Volterra-Wiener kernels are calculated for every approximated function. Finally, the response of the circuit is calculated by an algorithm that includes the sum of the convolutions based on the calculated kernels and an iterative approach that refines the parameters describing the response through a feedback loop is used. It has been shown that the method of spline kernels

where a single kernel is used for each chart-function is much more efficient in describing the response of an RC circuit compared to a more classical approach which uses three kernels.

A paper by Barahona and Poon [2], uses a discrete version of the Wiener series to detect the nonlinear characteristics in a noisy dynamical process. This is a frequent problem in nonlinear dynamics where deterministic chaos arising from such systems is usually mistaken for random noise. A formulation of the response in the form of Wiener series is used to represent the predictor time series of the nonlinear system. Then an optimization technique is used to minimize the error in the predictor in accordance with a suggested parsimony principle for the net error. The optimization technique was repeated while increasing the order of functionals used in the series and the degree of nonlinearity of the model until it converged to the best nonlinear model. This technique was found to detect the nonlinearities under high levels of noise up to a 50% of additive correlated noise and was even robust in the case of low intensity (compared to the actual system) random spikes.

A very similar approach to the one of Barahona and Poon above is used by Kumar *et al* in [38] to characterise chaos in air pollutants. The same prediction error function is minimized under the same parsimony principle to find best prediction model based on the Wiener series representation of the model for air pollutants which will give an indication of any chaotic behaviour present in the data.

A book by Ogunfunmi [52] uses the Volterra and Wiener theories as the main tool for adaptive nonlinear system identification. The book contains some introduction to Volterra and Wiener series as well as to Adaptive signal processing. It also includes some general background on methods based on local and global optimization used as system identification methods in nonlinear systems before going into adaptive methods based on the Volterra and Wiener models. The identification based Wiener models includes the investigation of second-order systems, third-order systems, a nonlinear LMF[11] [75] adaptation algorithm as well as work on RLS (recursive least square) and OLS (orthogonal least square) algorithms.

Back to [63], we find applications of Volterra theory on differential equations, free-swinging pendulum and nonlinear feedback systems. Particularly, a study case over a nonlinear differential equation with linear damping and sinusoidal stiffness which can describe the behaviour of gyroscopes, ferrites and phase-lock loops is undertaken where Volterra operators are extracted and some other interesting results that will be explored later in more detail such as the zero valued operators for symmetric stiffness are mentioned. In the end of this book Wiener theory is used along with Gate function model theory also explained

[11] The Least Mean Fourth (LMF) performs error minimization in the mean fourth. For example, if $y = \sum_{n=0}^{N} y_n \quad \Rightarrow \quad \mathcal{E}\{(y_{N+1} - y_N)^4\} \leq \mathcal{E}\{(y_N - y_{N-1})^4\}$

in the book to perform some optimization techniques on nonlinear models including the demonstration of this in an experiment over a given model.

Further work on Volterra theory is included in chapter 8 of [78]. Various applications of the theory are explored from characterising a shock absorber, to higher-order modal analysis and multiple-input-multiple-output system analysis.

A final application of Volterra and Wiener series can be found in speech recognition using the nonlinear signal decomposition based on the two functional series as presented by Krot and Tkachova in [37]. The authors use this new technique instead of the more classical methods such as hidden Markov models and neural networks in order to handle the nonlinear aspects in speech. These may include physical parameters such as vocal tract length and glottal size and personal learned abilities like different accents, pronunciations and speed of articulations. The way they approach this problem is be representing the speech signal as a Wiener series and calculating the kernels for each functional in it. Then, a nonlinear decomposition based on this Wiener kernels which act as the multidimensional nonlinear filters is performed to identify groups of phonemes in Belarusian language as an example.

1.3 Scope of work and summary of thesis contents

In this first chapter, an overview of the work pertaining to the Volterra and Wiener series and nonlinear random vibrations was presented. This included theoretical work and applications, both in engineering and elsewhere. The historical developments from Green's function to Volterra theory and eventually to Wiener theory was presented and the main differences between the Volterra and Wiener theories were explained.

In addition, the role of EL in engineering was demonstrated; and the aim of this thesis is to improve its performance. EL will be tested upon systems with nonlinear stiffness and nonlinear damping under white-noise input. Its limitations will be illustrated and analytical proofs will be used to explain them. Furthermore, an extension of EL will give rise to a new methodology to improve the current method. The validity and robustness of this new method will be tested and an investigation for its origination will be performed. The Wiener theory already introduced in this section forms the basis for the discovery of this new methodology.

Looking at the big picture, a new methodology for improving EL will enable an engineer to effectively calculate the power spectrum of a nonlinear system. This development could then be of great assistance in parameter estimation or predicting the response statistics of a nonlinear system. More suggestions about future expansion of this work will be discussed in the last chapter of this thesis.

Analytically, the break down of the work to be presented in the next chapters to support the plan mentioned above is as follows:

Chapter 2: An outline of the model system -the Duffing oscillator- used in this project is included together with the generation of white-noise excitation. The calculation and extraction of Wiener kernels is included and the comparison with EL is illustrated. It also includes the study of the coherence function as a tool for measuring the contribution of the first Wiener kernel as well as an analytical proof on the energy transfer between the kernels.

Chapter 3: The main result of the thesis is presented. This is a suggested method to enhance EL. Before introducing this new method a brief introduction into Characteristic functions and Cumulants is given to explain some of the limitations of EL.

Chapter 4: The suggested methodology illustrated in Chapter 3 is extended to a 2DOF system to show its robustness. Two different cases of a 2DOF system are investigated.

Chapter 5: Chapters 5 and 6 are intended to deal with the understanding of the method presented in the two previous chapters. Here, an investigation on an isolated nonlinear spring is performed. The aim is to build a model for the nonlinear spring to illustrate similar behaviour to the one observed when applying the suggested method in Chapter 5.

Chapter 6: An extension of the model of the nonlinear spring to a nonlinear system is implemented using an iterative procedure. The results aim to connect the pieces from Chapters 3 and 5 and explain the mechanisms of the nonlinear system that give rise to the results from the previous chapters.

Chapter 7: Discussion and conclusions of the results as well as possible future extensions for this work.

Chapter 2

The Wiener kernels and the comparison with Equivalent Linearisation

2.1 Introduction

In the first chapter, the vibration nature of the problem under investigation which combines nonlinear systems with random theory was introduced. In addition, the concept of EL was introduced and a few examples of how it is used in industry were demonstrated. Furthermore, an introduction in Volterra and Wiener theories was presented. The main differences between the two theories were highlighted and some theoretical work as well as industrial applications related to these theories were mentioned.

The aim in this chapter is to apply the Wiener theory on a simple nonlinear system under white-noise input and compare the results to that calculated by EL for the same system. This will involve the calculation and extraction of the first Wiener kernel of the system response. The investigation will be performed both for a system with nonlinear stiffness and a system with nonlinear damping.

We will then try to understand and explain the observed behaviour of the first Wiener kernel. This is to be done through various methods to quantify the contribution of the first Wiener kernel to the response. Two different methods are to be used for this, a direct method and the coherence function method.

Finally, the most important result for the chapter is to be presented. This is an analytical way to explain the behaviour of the first Wiener kernel using an energy transfer approach.

2.2 The test model

The model vibrational system used in this project is the popular Duffing oscillator. The volume of literature related to the Duffing oscillator is extremely large but a good reference on the theory behind the oscillator as well as on its applications can be found in [35]. The oscillator has a broad range of engineering applications from describing the motion of vibrational energy harvesters to signal detection and modelling current flow in electrical circuits. All these, together with the fact that is a simple nonlinear system with a well known and understood behaviour makes it an ideal model to use in this project. The single-degree-of-freedom Duffing equation is given by,

$$\ddot{x} + 2\beta\omega_0\dot{x} + \omega_0^2 x(1 + \hat{\varepsilon}_3 x^2) = f(t), \tag{2.1}$$

where x, $\dot{x}$, $\ddot{x}$ and f are all functions of time. In addition, β is the damping coefficient ω_0^2 is the natural frequency of the oscillator and f is the external white-noise excitation. The nonlinearity is introduced by the nonlinear term $\omega_0^2\hat{\varepsilon}_3 x^3$ on the left-hand side of the equation, also known as the Duffing term which represents the nonlinear restoring force of the oscillator. The Frequency Response Function (FRF) of the Duffing oscillator at a given amplitude of excitation is schematically plotted in Fig.2.1 along with the FRF of a linear oscillator. The hardening characteristic of the oscillator is demonstrated by the bending of the resonance peak due to the shifting of the natural frequency which is characterised by a backbone curve (dotted dark blue line in Fig.2.1).

Part of the project is to investigate a different form of the Duffing oscillator where the nonlinearity is introduced by some nonlinear damping. This gives rise to a new expression of the Duffing equation which also contains the nonlinear term $2\beta\omega_0\hat{\varepsilon}_2\dot{x}^3$ as shown below,

$$\ddot{x} + 2\beta\omega_0\dot{x}(1 + \hat{\varepsilon}_2\dot{x}^2) + \omega_0^2 x(1 + \hat{\varepsilon}_3 x^2) = f(t). \tag{2.2}$$

The coefficients ε_2 and ε_3 account for the amount of nonlinear damping and nonlinear stiffness of the oscillator respectively.

A very useful and elegant methodology we can employ to make the model simpler and analytically flexible is to use a nondimensionalised form of the Duffing equation Eq.(2.2). The nondimensionalised version of the equation takes the form,

$$\ddot{y} + 2\beta(1 + \varepsilon_2\dot{y}^2)\dot{y} + y(1 + \varepsilon_3 y^2) = g(\tau). \tag{2.3}$$

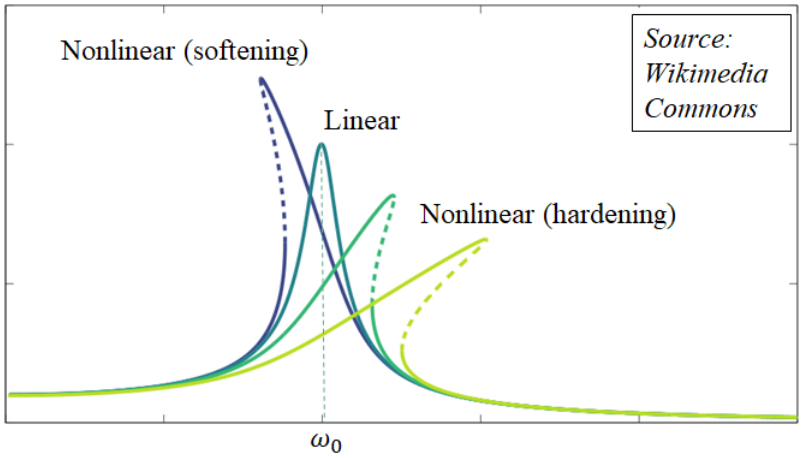

Fig. 2.1 The frequency response function of a typical Duffing oscillator. The linear case is when the nonlinear coefficient, ε_3 in Eq.(2.1), is 0. When $\varepsilon_3 > 0$ it is known as hardening and when $\varepsilon_3 < 0$ is known as softening. For the cases where $\varepsilon_3 \neq 0$ the resonance frequency is no longer equal to ω_0. The dashed parts of the frequency response are the unstable states of the response.

where $\varepsilon_2 = \hat{\varepsilon}_2 \sigma_0^2 \omega_n^2$ and $\varepsilon_3 = \hat{\varepsilon}_3 \sigma_0^2$ are the two nondimensionalised nonlinear coefficients for nonlinear damping and nonlinear stiffness respectively and σ_0^2 is the mean square response of the linearised system ($\varepsilon_3 = 0$ and $\varepsilon_2 = 0$) with natural frequency, $\omega_0^2 = 1$. In this way, the same equation can be expressed in terms of the damping coefficient (β) and the new nonlinearity coefficients (ε_2 and ε_3) only. Additionally, the power spectrum of the new excitation force $g(\tau)$ is dependent on the damping coefficient only such that $S_{gg} = \frac{4\beta}{\pi}$. This result is demonstrated in Appendix A and follows from the fact that an arbitrary value for the natural frequency ($\omega_0^2 = 1$) was chosen and the relationship between the RMS value of a process and the power spectrum of the input for a linear system. The nondimensionalised form enables the investigation of a wider range of oscillators with different characteristics, such as natural frequency, to take place under the same analysis. At the same time all the units are eliminated from the differential equation which is set to be dimensionless. All the steps of the nondimensionalisation process are included in Appendix A.

2.2.1 Generating the white-noise and simulating the system

White-noise can be modelled as the superposition of many periodic sinusoidal waves of the same amplitude but different phase which is randomly choosen. The generation of white-noise excitation can then be obtained through the Fast Fourier Transform (FFT), denoted FFT$\{\}$, over the ensemble of trigonometric functions with random phase such that,

$$g(\tau) = \sum_j \sqrt{2S_{gg}\mathrm{d}\omega}\cos(\omega_j\tau + \varphi_j) = \mathrm{Re}\left[\sum_j a_j e^{i\omega_j\tau}\right] = \mathrm{Re}[\mathrm{FFT}\{a_j\}]. \tag{2.4}$$

where,

$$a_j = \sqrt{2S_{gg}\mathrm{d}\omega}e^{i\varphi_j} \tag{2.5}$$

with φ_j being the randomly generated phase and S_{gg} the spectral density which is constant for white noise. For the nondimensionalised version of the Duffing oscillator this value will be $S_{gg} = \frac{4\beta}{\pi}$ as explained in the section above and calculated in Appendix A.

To calculate the response of the oscillator for different values and types of nonlinearities, the MATLAB time domain integration subroutine ODE45 was used over an ensemble of 200 simulations in each case where each simulation had a different realisation of noise input. Each of the simulations run for 125 seconds which corresponds to about 22 cycles of the linear oscillator. Fig.2.2 shows two realisations of the Duffing oscillator response. The first column includes the time history for the displacement, velocity and white-noise excitation for the linear oscillator while the second column shows the same information but for a nonlinear oscillator this time. The standard values used for these simulations and which are kept constant through out the project unless otherwise stated are $\beta = 0.15$ and $S_{gg} = S_0 = 0.191$. The most interesting observation from this figure which forms the main reason for doing this research is when looking at the decrease in the amplitude of the oscillations as well as the increase in the frequency when nonlinear stiffness is introduced in the system for the same input ($g(\tau)$). This can be seen when comparing the top two plots of the response ($y(\tau)$) of the system in Fig.2.2. For this to happen the change in velocity needs to be quicker. This is illustrated in the third and fourth plots (second row) of the same figure where the frequency of the velocity plot ($\dot{y}(\tau)$) is much higher for the nonlinear system compared to the linear one.

Following these observations someone can ask: What is the cause of this damping phenomenon? Can we explain this through analytic expressions? Can we even predict or quantify the changes in damping and frequency? These are some of the questions aim to be investigated in this thesis.

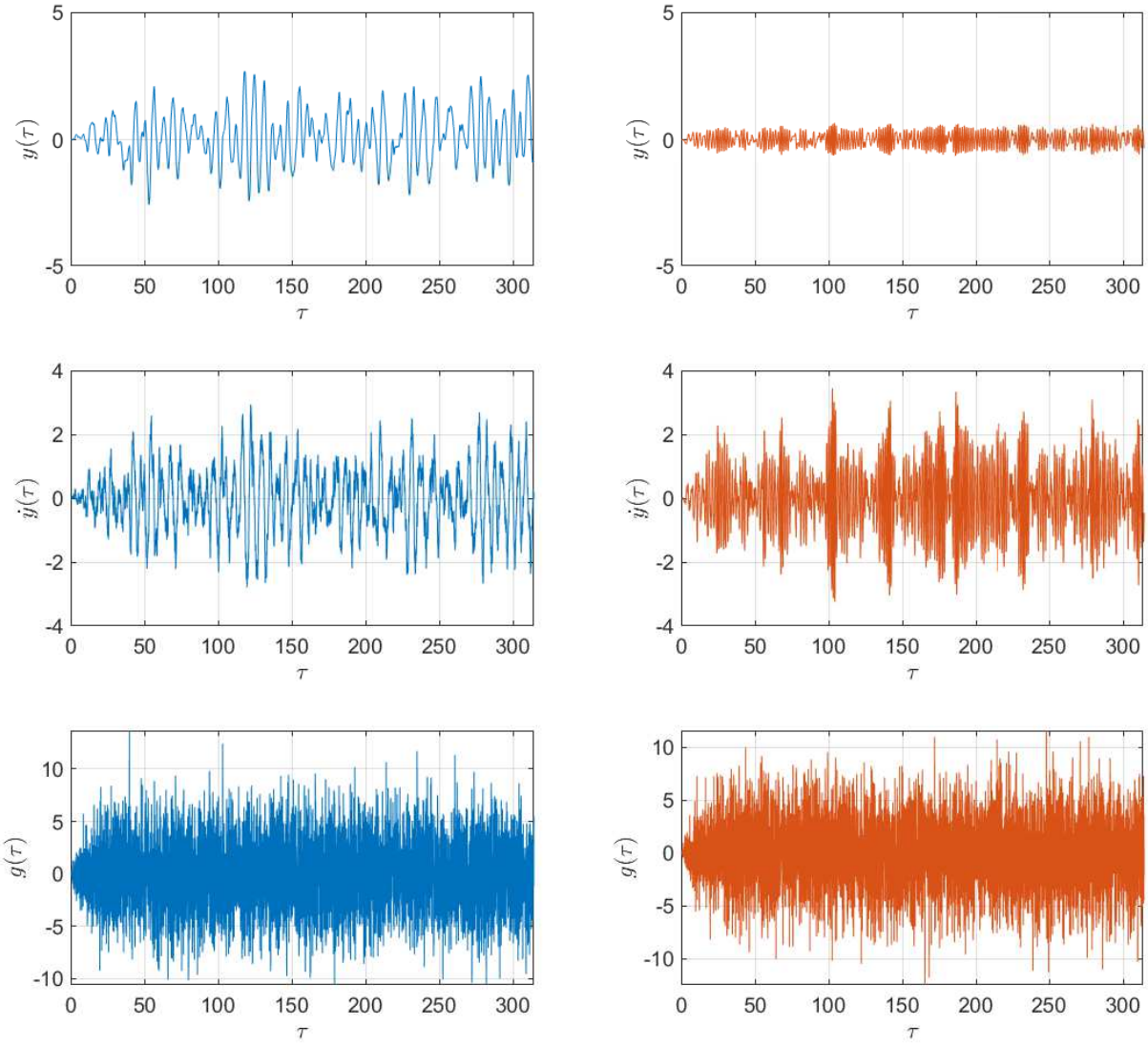

Fig. 2.2 An example of time history from two realisations of the Duffing oscillator. The first column (blue) is a linear oscillator where $\varepsilon_2 = 0$ and $\varepsilon_3 = 0$ while the second column (red) is a nonlinear oscillator where $\varepsilon_2 = 0$ and $\varepsilon_3 = 110$. In each case, the first row shows the displacement time history, the second row the velocity time history of the oscillator and the third row is the white-noise excitation time history for one realisation.

2.3 Calculation and extraction of the Wiener kernels

In this section, the process for calculating the Wiener kernels of the nonlinear Duffing oscillator is explained and implemented. This includes the extraction of the first and second Wiener kernel for both stiffening and damping nonlinearities which are then studied and analysed. The work of this chapter is mostly based on Chapter 13 of [63].

2.3.1 Generalised Nth Wiener kernel

It has already been mentioned in the previous chapter that the first order Wiener kernel is the impulse response function of a linear system. However, for the purpose of this project, it is more useful to extract the kernels describing the velocity response of the system instead of the displacement, since it has a direct relation to the power dissipated from the system (as shown later in Eq.(2.17), where $K_1(\omega)$ is the velocity kernel). However, the relationship between the velocity and the displacement kernels follows through the usual derivative between the two quantities, such as $k_n^{vel}(t) = \frac{d(k_n^{disp}(t))}{dt}$ for the n^{th} order kernel. These kernels can be calculated by cross-correlation between the displacement $y(t)$ or the velocity $\dot{y}(t)$ and the input $g(t)$ as illustrated by Schetzen in [63].

In the frequency domain the first kernel, as we will see later, is directly related to the power spectrum of the process. As a result, it is sufficient to work with the kernels mainly in the frequency domain. The following analysis makes use of Schetzen's time-domain representation of the kernels to find the frequency-domain representation form of the kernels.

From [63], we combine equations (13.5-11),

$$k_n(\hat{\sigma}_1,...,\hat{\sigma}_n) = \frac{1}{n!A^n}\mathrm{E}[\dot{y}(t)\mathbf{H}_n[g(t)]] \tag{2.6}$$

and (13.1-5),

$$\mathbf{H}_n[g(t)] = g(t-\hat{\sigma}_1)...g(t-\hat{\sigma}_n) \tag{2.7}$$

to obtain the equation of the n^{th} order kernel in the form,

$$k_n(\hat{\sigma}_1,...,\hat{\sigma}_n) = \frac{1}{n!A^n}\mathrm{E}[\dot{y}(t)g(t-\hat{\sigma}_1)...g(t-\hat{\sigma}_n)] \tag{2.8}$$

where A defines the level of the spectral density of the white-noise input and E[] is the ensemble average. $\mathbf{H}_n[g(t)]$ is the n-dimensional delay functional (or n^{nt} degree Volterra functional) and $\hat{\sigma}_n$ is some time delay applied on the input $g(t)$.

The Fourier transforms of the terms in the ensemble from Eq.(2.8) are equal to,

$$\dot{y}(t)g(t-\hat{\sigma}_1)...g(t-\hat{\sigma}_n) = \int_{-\infty}^{\infty}\int_{-\infty}^{\infty}...\int_{-\infty}^{\infty}\dot{Y}(\omega_1)e^{i\omega_1 t}G^*(\omega_2)e^{-i\omega_2(t-\hat{\sigma}_1)} \\ ...G^*(\omega_{n+1})e^{-i\omega_{n+1}(t-\hat{\sigma}_n)}\mathrm{d}\omega_1\mathrm{d}\omega_2...\mathrm{d}\omega_{n+1}. \tag{2.9}$$

where $\dot{Y}(\omega) = \mathscr{F}\{y(t)\}$ and $G(\omega) = \mathscr{F}\{g(\tau)\}$ and $\mathscr{F}\{\}$ is the Fourier transform. Substituting Eq.(2.9) in Eq.(2.8) we get,

$$k_n(\hat{\sigma}_1,...,\hat{\sigma}_n) = \frac{1}{n!A^n}E\Big[\int_{-\infty}^{\infty}\int_{-\infty}^{\infty}...\int_{-\infty}^{\infty}\dot{Y}(\omega_1)e^{i\omega_1 t}G^*(\omega_2)e^{-i\omega_2(t-\hat{\sigma}_1)} \\ ...G^*(\omega_{n+1})e^{-i\omega_{n+1}(t-\hat{\sigma}_n)}\mathrm{d}\omega_1\mathrm{d}\omega_2...\mathrm{d}\omega_{n+1}\Big]. \tag{2.10}$$

Rearranging the exponential terms and averaging over time the expression becomes,

$$k_n(\hat{\sigma}_1,...,\hat{\sigma}_n) = \frac{1}{n!A^n}\frac{1}{T}\int_0^T\int_{-\infty}^{\infty}\int_{-\infty}^{\infty}...\int_{-\infty}^{\infty}\dot{Y}(\omega_1)G^*(\omega_2)...G^*(\omega_{n+1}) \\ e^{i(\omega_1-\omega_2-...-\omega_{n+1})t}e^{i\omega_2\hat{\sigma}_1}...e^{i\omega_{n+1}\hat{\sigma}_n}\mathrm{d}\omega_1\mathrm{d}\omega_2...\mathrm{d}\omega_{n+1}\mathrm{d}t. \tag{2.11}$$

Integrating with respect to time t introduces the delta function term since $\int e^{i\Omega t}dt = 2\pi\delta(\Omega)$,

$$k_n(\hat{\sigma}_1,...,\hat{\sigma}_n) = \frac{1}{n!A^n}\frac{2\pi}{T}\int_{-\infty}^{\infty}\int_{-\infty}^{\infty}...\int_{-\infty}^{\infty}\dot{Y}(\omega_1)G^*(\omega_2)...G^*(\omega_{n+1}) \\ \delta(\omega_1-\omega_2-...-\omega_{n+1})e^{i\omega_2\hat{\sigma}_1}...e^{i\omega_{n+1}\hat{\sigma}_n}\mathrm{d}\omega_1\mathrm{d}\omega_2...\mathrm{d}\omega_{n+1} \tag{2.12}$$

Next, integrating with respect to ω_1 results in,

$$k_n(\hat{\sigma}_1,...,\hat{\sigma}_n) = \frac{1}{n!A^n}\frac{2\pi}{T}\int_{-\infty}^{\infty}...\int_{-\infty}^{\infty}\dot{Y}(\omega_2+...+\omega_{n+1})G^*(\omega_2)...G^*(\omega_{n+1}) \\ e^{i\omega_2\hat{\sigma}_1}...e^{i\omega_{n+1}\hat{\sigma}_n}\mathrm{d}\omega_2...\mathrm{d}\omega_{n+1}. \tag{2.13}$$

Then, we can rearrange and take the Fourier transform of k_n which equals to the average between the velocity and excitation function on the right-hand side of the expression,

$$K_n(\omega_2,...,\omega_{n+1}) = \frac{1}{n!A^n}\frac{2\pi}{T}(2\pi)^n\mathrm{E}\left[\dot{Y}(\omega_2+...+\omega_{n+1})G^*(\omega_2)...G^*(\omega_{n+1})\right]. \tag{2.14}$$

The final step is to substitute $A = \pi S_0$, simplify the coefficients and replace the variables for easiness of definition and analytical consistency to give us the final expression,

$$K_n(\omega_1,...,\omega_n) = \frac{(2\pi)^{(n+1)}}{n!(\pi S_0)^n T} E\left[\dot{Y}(\omega_1 + ... + \omega_n) G^*(\omega_1)...G^*(\omega_n)\right] \tag{2.15}$$

A different and more elegant form of the above expression is,

$$K_n(\omega_1,...,\omega_n) = \frac{2^{(n+1)}\pi}{n!S_0^n T} E\left[\dot{Y}\left(\sum_{n=1}^{n}\omega_n\right)\prod_{n=1}^{n} G^*(\omega_n)\right] \tag{2.16}$$

An obvious observation from this expression is the fact that the number of dimensions required to define a kernel is directly related to the order of the kernel. So, the first order kernel is an one dimensional function, the second kernel is a two dimensional function and the n^{th} order kernel is of n dimensions indicating the computational difficulties of calculating the higher order kernels. The relationship between the velocity and the displacement kernels in the frequency domain is given by $K_n^{vel}(\omega) = i\omega K_n^{disp}(\omega)$.

Finally, for the purposes of this project the ensemble average for calculating the kernels will be taken over 200 realisations unless stated otherwise. This number of realisations was chosen because it is satisfactory for convergence.

2.3.2 First Wiener kernel

The first Wiener kernel is probably the most important kernel in the series, the reasons of which we will see in this section. Thus, a big portion of the research is dedicated for the study of this kernel. The most basic but very important fact to understand about the first kernel is that for a linear system the first kernel represents the impulse response function of the system. Some other most important properties of the first kernel for nonlinear systems are given by Langley [40]. He defines the total power input to the system in terms of the real part of the first Wiener kernel and the level of white-noise excitation by,

$$\langle E[P_{in}]\rangle = S_0 \int_0^\infty Re[K_1(\omega)]\mathrm{d}\omega. \tag{2.17}$$

Using the above result and some further analysis, Langley showed that for broadband excitation the power spectrum of the velocity for a system with linear damping β can be described by,

$$S_{\dot{y}\dot{y}}(\omega) = \frac{S_0}{2\beta} Re[K_1(\omega)]. \tag{2.18}$$

These two results are very important for any system with white-noise excitation since they can allow for the calculation of some very important statistical properties of a stochastic process such as the mean square for the velocity, $\sigma_{\dot{y}}^2$ and the displacement, σ_y^2.

Using equation Eq.(2.16) for $n = 1$, the first Wiener kernel, $K_1(\omega)$, which is a complex function in the frequency domain is defined as,

$$K_1(\omega) = \frac{4\pi}{S_0 T} E\left[\dot{Y}(\omega) G^*(\omega)\right] \tag{2.19}$$

This is calculated over a range of nonlinear stiffness values and its real and imaginary parts are plotted in Fig.2.3. The values of the parameters for the Duffing oscillator in this case are $\beta = 0.15$, $\varepsilon_2 = 0$ and ε_3 =0, 10, 30, 70 and 110.

The velocity power spectrum can also calculated using Eq.(2.18) and plotted in Fig.2.4. As you can see the relationship between the velocity power spectrum and the real part of the first kernel is just of a factor, $S_0/2\beta$ as expected from Eq.(2.18).

2.3.3 Second Wiener kernel

In this section, the second Wiener kernel is calculated. However, for cubic nonlinear stiffness as in Eq.(2.3) the second kernel is theoretically equal to zero. The proof and analysis for this statement is explored by Chatterjee and Vyas in [12]. They explored the symmetry of the nonlinear restoring force and found that for a symmetrical restoring force the kernels of even order are all zero. Any function $q[y(t)]$ that satisfies,

$$q[y(t)] = -q[-y(t)] \tag{2.20}$$

is said to be symmetrical. The above expression holds for the cubic stiffness term ($x^3 = -(-x)^3$) used for the Duffing oscillator in Eq.(2.3). For restoring forcing of this nature Chatterjee and Vyas have proved that the even order response components as they appear in Eq.(1.14) entirely consist of even order harmonic excitations which for a symmetrical system are all equal to zero; setting all the individual even components of the response to zero at the same time. From this, it follows that all the even order kernels which characterize the even order response components are also equal to zero.

To overcome this problem a quadratic stiffening term is introduced so that the new form of the Duffing equation looks like,

$$\ddot{y} + 2\beta(1+\varepsilon_2)\dot{y} + y(1 + \varepsilon_{2s} y + \varepsilon_3 y^2) = g(\tau). \tag{2.21}$$

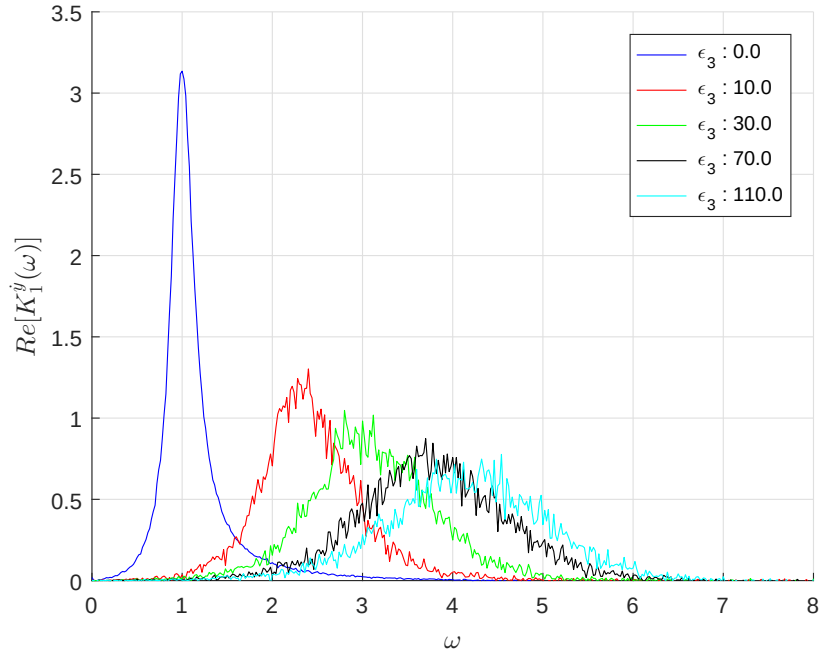

(a) Real part

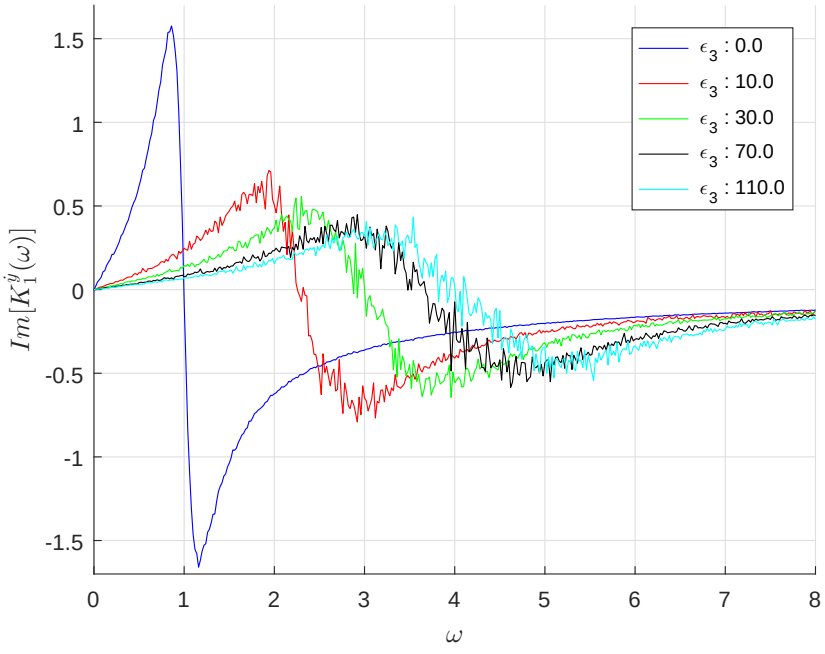

(b) Imaginary part

Fig. 2.3 The first Wiener kernel with varying nonlinear stiffness.

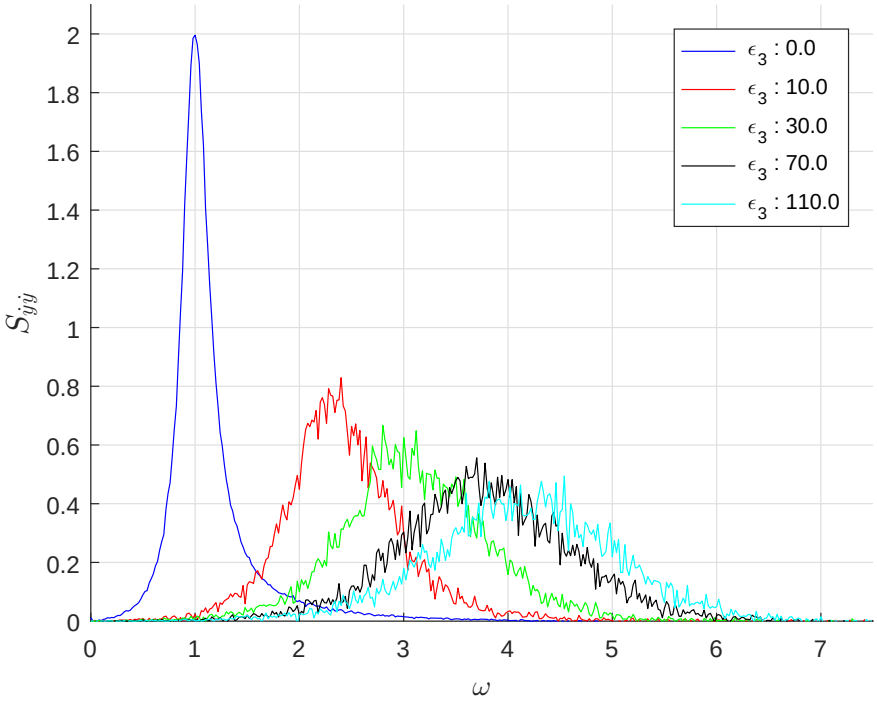

Fig. 2.4 The velocity power spectrum ($S_{\dot{y}\dot{y}}$) with varying nonlinear stiffness.

where $\varepsilon_{2s} < 0$ is the coefficient for the quadratic nonlinearity which incorporates the asymmetry in the restoring force. For the results that follow we use $\varepsilon_{2s} = -0.1$ and $\varepsilon_2 = 0$.

Going back to the kernels, according to Eq.(2.16) the second order Wiener kernel is a two dimensional function. Setting n=2 in Eq.(2.16) the equation for the second kernel is,

$$K_2(\omega_1, \omega_2) = \frac{4\pi}{S_0^2 T} E\left[\dot{Y}(\omega_1 + \omega_2) G^*(\omega_1) G^*(\omega_2)\right]. \tag{2.22}$$

As with the first kernel this is a complex function whose absolute value is calculated and plotted in Fig.2.5 for two values of nonlinear stiffness, $\varepsilon_3 = 10$ and $\varepsilon_3 = 130$. Note that for this figure a smoothing algorithm was used to minimize the effect of noise on the kernels.

The red areas where the amplitude is maximum correspond to the natural frequency which lies on the lines satisfying $\omega_2 = \mid \omega_1 \mid + \mid n_l \mid$, where $n_l = 1 + 2\varepsilon_{2s}\mu + 3\varepsilon_3(\mu^2 + \sigma^2)$ is the linearised natural frequency (see next chapter for theory and Appendix B for the proof); with μ being the mean value and σ the standard deviation of the process. The kernel seems to get more damped with increasing nonlinearity; it widens around the natural frequency and its amplitude decreases, in the same way the first Wiener kernel does. The explanation for

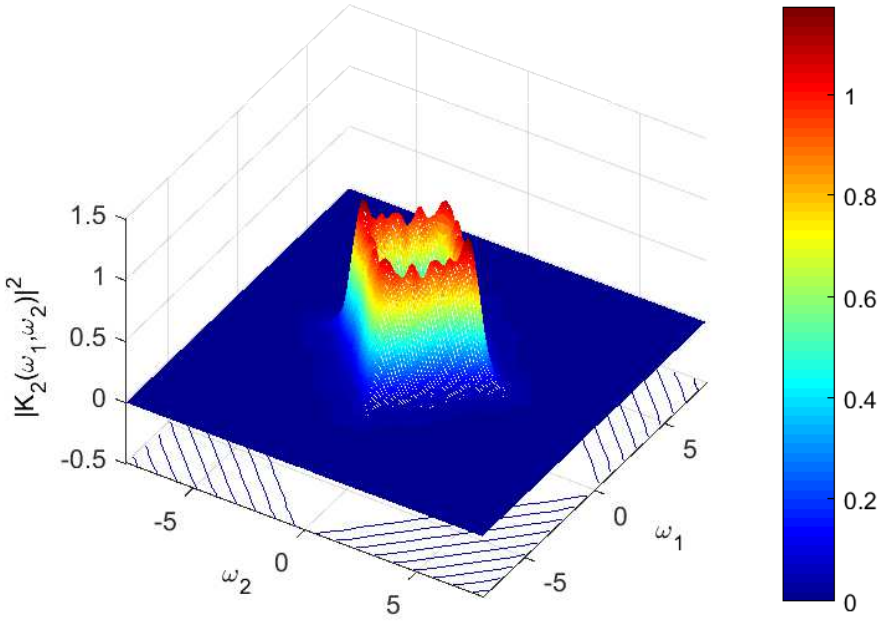

(a) $\varepsilon_3 = 10$

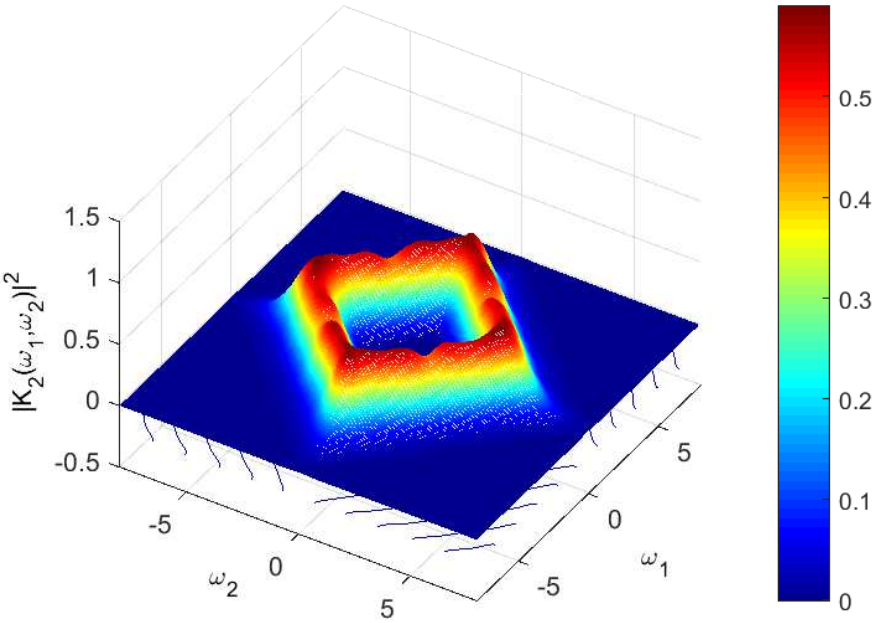

(b) $\varepsilon_3 = 130$

Fig. 2.5 The absolute value squared of the second Wiener kernel, $|K_2(\omega_1,\omega_2)|^2$, for $\varepsilon_2 = 0$, $\varepsilon_{2s} = -0.1$ and (a) $\varepsilon_3 = 10$ and (b) $\varepsilon_3 130$.

this result was mentioned in the previous chapter and is related to the energy transferred from the second Wiener kernel to higher order kernels when nonlinear stiffness increases.

2.4 Wiener kernels versus Equivalent Linearisation

A very common technique for studying and finding solutions of nonlinear systems is the Equivalent Linearisation (EL) [58]. This method tries to approximate a given nonlinear system with a linear system with similar statistical and dynamical characteristics by minimizing some measure of the error between the two. Below, the steps for the EL of the Duffing equation for both nonlinear stiffness and nonlinear damping are illustrated. The resulting first Wiener kernels characterizing both the nonlinear and equivalent linear system in each case are plotted and compared. In the case of the linear system, the first kernel in the frequency is the same as the transfer function of the system.

2.4.1 Nonlinear stiffness

Setting $\varepsilon_2 = 0$ in equation Eq.(2.3), we get the nondimensional Duffing equation with nonlinear stiffness only,

$$\ddot{y} + 2\beta\dot{y} + y(1 + \varepsilon_3 y^2) = g(\tau) \tag{2.23}$$

where the excitation $g(\tau)$ is white noise. By substituting the nonlinear term in the equation with a linear term of an arbitrary coefficient k_l we get the linearised form of the Duffing oscillator,

$$\ddot{y} + 2\beta\dot{y} + y(1 + k_l) = g(\tau). \tag{2.24}$$

For this linear process the mean square displacement is given by,

$$\sigma_y^2 = \frac{\pi S_0}{4\beta(1 + k_l)} \tag{2.25}$$

where S_0 is the level of the single sided spectrum of white-noise excitation, $g(\tau)$.

To find the optimal value of k_l, we aim to minimise the error between Eq.(2.23) and Eq.(2.24) with respect to k_l. The squared error is found by subtracting the linearised equation from the nonlinear equation and squaring, resulting in,

$$\epsilon^2 = (\varepsilon_3 y^3 - k_l y)^2 \tag{2.26}$$

The minimum value of the squared error is found by calculating the partial derivative with respect to k_l and setting the result to zero,

$$\frac{\partial \epsilon^2}{\partial k_l} = -2y(\varepsilon_3 y^3 - k_l y) = 0. \tag{2.27}$$

The ensemble average of the above expression is taken yielding,

$$E[2y(\varepsilon_3 y^3 - k_l y)] = 0 \;\rightarrow\; \varepsilon_3 E[y^4] - k_l E[y^2] = 0. \tag{2.28}$$

Assuming Gaussian approximation for the process and the fact that $\mathrm{E}[y^4] = 3\mathrm{E}[y^2]^2$, the above expression results in a new relationship for an optimal value of k_l in terms of σ_y^2,

$$3\varepsilon_3 \sigma_y^4 - k_l \sigma_y^2 = 0 \;\rightarrow\; k_l = 3\varepsilon_3 \sigma_y^2. \tag{2.29}$$

In order to find the exact value for σ_y^2 analytically, we substitute the result from Eq.(2.29) into Eq.(2.25) which leads to a quadratic equation,

$$\sigma_y^2 = \frac{\pi S_0}{4\beta(1+3\varepsilon_3\sigma_y^2)} \;\rightarrow\; 12\beta\varepsilon_3(\sigma_y^2)^2 + 4\beta\sigma_y^2 - \pi S_0 = 0 \tag{2.30}$$

whose solutions for different nonlinear stiffness coefficients are plotted in Fig.2.6 where they are compared with the RMS values of the Monte-Carlo simulations. The values used are $\beta = 0.15$ and $S_0 = 4\beta/\pi$ for an ensemble of 200 realisations. The agreement between the analytic and numerical results is strong.

Having the analytical result for σ_y^2 the natural frequency of the linearised system can be found using,

$$\omega_l^2 = 1 + k_l = 1 + 3\varepsilon_3\sigma_y^2 \;\rightarrow\; \omega_l = \sqrt{1+3\varepsilon_3\sigma_y^2}. \tag{2.31}$$

Table 2.1 summarizes the analytic results for the mean square displacement and the new linearised natural frequency for various values of nonlinear stiffness.

The velocity power spectrum of the nonlinear system illustrated in Fig.2.4 is plotted in Fig.2.7 where it is compared with the power spectrum of the equivalent linearised equation. The area under the two graphs is very similar confirming the results from Fig.2.6. The shift in the natural frequency due to the nonlinear stiffness is achieved nicely by the EL method. However, the linearisation does not account for the additional damping incorporated by the extra stiffness in the system. This very important discrepancy forms the basis of this research. Our aim is to try and understand the underlying mechanisms of the system that drive this phenomenon of additional damping which will hopefully lead to some useful and solid conclusions.

ε_3	0	10	30	70	110
σ_y^2	1.00	0.167	0.100	0.0667	0.0536
ω_l	1.00	2.45	3.16	3.87	4.32

Table 2.1 Analytic results for linearised natural frequency

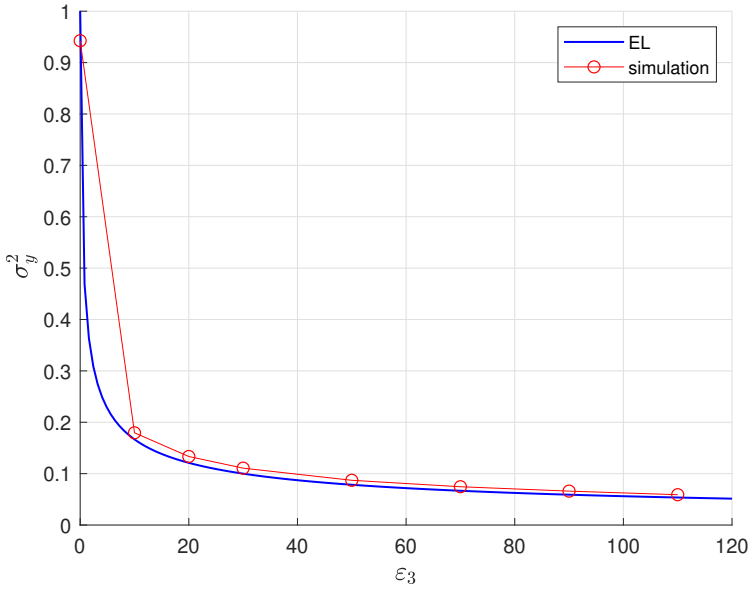

Fig. 2.6 The displacement RMS value versus the stiffening nonlinearity. The two curves correspond to the RMS values from the Monte-Carlo simulations (red) and the analytic value calculated from EL (blue).

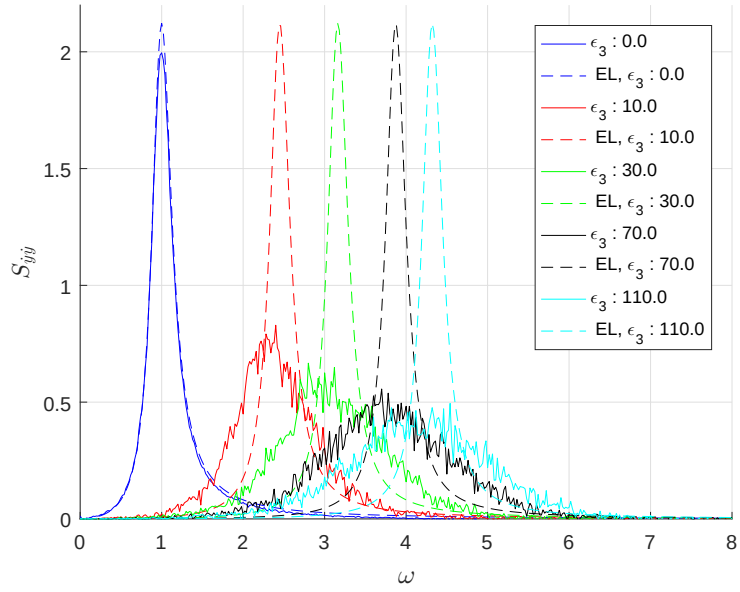

Fig. 2.7 The velocity power spectrum ($S_{\dot{y}\dot{y}}$) of the Duffing oscillator with nonlinear stiffness only (solid line) compared to the power spectrum of the EL (dotted line).

2.4.2 Nonlinear damping

Setting $\varepsilon_3 = 0$ in Eq.(2.3), results in the nondimensional Duffing equation with nonlinear damping only,

$$\ddot{y} + 2\beta\dot{y}(1 + \varepsilon_2\dot{y}^2) + y = g(\tau) \tag{2.32}$$

for white-noise excitation, $g(\tau)$. By substituting the nonlinear term in the equation with a linear term of an arbitrary constant q_l we get the linearised equation,

$$\ddot{y} + 2\beta\dot{y}(1 + q_l) + y = g(\tau). \tag{2.33}$$

For this linear oscillator the mean square velocity is given by,

$$\sigma_{\dot{y}}^2 = \frac{\pi S_0}{4\beta(1 + q_l)} \tag{2.34}$$

where S_0 is the level of the single sided spectrum of the white-noise excitation.

To find the optimal value of q_l, we aim to minimise the error between Eq.(2.32) and Eq.(2.33) with respect to q_l. Like with the nonlinear stiffness, the squared error is found by subtracting the linearised equation from the original equation and squaring the result so that,

$$\epsilon^2 = (\varepsilon_2\dot{y}^3 - q_l\dot{y})^2. \tag{2.35}$$

The minimum value is then found by calculating the partial derivative with respect to q_l and setting the result to zero,

$$\frac{\partial \epsilon^2}{\partial q_l} = -2\dot{y}(\varepsilon_2\dot{y}^3 - q_l\dot{y}) = 0. \tag{2.36}$$

Taking the ensemble average of the above expression yields,

$$\mathrm{E}[2\dot{y}(\varepsilon_2\dot{y}^3 - q_l\dot{y})] = 0 \;\rightarrow\; \varepsilon_2\mathrm{E}[\dot{y}^4] - q_l\mathrm{E}[\dot{y}^2] = 0 \tag{2.37}$$

and assuming the Gaussian approximation for the process with $\mathrm{E}[\dot{y}^4] = 3\mathrm{E}[\dot{y}^2]^2$, leads to a new relationship with the optimal value for q_l in terms of $\sigma_{\dot{y}}^2$,

$$3\varepsilon_2\sigma_{\dot{y}}^4 - q_l\sigma_{\dot{y}}^2 = 0 \;\rightarrow\; q_l = 3\varepsilon_2\sigma_{\dot{y}}^2. \tag{2.38}$$

As with the case of nonlinear stiffness, in order to find the exact value for $\sigma_{\dot{y}}^2$ analytically, we substitute the result from Eq.(2.38) into Eq.(2.34) resulting in a quadratic equation,

$$\sigma_{\dot{y}}^2 = \frac{\pi S_0}{4\beta(1+3\varepsilon_2\sigma_{\dot{y}}^2)} \rightarrow 12\beta\varepsilon_2(\sigma_{\dot{y}}^2)^2 + 4\beta\sigma_{\dot{y}}^2 - \pi S_0 = 0 \tag{2.39}$$

whose solutions for different nonlinear damping coefficients are plotted in Fig.2.8 where they are compared with the RMS values of the Monte-Carlo simulations. The values used are $\beta = 0.15$ and $S_0 = 4\beta/\pi$ for an ensemble of 200 realisations. The agreement between the analytical and numerical results is again very clear.

The linearised oscillators are plotted together with their nonlinear counterparts in Fig.2.9. The results suggest that EL is very efficient in the case of nonlinear damping since the two graphs match nicely.

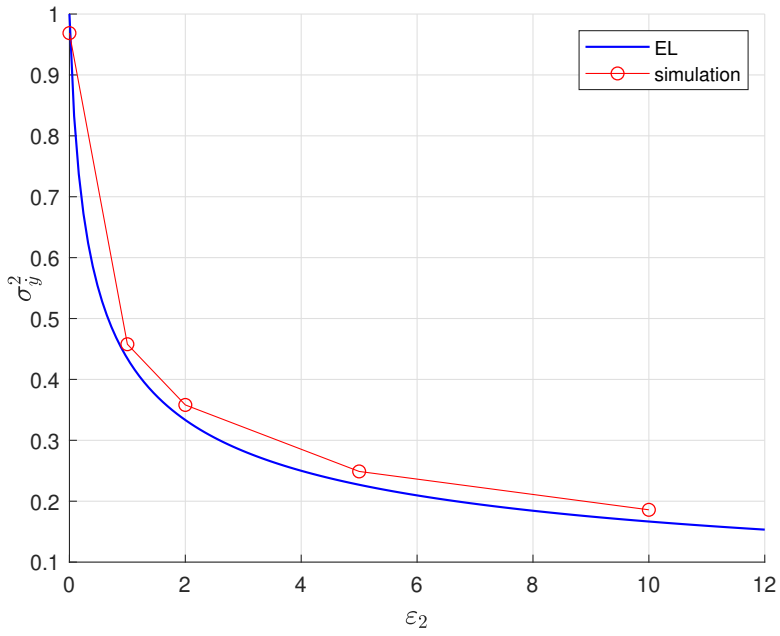

Fig. 2.8 The velocity RMS value versus the nonlinear damping. The two curves correspond to the RMS values from the Monte-Carlo simulations (red) and the analytic results from the EL (blue).

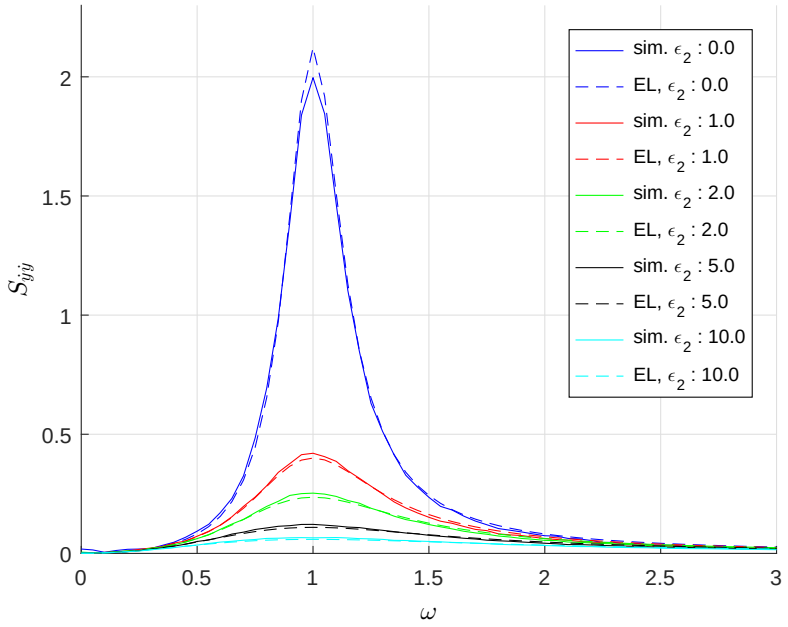

Fig. 2.9 The velocity power spectrum of the Duffing oscillator with nonlinear damping (solid line) compared to the power spectrum of the EL (dotted line).

2.4.3 Nyquist representations

A different way of looking at the results in Fig.2.7 and Fig.2.9 is through the Nyquist plots of the kernel in each case. These are plots of the real part against the imaginary part of a complex quantity. Note that a smoothing algorithm was applied on the first Wiener kernels obtained from the simulations (Fig.2.7 and Fig.2.9) before the creation of the Nyquist plots to eliminate the effect of noise.

2.4.3.1 Nonlinear stiffness

In the case of nonlinear stiffness, the Nyquist plots for the kernels of the Duffing oscillator are illustrated in Fig.2.10. The straight lines in the circles indicate the position of the natural frequency in each case.

The additional damping in the system visualised in Fig.2.7 due to the nonlinear stiffness is reflected by a decrease in the diameter of the circles in Fig.2.10. Another interesting observation is the fact that the 'circles' are getting more elliptical as the nonlinearity increases indicating that there must be something more than just some added damping when nonlinearity is incorporated in the system. The ratio between the diameters of the ellipses is shown in Table 2.2. Also, there is some shifting in the position where the natural frequency

of the system is relative to the linear system. This is demonstrated by the rotation of the dotted lines in each case from the horizontal axis which marks the position of the linear equivalent.

On the other hand, for the equivalent linearised system there is no additional damping to the system. Thus, the Nyquist plots shown in Fig.2.11 are perfect circles with fixed radius implying no additional effective damping in the system. This goes in line with the results in Fig.2.7. Also, the dotted lines are aligned with the horizontal axis which implies the description of a purely linear system in terms of stiffness since the imaginary part in zero.

ε_3	0	10	30	70	110
Diameters' ratio	1.007	1.186	1.197	1.261	1.228

Table 2.2 Nyquist plots: Diameters' ratio for nonlinear stiffness, Fig.2.10.

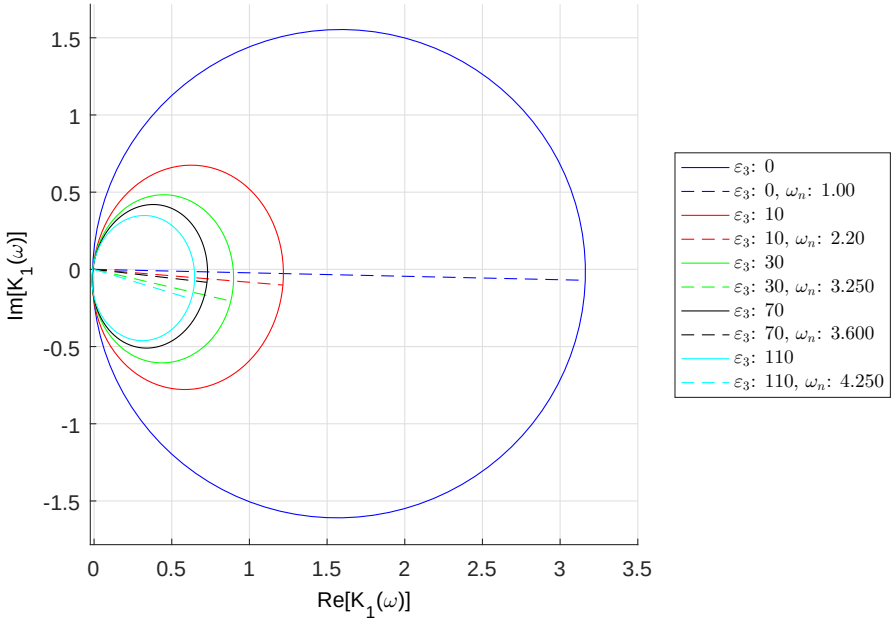

Fig. 2.10 Nyquist representation of the first Wiener kernel for nonlinear stiffness from simulations.

2.4.3.2 Nonlinear damping

In the case of nonlinear damping, the Nyquist plots for the kernels of the version of Duffing oscillator given in Eq.(2.32) are illustrated in Fig.2.12. The straight lines in the circles indicate the position of the natural frequency in each case. The effect of damping on the plots

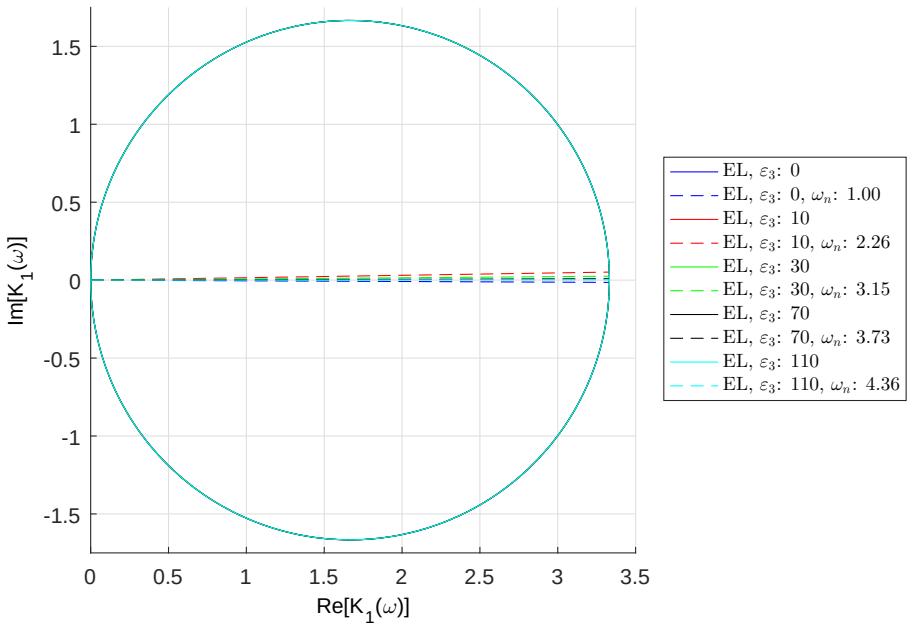

Fig. 2.11 Nyquist representation of the first Wiener kernel for the linearised oscillator in the case of nonlinear stiffness.

is obvious; increasing damping decreases the diameter of the circles as expected. However, unlike the plots for nonlinear stiffness in Fig.2.10 the circles do not become elliptical. In Fig.2.9 was shown that EL works nicely for nonlinear damping. This is confirmed by the Nyquist plots of the linearisation in Fig.2.13 which match perfectly when compared to the plots of the nonlinear system from Fig.2.12.

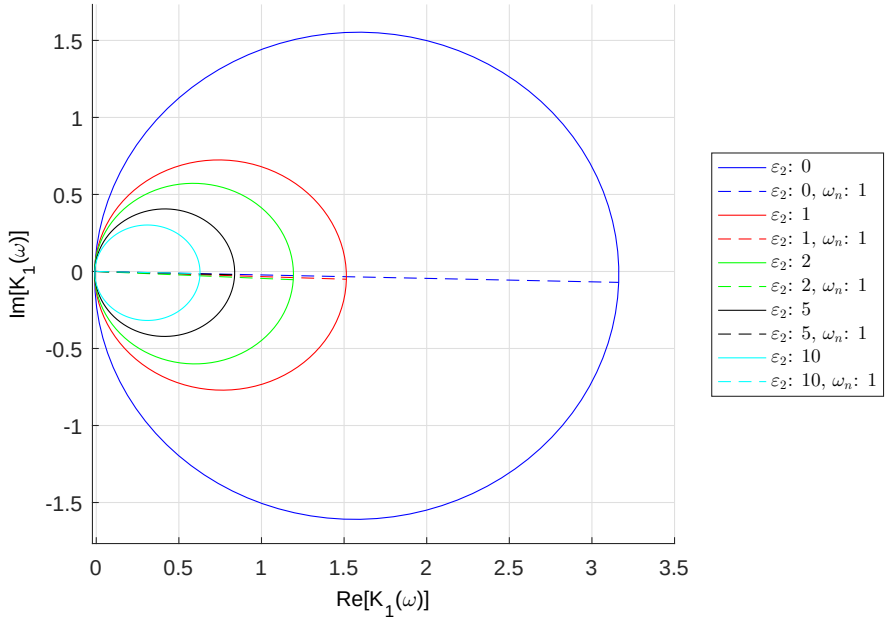

Fig. 2.12 Nyquist representation of the first Wiener kernel for nonlinear damping from simulations.

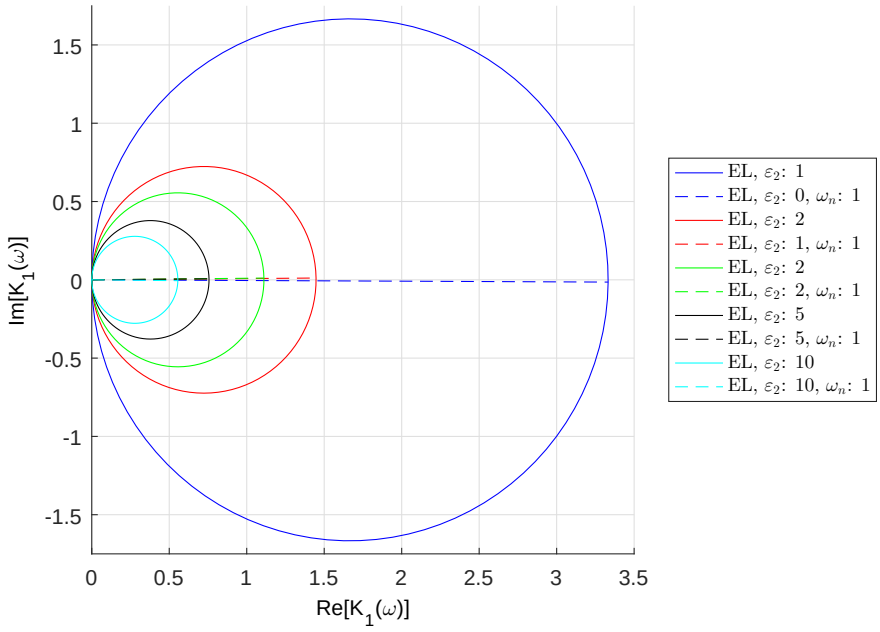

Fig. 2.13 Nyquist representation of the first Wiener kernel for the linearised oscillator in the case of nonlinear damping.

2.5 Kernel contribution

In the previous sections, the method for calculating the first Wiener kernel and visualizing it in various ways were explored. In this section, we seek to quantify the role of each kernel in the total process in order to determine its importance.

To achieve this, a new expression for the the velocity power spectrum is considered based on the expression of the system's response given in Eq.(1.14). This states that the total spectrum is the sum of the power spectrum of each of the individual kernels such as,

$$S_{\dot{y}\dot{y}}(\omega) = S_{\dot{y}_1\dot{y}_1}(\omega) + S_{\dot{y}_2\dot{y}_2}(\omega) + ... + S_{\dot{y}_n\dot{y}_n}(\omega), \quad \text{for } n = 1...\infty \tag{2.40}$$

where,

$$\begin{aligned}
&S_{\dot{y}_1\dot{y}_1} = S_0 \left|K_1(\omega)\right|^2 \\
&S_{\dot{y}_2\dot{y}_2} = \frac{S_0}{2\pi}\int_{-\infty}^{+\infty} \left|K_2(\omega_1, \omega-\omega_1)\right|^2 \mathrm{d}\omega_1 \\
&... \\
&S_{\dot{y}_n\dot{y}_n} = \frac{S_0}{(2\pi)^{n-1}}\int_{-\infty}^{+\infty} ... \int_{-\infty}^{+\infty} \left|K_n(\omega_1, ..., \omega_{n-1}, \omega-\omega_1-...-\omega_{n-1})\right|^2 \mathrm{d}\omega_1 ... \mathrm{d}\omega_{n-1}.
\end{aligned} \tag{2.41}$$

The above equations allow the calculation of the velocity power spectrum generated by a single Wiener kernel only. In the next chapters the the velocity power spectrum of the first kernel will be measured and compared with the spectrum of the whole process in order to measure its contribution.

2.5.1 The coherence function

A robust way of measuring the extent to which two data sets are correlated is by calculating the coherence function [5][51] between them. In the following sections, the coherence function is used to calculate the power transfer between the white-noise input and the power dissipated due to the first Wiener kernel. Different forms of the coherence function are used in literature but for the purposes of this project the following equation is used,

$$C(\omega) = \frac{\left|S_{\dot{y}g}\right|^2}{S_{\dot{y}\dot{y}}S_{gg}} \equiv \frac{\left|S_{\dot{y}_1\dot{y}_1}\right|^2}{S_{\dot{y}\dot{y}}S_{gg}} \tag{2.42}$$

The equation above defines the coherence function as the ratio of the absolute value of the cross-spectral density ($S_{\dot{y}g}$) between the response velocity and the excitation to the product

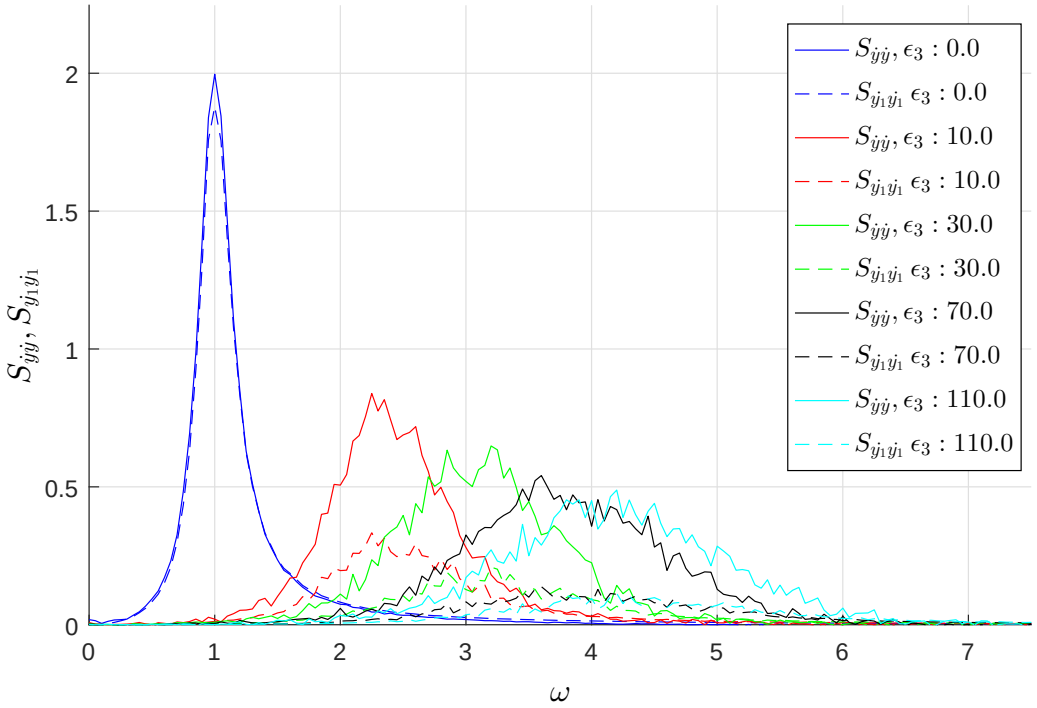

Fig. 2.14 The velocity power spectrum (solid line) of the whole process compared to the contribution of the first Wiener kernel (dotted line) for different measures of nonlinear stiffness.

of the auto-spectral densities of the velocity ($S_{\dot{y}\dot{y}}$) and the excitation (S_{gg}). The coherence is calculated in the following sections for both nonlinear stiffness and nonlinear damping.

The function has a range from zero to one for uncorrelated and correlated data respectively. For a linear system the power dissipated is entirely due to the first kernel, thus the coherence function between the power spectrum from the first kernel and the input excitation should be one. The proof for this can be found in page 172 of [5].

2.5.2 Nonlinear stiffness

The power spectrum from the contribution of the first kernel is calculated using the expression in Eq.(2.41). The result is illustrated graphically in Fig.2.14 where it is plotted together with the power spectrum of the whole process for different values of nonlinear stiffness. In the case of the linear system the strong agreement between the two curves confirms the expected result that the energy dissipated entirely depends on the first Wiener kernel. The disagreement at the top of the peaks is due to numerical limitations of the computations and the resolution of the solutions. However, as the systems becomes more nonlinear, the

ε_3	0	10	30	70	110
$\sigma^2_{\dot{y}}$	0.984	0.987	0.984	0.991	0.979
$\sigma^2_{\dot{y}_1}$	0.940	0.449	0.339	0.289	0.252
$1-\left((\sigma^2_{\dot{y}}-\sigma^2_{\dot{y}_1})/\sigma^2_{\dot{y}}\right)$	≈ 1	0.455	0.345	0.292	0.257
$\sigma^2_{\dot{y}_1}/\sigma^2_{\dot{y}}$	≈ 1	0.454	0.344	0.292	0.258

Table 2.3 Quantification of the contribution of the first Wiener kernel for nonlinear stiffness

energy from the first kernel is transferred to the higher order kernels in which the energy is dissipated as it has been explained in section 1.2.2.2 reducing the contribution of the first kernel. A quantified measure of the kernel contribution is given in table 2.3 where the ratio of the RMS velocity from the first kernel to the total is calculated. The calculations are based on the fact that,

$$\sigma^2_{\dot{y}} = \int_0^\infty S_{\dot{y}\dot{y}} d\omega \quad \text{and} \quad \sigma^2_{\dot{y}_1} = \int_0^\infty S_{\dot{y}_1\dot{y}_1} d\omega. \tag{2.43}$$

Figure 2.15 shows the coherence function as a function of frequency for the various values of nonlinear stiffness. In the case of the linear system the coherence function is one for almost all the frequencies as expected. The fact that for a few low frequencies, the coherence is not ones is due to the limitations of the numerical computations. For the nonlinear cases the coherence experiences an increasing drop with an interesting further drop at the natural frequency. The value at the natural frequency follows the drop rate of the ratio between the velocity RMS values shown in Table 2.3. This decreasing behaviour both in the ratio of the velocity RMS values and of the coherence at the natural frequency suggest that the importance or the contribution of the first Wiener kernel to the total process gets less with increasing nonlinear stiffness. As it has been explained in previous chapters this can be explained by the fact that the energy from the first kernel is dissipated to the higher order kernels when the system becomes more nonlinear.

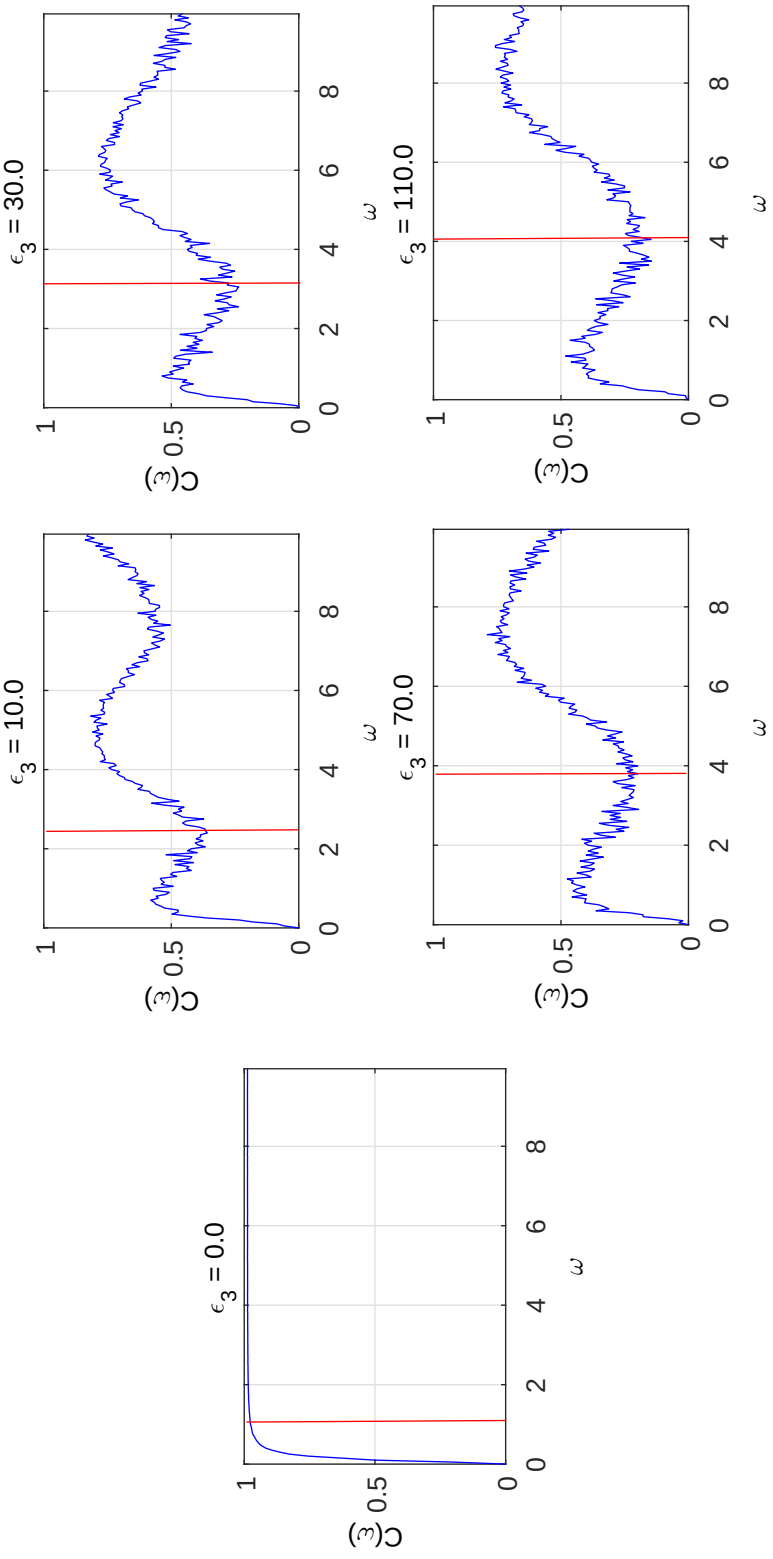

Fig. 2.15 The coherence as a function of frequency for different values of nonlinear stiffness, ε_3. The red lines marks the shifted natural frequency.

2.5.3 Nonlinear damping

The contribution of the first kernel for the Duffing oscillator with nonlinear damping is calculated and plotted together with the total velocity spectrum in Fig.2.16. Unlike nonlinear stiffness, for nonlinear damping the first Wiener kernel is the dominant kernel in the process despite the increase in nonlinearity. The matching between the two curves is obvious suggesting a negligible effect on the role of the first kernel when nonlinear damping is incorporated in the system. This is confirmed by the the ratio between the velocity RMS values of the two curves for a range of nonlinear damping values which is constantly very close to one as demonstrated in table 2.4. The RMS values are calculated using the relevant equation from Eq.(2.43).

Here, it should be noted that the velocity power spectrum of the process for nonlinear damping was calculated using the velocity auto-correlation function given by,

$$S_{\dot{y}\dot{y}}(\omega) = \frac{S_0 T}{2\pi} \mathrm{E}[\dot{Y}^2(\omega)]. \tag{2.44}$$

This is due to the fact that the expression in Eq.(2.18) is only valid for systems with linear damping.

In the next page, Fig.2.17 shows the coherence function as a function of frequency for the different values of nonlinear damping already used in the previous examples. For the linear system, the coherence function is one as expected. The same trend holds true for the nonlinear cases where the coherence is constant very close to one just like with the ratio between the velocity RMS values shown in the table above with a general tendency of this value to drop slightly when increasing nonlinear damping. This behaviour both between the ratio of the RMS values and of coherence suggest that the first Wiener kernel is the main contributor to the total process independently of the amount of damping in the system.

Table 2.4 Quantification of the contribution of the first Wiener kernel for nonlinear damping

ε_2	0	1	2	5	10
$\sigma^2_{\dot{y}}$	0.964	0.452	0.353	0.243	0.180
$\sigma^2_{\dot{y}_1}$	0.940	0.438	0.340	0.233	0.172
$1-\left((\sigma^2_{\dot{y}}-\sigma^2_{\dot{y}_1})/\sigma^2_{\dot{y}}\right)$	≈ 1	0.969	0.963	0.958	0.955
$\sigma^2_{\dot{y}_1}/\sigma^2_{\dot{y}}$	≈ 1	0.969	0.964	0.958	0.954

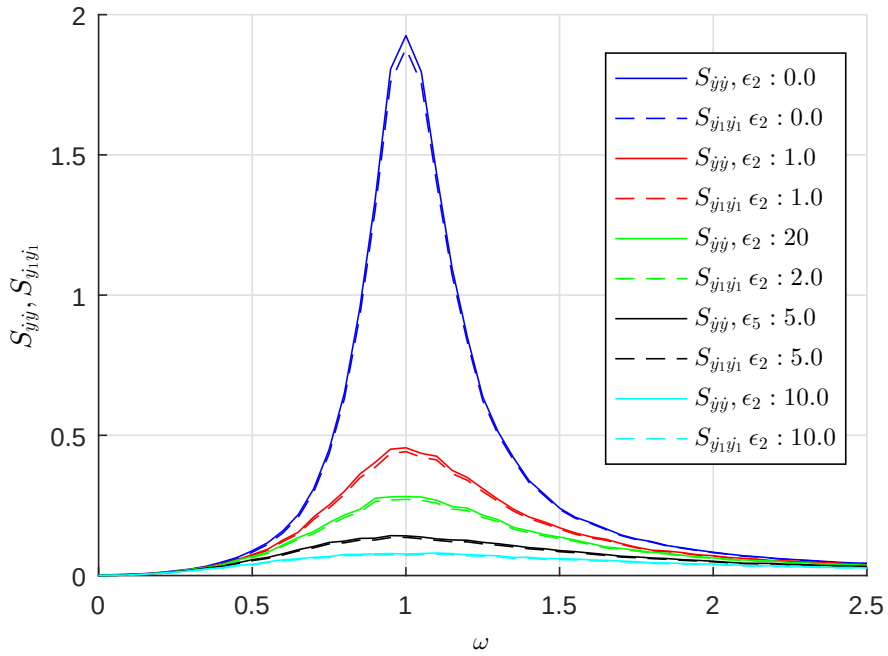

Fig. 2.16 The velocity power spectrum (solid line) of the whole system compared to the contribution of the first Wiener kernel (dotted line) for different measures of nonlinear damping.

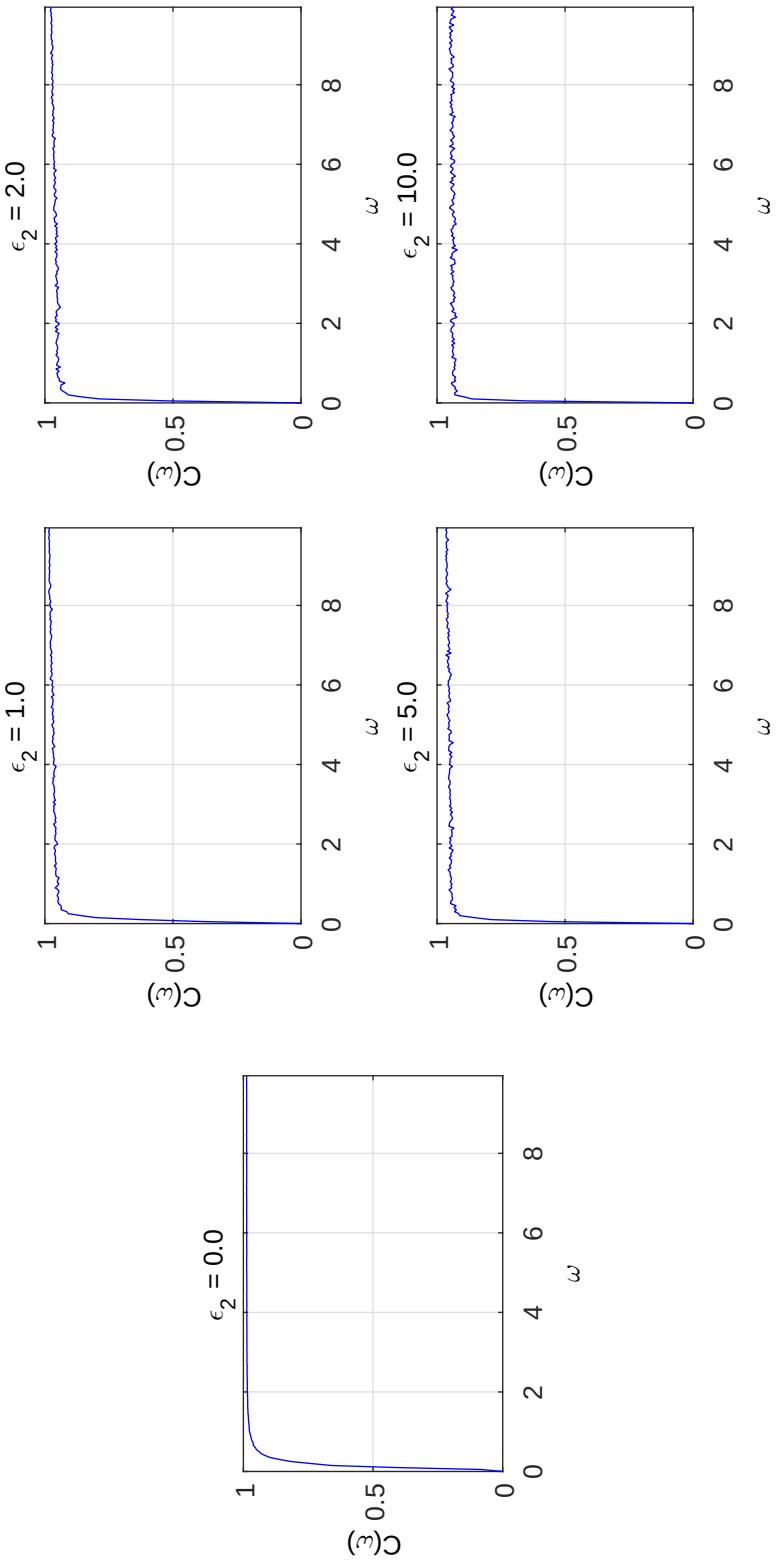

Fig. 2.17 The coherence as a function of frequency for different values of nonlinear damping, ε_2. The red lines marks the natural frequency.

2.6 An analytical energy transfer approach to explain the kernels' behaviour in the case of nonlinear stiffness

In order to understand the behaviour of nonlinear systems under white-noise input and the role the kernels play in this, it is essential to investigate the mechanism describing the energy transfer between the kernels in these systems. For this consider a nonlinear system described by the following equation of motion

$$\ddot{y} + c\dot{y} + ky + W(y) = \xi(t) \tag{2.45}$$

with nonlinear stiffness term $W(y) = y^n$ for an odd power $n(n > 1)$ and c and k the linear damping and stiffness coefficients respectively and $\xi(t)$ the white-noise input force.

The velocity response of the above system can be expressed by its Wiener series

$$\dot{y}(t) = \sum_{n=0}^{\infty} G_n[k_{n,\dot{y}}; \xi(t)] = \sum_{n=0}^{\infty} \dot{y}_n \tag{2.46}$$

and in a similar way the nonlinear force can be expressed as

$$W(y) = \sum_{n=0}^{\infty} G_n[k_{n,W}; \xi(t)] = \sum_{n=0}^{\infty} W_n. \tag{2.47}$$

Due to the statistical independence of the terms in the series as expressed by Eq.(1.16) the following expressions between the two quantities of interest -velocity and nonlinear force- need to be noted:

$$E[\dot{y}_n \dot{y}_m] = 0,\ E[W_n W_m] = 0,\ E[\dot{y}_n W_m] = 0 \ \text{ for } n \neq m,\ n \in \mathbb{Z},\ m \in \mathbb{Z}. \tag{2.48}$$

The above definitions and results are now to be used for the proof in this section which will show how the energy in the system is transferred between the kernels.

The structure of the following proof consists of two intermediate results which are then combined to explain an interesting result. To obtain the first intermediate result, multiply Eq.(2.45) by the velocity $\dot{y}$ and take the expected value $E[]$ on both sides of the equation

$$\begin{aligned} &\dot{y}\ddot{y} + c\dot{y}^2 + k\dot{y}y + \dot{y}W(y) = \dot{y}\xi(t) \overset{E[\,]}{\rightarrow} \\ &E[\dot{y}\ddot{y}] + cE\left[\dot{y}^2\right] + kE[\dot{y}y] + E[\dot{y}W(y)] = E[\dot{y}\xi(t)]. \end{aligned} \tag{2.49}$$

The first and third terms on the LHS of the above equation are always zero because the process is stationary. This can be demonstrated by

$$E\left[\dot{y}\ddot{y}\right] = E\left[\frac{1}{2}\frac{d}{dt}\dot{y}^2\right] = \frac{1}{2}\frac{d}{dt}E\left[\dot{y}^2\right] = 0 \quad \text{and} \quad E\left[\dot{y}y\right] = E\left[\frac{1}{2}\frac{d}{dt}y^2\right] = \frac{1}{2}\frac{d}{dt}E\left[y^2\right] = 0. \tag{2.50}$$

In a similar way, the expected value of the product in the fourth term which can be redefined as $\dot{y}\frac{dU}{dy}$ where U is the potential energy of the system arising from the nonlinearity (excluding $\frac{1}{2}ky^2$) can also be shown to be zero.

$$E\left[\dot{y}W(y)\right] = E\left[\dot{y}\frac{dU}{dy}\right] = \frac{d}{dt}E\left[U\right] = 0. \tag{2.51}$$

Substituting the results from Eq.(2.50) and Eq.(2.51) back to Eq.(2.49) yields

$$cE\left[\dot{y}^2\right] = E\left[\dot{y}\xi(t)\right]. \tag{2.52}$$

Based on the orthogonality properties of the terms in the Wiener series the expected value of the response velocity can be expressed as

$$E\left[\dot{y}^2\right] = E\left[\sum_{n=0}^{\infty}\dot{y}_n\sum_{m=0}^{\infty}\dot{y}_m\right] = E\left[\sum_{n=0}^{\infty}\sum_{m=0}^{\infty}\dot{y}_n\dot{y}_m\right] = E\left[\sum_{n=0}^{\infty}\dot{y}_n^2\right] = \sum_{n=0}^{\infty}E\left[\dot{y}_n^2\right] \tag{2.53}$$

In addition, it is known that any effect of the white-noise excitation comes only from the contribution of the first kernel of the force. Therefore, due to the orthogonality condition the RHS term in Eq.(2.52) can be simplified to

$$E\left[\dot{y}\xi(t)\right] = E\left[\sum_{n=0}^{\infty}\dot{y}_n\xi_1(t)\right] = E\left[\dot{y}_1\xi_1(t)\right] = E\left[\dot{y}_1\xi(t)\right]. \tag{2.54}$$

The expressions from Eq.(2.53) and Eq.(2.54) are then substituted back into Eq.(2.52) to give rise to the first intermediate result:

$$c\sum_{n=0}^{\infty}E\left[\dot{y}_n^2\right] = E\left[\dot{y}_1\xi(t)\right] \tag{2.55}$$

which suggests the well-known fact that the sum of the dissipated power from each individual kernel equals to the total input power to the system (Conservation of Energy).

A similar methodology is used to obtain the second intermediate result. In this case, Eq.(2.45) is multiplied by a single velocity response Wiener term before taking the expected

value of both sides of the equation

$$\begin{aligned} &\dot{y}_m\ddot{y} + c\dot{y}_m\dot{y} + k\dot{y}_m y + \dot{y}_m W(y) = \dot{y}_m\xi(t) \overset{E[\,]}{\rightarrow} \\ &E\left[\dot{y}_m\ddot{y}_m\right] + cE\left[\dot{y}_m^2\right] + E\left[\dot{y}_m y_m\right] + E\left[\dot{y}_m W_m(y)\right] = E\left[\dot{y}_m\xi(t)\right] = P(t)\delta_{1m} \end{aligned} \tag{2.56}$$

where δ_{1m} is the Kronecker delta[1] function such that the RHS power term is non-zero only for $m = 1$ since the power input to the system -now defined by P- is only dependent on the first kernel. The first and third terms in the above equation are equal to zero like with the expressions in Eq.(2.50), because

$$E\left[\dot{y}_m\ddot{y}_m\right] = E\left[\frac{1}{2}\frac{d}{dt}\dot{y}_m^2\right] = \frac{1}{2}\frac{d}{dt}E\left[\dot{y}_m^2\right] = 0 \text{ and } E\left[\dot{y}_m y_m\right] = E\left[\frac{1}{2}\frac{d}{dt}y_m^2\right] = \frac{1}{2}\frac{d}{dt}E\left[y_m^2\right] = 0 \tag{2.57}$$

reducing Eq.(2.56) into the second intermediate result

$$cE\left[\dot{y}_m^2\right] + E\left[\dot{y}_m W_m(y)\right] = P(t)\delta_{1m}. \tag{2.58}$$

Writing the explicit expressions from the contributions of the first n individual kernels emerging from the above equation results in the following set of equations

$$\begin{aligned} cE\left[\dot{y}_1^2\right] + E\left[\dot{y}_1 W_1(y)\right] &\leq P(t) \\ cE\left[\dot{y}_2^2\right] + E\left[\dot{y}_2 W_2(y)\right] &= 0 \\ &\cdots \\ cE\left[\dot{y}_n^2\right] + E\left[\dot{y}_n W_n(y)\right] &= 0. \end{aligned} \tag{2.59}$$

For a linear system ($W(y) = 0$) the inequality above becomes a strict equality since all the input energy is exclusively used by the first kernel. But for a nonlinear system, $E\left[\dot{y}_1 W_1\right] \geq 0$ and from Eq.(2.51) which can be generalised to

$$E\left[\dot{y}W(y)\right] = \sum_{m=0}^{\infty} E\left[\dot{y}_m W_m(y)\right] = 0 \tag{2.60}$$

it follows that

$$E\left[\dot{y}_m W_m(y)\right] \leq 0 \quad \text{for } m > 1 \tag{2.61}$$

[1] $\delta_{ij} = \begin{cases} 0 & \text{if } i \neq j \\ 1 & \text{if } i = j \end{cases}$

and consequently from Eq.(2.59)

$$cE\left[\dot{y}_m^2\right] \geq 0 \quad \text{for} \quad m > 1. \tag{2.62}$$

This result suggests that for a system with nonlinear stiffness some of the power taken in by the first kernel is transferred to the higher order kernels where it is expressed as additional dissipation power by the system. The additional dissipation characteristic emerging from the energy transfer to the higher order kernels has a broadening effect on the shape of first Wiener kernel. This is already visualized in Fig.2.4 and Fig.2.7 and it will be discussed further in the next chapter.

2.7 Conclusion

Firstly, the Wiener kernels for a nonlinear system were calculated and extracted. A generalised form of the n^{th} order Wiener kernel was presented with only the first (Fig.2.3) and second kernels (Fig.2.5) to be extracted from the system which show similarities in their behaviour such as the widening effect for increasing nonlinear stiffness.

Next, the first Wiener kernel was compared to EL. For nonlinear stiffness, EL captures the RMS value of the response well as shown in Fig.2.8. The shift in the natural frequency due to the additional stiffness was also followed by EL especially for weak nonlinearity. However, it is clear that EL cannot capture the true shape of the velocity spectrum which gets damped with nonlinear stiffness. This result is itself surprising enough due to the fact that no damping is added in the system but still a clear damping effect is present in the system as reflected in the power spectrum of the response (Fig.2.4) since it is known that the power spectrum and the first Wiener kernel are linearly related (Eq.(2.18)) for systems with linear damping.

To understand the damping effect, the contribution of the first Wiener kernel was calculated for varying nonlinear stiffness using a direct method (Tab.2.3) and the coherence function (Fig.2.15). The two methodologies agree with each other as expected and suggest that the contribution of the first Wiener kernel to the system decreases with increasing nonlinear stiffness. A further detail obtained from the graphical illustration of the coherence function suggests that around the natural frequency the the contribution from the kernel is at its minimum in each case.

Finally, an energy transfer approach to give an analytical explanation to the damping effect on the first Wiener kernels. It was shown that for nonlinear stiffness some of the energy input in the first Wiener kernel is transferred to higher order kernel. This loss of energy from

the first kernel is what causes the additional damping on it despite no external damping being added to the system.

Before going on to the next chapter, it needs to be mentioned that through the work presented above it is shown that EL works very well for systems with nonlinear damping and linear stiffness. This is demonstrated in Fig.2.9 and supported by the contribution results of the first Wiener kernel (Fig.2.17) which suggest that for nonlinear damping the full contribution to the energy of the system comes from the first Wiener kernel alone.

Chapter 3

An enhancement to Equivalent Linearisation

3.1 Introduction

In Chapter 2, the failure of EL to capture the true shape of the first Wiener kernel of systems with nonlinear stiffness was presented. In addition, the reason behind this failure was demonstrated by calculating the contribution of the first Wiener kernel to the overall system which decreases with increasing nonlinear stiffness. Furthermore, an analytical proof of an energy approach method was presented to show that the effective damping on the first kernel caused by stiffening nonlinearities is caused due to the energy transfer from the first Wiener kernel to the higher order kernels.

In this chapter, an analytical explanation to why EL fails for systems with nonlinear stiffness is presented using the cumulant and characteristic function representation for distributions.

Next, the main result of this project is to be presented. This is a method to improve EL using a single-pole fit (SPF) function over the transfer function (TF) between the first Wiener kernel of the nonlinear force and the first Wiener kernel of the original system.

3.2 Limitations of Equivalent Linearisation

3.2.1 A brief introduction to Characteristic functions and Cumulants

EL assumes that the nonlinear stiffening force has a Gaussian distribution like a linear force does. However, this property is no longer true in the case of the nonlinear force. Here,

an analytical proof is presented in order to show why EL does not work. The proof uses the characteristic function and the cumulant representation of the first Wiener kernel of the nonlinear force and therefore, a short introduction to this theory follows.

The cumulants, $\kappa_i[X_1 \dots X_n]$, are an alternative to the moments representation of the joint probability density function of variables $X_1 \dots X_n$. They are the coefficients of the Taylor expansion of the logarithmic characteristic function of a probability distribution of a set of jointly distributed random variables such as

$$\kappa_{m_1+\dots+m_n}[X_1 \dots X_n] = \frac{1}{i^{m_1+\dots+m_n}} \left(\frac{\partial^{m_1+m_2+\dots+m_n}}{\partial \theta_1^{m_1} \dots \partial \theta_n^{m_n}} L_{X_1 \dots X_n}(\theta_1, \dots, \theta_n) \right)_{\theta_1=\dots=\theta_n=0} \tag{3.1}$$

where $L_{X_1 \dots X_n} = \ln(M_{X_1 \dots X_n})$ and $M_{X_1 \dots X_n}$ is the characteristic function defined as the Fourier Transform of the joint probability density function of $X_1 \dots X_n$. This is defined as

$$M_{X_1 \dots X_n} = \int_{-\infty}^{\infty} \int_{-\infty}^{\infty} p_{X_1 \dots X_n}(x_1 \dots x_n) e^{i(\theta_1 x_1 + \dots + \theta_n x_n)} \mathrm{d}x_1 .. \mathrm{d}x_n. \tag{3.2}$$

It is also known that the expected value of joint random variables is

$$E\left[X_1^{m_1} \dots X_n^{m_n}\right] = \frac{1}{i^{m_1+\dots+m_n}} \left(\frac{\partial^{m_1+m_2+\dots+m_n}}{\partial \theta_1^{m_1} \dots \partial \theta_n^{m_n}} M_{X_1 \dots X_n}(\theta_1, \dots, \theta_n) \right)_{\theta_1=\dots=\theta_n=0}. \tag{3.3}$$

Detailed information on cumulants and the characteristic function can be found in the second chapter of [44].

3.2.2 Cumulants and Equivalent Linearisation

The first kernel of the nonlinear force y^3 is given by $E\left[Y^3(\omega)\Xi(\omega)\right]$ where $\Xi(\omega)$ is the white-noise input (Eq.(2.45)) in the frequency domain, $\mathrm{FFT}\{\xi(t)\} = \Xi(\omega)$. For simplicity we can set $Y(\omega) = \theta_1$ and $\Xi(\omega) = \theta_2$. From Eq.(3.3) it follows

$$E\left[{\theta_1}^3 \theta_2\right] = \frac{1}{i^4} \left(\frac{\partial^4}{\partial^3 \theta_1 \partial \theta_2} M(\theta_1, \theta_2) \right)\Bigg|_{\theta_1=\theta_2=0} = \left(\frac{\partial^4}{\partial^3 \theta_1 \partial \theta_2} e^{L(\theta_1,\theta_2)} \right)_{\theta_1=\theta_2=0}\Bigg|. \tag{3.4}$$

Taking the partial derivatives with respect to θ_1 and θ_2 such that $L_i = \frac{\partial L}{\partial \theta_i}$ and $L_{ij} = \frac{\partial^2 L}{\partial \theta_i \partial \theta_j}$,

$$E\left[{\theta_1}^3 \theta_2\right] = \left(\begin{array}{c} L_1^3 L_2 + 3L_1^3 L_{12} + 3L_{11} L_{12} + 3L_1 L_{112} + \\ 3L_1 L_2 L_{11} + L_{1112} + L_{111} L_2 \end{array} \right) e^{L(\theta_1,\theta_2)}\Bigg|_{\theta_1=\theta_2=0}. \tag{3.5}$$

Since $L_1 = L_2 = 0$ ($\mu_{\theta_1} = \mu_{\theta_2} = 0$) and $e^{L(\theta_1,\theta_2)}|_{\theta_1=\theta_2=0} = 1$ the above expression can be simplified into

$$E\left[{\theta_1}^3\theta_2\right] = 3L_{11}L_{12} + L_{1112} \tag{3.6}$$

and finally using Eq.(3.1) to write the result in terms of the cumulants between the nonlinear force and the white-noise excitation

$$\begin{aligned} E\left[{\theta_1}^3\theta_2\right] &= 3\kappa_2\left[\theta_1\theta_2\right]\kappa_2\left[\theta_1^2\right] + \kappa_4\left[\theta_1^3\theta_2\right] \\ \therefore E\left[Y^3(\omega)\,\Xi(\omega)\right] &= 3\kappa_2\left[Y(\omega)\,\Xi(\omega)\right]\kappa_2\left[Y^2(\omega)\right] + \kappa_4\left[Y^3(\omega)\,\Xi(\omega)\right]. \end{aligned} \tag{3.7}$$

A linear force can be shown to be dependent solely on κ_2 and therefore exhibiting a Gaussian distribution. However, the above result suggests a property for systems with nonlinear stiffening force. The second term in the expression includes the forth cumulant between the nonlinear force and the excitation. Remember that for a Gaussian distribution, $\kappa_n = 0$ for $n > 2$. Thus, the quantity of interest which is the first Wiener kernel of nonlinear force does not have a Gaussian distribution since $\kappa_4 > 0$. This property of the nonlinear force is ignored by EL. This also explains the mismatch between the curves in Fig.2.7. In the next chapter an improved method to EL is suggested which exploits the result above to find a function to characterise the forth cumulant of the first Wiener kernel of the nonlinear force in the form,

$$\begin{aligned} E\left[Y(\omega)^3\Xi(\omega)\right] &= K_{1,y^3}(\omega) \\ &= 3\sigma_y^2 K_1(\omega) + Q(\omega) = \left(3\sigma_y^2 + P(\omega)\right)K_1(\omega) = G(\omega)\,K_1(\omega). \end{aligned} \tag{3.8}$$

where $K_{1,y^3}(\omega)$ is the first Wiener kernel of the nonlinear force and $Q(\omega)$, $P(\omega)$ and $G(\omega)$ are non-constant functions to be quantified.

3.2.3 Visualisation of the non-Gaussian behaviour

Two famous series, the Gram-Charlier[27][11] and Edgeworth[34][29] series make use of the cumulants to express the probability distribution of a process. The two series are equivalent with the only difference being the rearrangement of the terms in the series which play a role on the truncation of the series.

The first three terms in the Gram-Charlier series are given by [76],

$$F(x) \approx \frac{1}{\sqrt{2\pi}\sigma} e^{-\frac{(x-\mu)^2}{2\sigma^2}} \left[1 + \frac{\kappa_3}{3!\sigma^3} H_3\left(\frac{x-\mu}{\sigma}\right) + \frac{\kappa_4}{4!\sigma^4} H_4\left(\frac{x-\mu}{\sigma}\right)\right] \tag{3.9}$$

where $H_n(x)$ is the nth order Hermite polynomial[1] [41][19] and μ and σ are the mean and standard deviation or the first and second cumulants respectively. Note, that there are many versions of the Gram-Charlier series such as 'Gram-Charlier Type A' and 'Gram-Charlier Type C' but there is no need here to go into their details here.

Equivalently, the first terms of the Edgeworth series are given by [76],

$$F_n(x) \approx \Phi(x) - \frac{1}{n^{1/2}}\left(\frac{1}{6}\frac{\kappa_3}{\sigma^3}\Phi^{(3)}(x)\right) + \frac{1}{n}\left(\frac{1}{24}\frac{\kappa_4}{\sigma^4}\Phi^{(4)}(x) + \frac{1}{72}\left(\frac{\kappa_3}{\sigma^3}\right)^2\Phi^{(6)}(x)\right) \quad (3.10)$$

where $\Phi^{(n)}(x) = (-1)^n H_n(x)\Phi(x)$ and $\Phi(x) = \int_{-\infty}^{x} \frac{1}{\sqrt{2\pi}} \exp^{-\frac{1}{2}q^2}\, dq$.

The individual cumulants in both cases are calculated using the following recursive formula[60]

$$\kappa_n = \mu'_n - \sum_{m=1}^{n-1} \binom{n-1}{m-1} \kappa_m \mu'_{n-m} \quad (3.11)$$

where $\mu'_n = \frac{1}{n}\sum^n x^n$ is the nth central moment of the random variable.

The pdfs of the random response for the nonlinear system under investigation, Duffing oscillator Eq.2.24, as approximated by the Gram-Charlier and Edgeworth series are illustrated in Fig.3.1. This is demonstrated for two different cases of the nonlinear coefficient and each the approximated pdfs are compared to the corresponding Gaussian (or Normal) distribution. It is obvious that the two approximations which match as expected, do not match with the Gaussian distribution but they rather have a much lowered peak. This is due to the the non-zero fourth cumulant of the response, an effect known as 'kurtosis'. Kurtosis is defined by the fourth cumulant and is a measure that describes the 'pointedness' of the peak of the probability distribution. In the cases below, a positive fourth cumulant results in a peak lower and smoother peak than that of the Normal distribution and hence, a wider pdf since the area under all the pdfs has to be the same. This mismatch of the pdf with the Normal distribution suggests why EL fails to capture the first Wiener kernel of a system with nonlinear stiffness since it assumes it has a Gaussian distribution.

[1] Probabilistic Hermite polynomials are used in this case. There is another type of Hermite polynomials known as physical which are not relevant with this work.

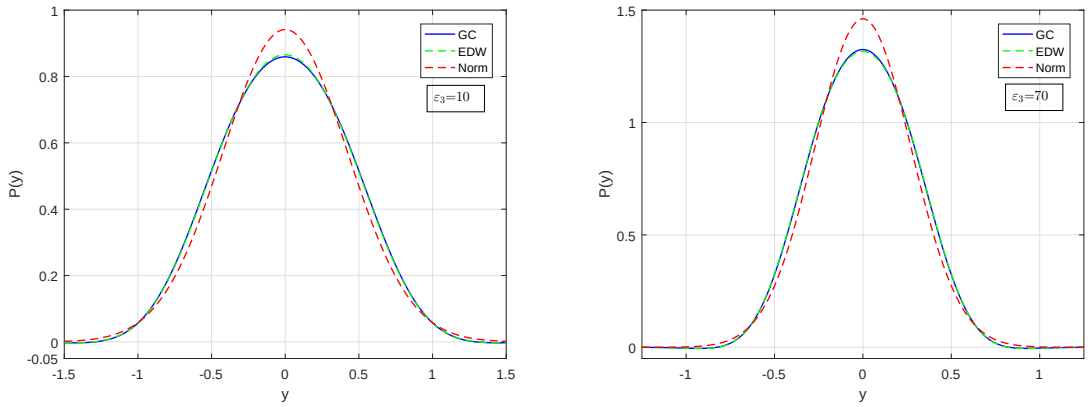

(a) $\varepsilon_3 = 10$ (b) $\varepsilon_3 = 70$

Fig. 3.1 The probability distribution of the response given by the Gram-Charlier and Edgeworth series approximation compared to the Normal distribution.

3.3 An alternative to Equivalent Linearisation: The single-pole fit method (SPF)

In this section an analytical representation for the first Wiener kernel is presented for systems such as in Eq.(2.23). The nonlinear force in the system can be expressed by its Wiener series

$$z = y^3 \rightarrow z = \sum_n z_n \tag{3.12}$$

where z_n is the n^{th} order functional. Hence,

$$z_1(t) = \int_{-\infty}^{\infty} k_{1,z}(t-\tau)\,\xi(\tau)\,d\tau \quad \rightarrow \quad Z_1(\omega) = K_{1,z}(\omega)\Xi(\omega) \tag{3.13}$$

with $K_{1,z}(\omega) = E\left[Y^3(\omega)\Xi(\omega)\right]$ being the first Wiener kernel of the nonlinear force $Z(\omega)$. Also, for notation purposes the first Wiener kernel of the system is now $K_{1,y}(\omega)$ such that

$$y_1(t) = \int_{-\infty}^{\infty} k_{1,y}(t-\tau)\,\xi(\tau)\,d\tau \quad \rightarrow \quad Y_1(\omega) = K_{1,y}(\omega)\Xi(\omega). \tag{3.14}$$

EL suggests that in Eq.(3.8), $P(\omega) = 0$. From this, it follows that the transfer function $G(\omega)$ between the first kernel of the nonlinear force ($K_{1,z}(\omega)$) and the system's response ($K_{1,y}(\omega)$) is $3\sigma_y^2$. However, for a nonlinear system this statement is not true. On the contrary

$$G(\omega) = \frac{Z_1(\omega)}{Y_1(\omega)} = \frac{K_{1,z}(\omega)}{K_{1,y}(\omega)} = 3\sigma_y^2 + P(\omega) \neq 3\sigma_y^2, \;\; P(\omega) \neq 0. \tag{3.15}$$

Before any recommendations are made on what $P(\omega)$ should look like an introduction to Mittag-Leffler's theorem (M-L) [13][4][5] is necessary. M-L states that any complex meromorphic[2] function $f(w)$ of real variable w which can be expressed as the ratio between two holomorphic[3] functions (i.e. $g(w)$ and $h(w)$) can also be expressed by the sum of its poles

$$f(w) = \frac{g(w)}{h(w)} = \sum_i \frac{a_i}{w - k_i}. \tag{3.16}$$

Using the M-L theorem and the fact that the function in Eq.(3.15) can be expressed as the ratio of the first Wiener kernels of the nonlinear force and the response both of which are holomorphic functions, it is attempted to fit in this complex function $G(\omega)$ a single-pole function corresponding to the first term of its M-L expansion. In addition, the conjugate pole is added to constrain the new function of being purely real in the time domain hence physical. This requires $G^*(\omega) = G(-\omega)$ also known as the reality condition.

Hence, the final form suggested for the function $G(\omega)$ is

$$\begin{aligned} G(\omega) = \frac{K_{1,z}(\omega)}{K_{1,y}(\omega)} &= \frac{\alpha}{(-\omega - \omega_p) + i\gamma} + \frac{\alpha}{(\omega - \omega_p) - i\gamma} + 3\sigma_y^2 \\ &= \frac{-2\alpha\omega_p}{-\omega^2 + \omega_p^2 + \gamma^2 + 2i\gamma\omega} + 3\sigma_y^2 \end{aligned} \tag{3.17}$$

with γ, α and ω_p being parameters to be found. Then, the EoM from Eq.(2.3) with a general nonlinear stiffness term can be obtained in the frequency domain where $Z_1(\omega)$ is the contribution of the first Wiener kernel of the nonlinear force

$$\begin{aligned} \left(-\omega^2 + 2i\beta\omega + 1\right) Y_1(\omega) + \varepsilon_3 Z_1(\omega) &= \Xi(\omega) \\ \left(-\omega^2 + 2i\beta\omega + 1 + \varepsilon_3 \frac{Z_1(\omega)}{Y_1(\omega)}\right) Y_1(\omega) &= \Xi(\omega). \end{aligned} \tag{3.18}$$

The first Wiener kernel of the response can be calculated so that

$$K_{1,y}(\omega) = \frac{Y_1(\omega)}{\Xi(\omega)} = \left(-\omega^2 + 2i\beta\omega + 1 + \varepsilon_3 \frac{Z_1(\omega)}{Y_1(\omega)}\right)^{-1}. \tag{3.19}$$

[2] A single-valued analytic function except on a subset of its domain where isolated poles exist. Such functions can be expressed as the ratio between two holomorphic functions.

[3] Complex-valued functions which are analytic in the whole domain.

Finally, the ratio $G(\omega) = \frac{Z_1(\omega)}{Y_1(\omega)}$ from Eq.(3.17) can be substituted in the expression above to give the analytic expression for $K_1(\omega)$

$$K_1(\omega) = K_{1,y}(\omega) = \frac{1}{-\omega^2 + 2i\beta\omega + 1 + \varepsilon_3 G(\omega)} \tag{3.20}$$

where $G(\omega)$ has the form given in Eq.(3.17).

3.3.1 SDOF application

3.3.1.1 Nonlinear stiffness

The single-pole (SP) model described above is to be applied on the SDOF system with equation of motion as in Eq.(2.3) but with a more general nonlinear stiffness term

$$\ddot{y} + 2\beta\dot{y}(1 + c_3\dot{y}^2) + y(1 + \varepsilon_3 y^n) = \xi(t) \tag{3.21}$$

where n is an even integer greater than two ($n \geq 2$). For a system with $\beta = 0.15$, $c_3 = 0$, $n = 2$ (i.e. cubic nonlinear stiffness) and $\varepsilon_3 = 10$ and with the SP parameters in Eq.(3.17) chosen such that $\alpha = -0.13$, $\omega_p = 2.55$ and $\gamma = 1.00$. At this stage the parameters are chosen empirically to fit the targeted function and consequently the first Wiener kernel. To improve accuracy, the SP parameters can be obtained by optimisation techniques, but this is not of an important interest in this project. The main goal here is to show that the SP is a good fit and the ideal way for getting these parameters would have been through an analytical method relating the SP parameters to the system's parameters. Some preliminary work on this task is shown later in section 3.4.

Back to the results, it can be seen from Fig.3.2a that the function $G(\omega)$ can be efficiently described by the single pole model, unlike the EL which incorrectly suggests a constant value at $3\sigma_y^2$ for $G(\omega)$. In Fig.3.2b the matching of the first kernel by the SP model after it is substituted in Eq.(3.20) is illustrated and compared along with the equivalent EL graph. As expected, the SP model matches the first kernel from the simulated data. This is because the step in Eq.(3.20) is deterministic which implies that as long as the fit for $G(\omega)$ is accurate the first kernel has to be accurate too.

Systems of higher power nonlinearity are also tested to check the consistency and robustness of the SP model. For the next example which is again based on the system from Eq.(2.3) with $n = 4$ (i.e. quintic nonlinear stiffness) so that the equation of motion is,

$$\ddot{y} + 2\beta\dot{y} + y + \varepsilon_5 y^5 = \xi(t) \tag{3.22}$$

with the nonlinear coefficient in this case being $\varepsilon_5 = 70$. The single pole parameters referring to Eq.(3.17) for this case are chosen to be $\alpha = -0.11$, $\omega_p = 3.60$ and $\gamma = 2.30$. The accuracy and agreement of the single pole model describing the first Wiener kernel is again very apparent. This is visualized in Fig.3.3.

The results look accurate and robust. Consequently, one would ask the question: Why the single-pole? What is the physical explanation for it? As it has already been seen, the SPF provides the damping characteristic required to capture the true shape of the first Wiener kernel unlike the EL. The source of this damping relies on the nature of the TF between the first kernel of the nonlinear force and that of the system intoduced above as $G(\omega)$. This function is therefore required to have a positive not constant imaginary part. Consequently, the Hilbert transform[4] of this requires the real part not to be constant contrary to EL. This is required by the Kramers–Kronig relations[36][17] which connect the real and imaginary parts of any complex analytic function in the upper half-plane. More specifically, the Kramers–Kronig relations state that, "the real part can be obtained from the imaginary part -or vice versa- of response functions in physical systems, because for stable systems, causality[5] implies the analyticity condition, and conversely, analyticity implies causality of the corresponding stable physical system.", [69]. The SP complies with all these conditions making it a good fit for function $G(\omega)$. A final note would be the extend to which additional poles from higher order terms of the M-L expansion can improve the accuracy of the results. Theoretically these additional terms, if they exist, can improve the fit. However, this will bring in additional complexity to the problem since three parameters will need to be introduced and estimated for each additional pole. The agreement in the results for these specific cases is satisfactory enough and therefore no attempt is to be made in bring in additional terms from the M-L expansion at this moment.

[4]The Hilbert transform is a linear operator described by an improper integral which takes a function, $f(x)$ of a real variable and produces another function of a real variable $g(y)$, [22]. The transform is defined by the integral, $g(y) = \mathscr{H}[f(x)] = \frac{1}{\pi} PV \int_{-\infty}^{\infty} \frac{f(x)}{x-y} dx$ where PV is Cauchy's principal value.

[5]A system is said to be causal if its output depends only on current and previous input values.

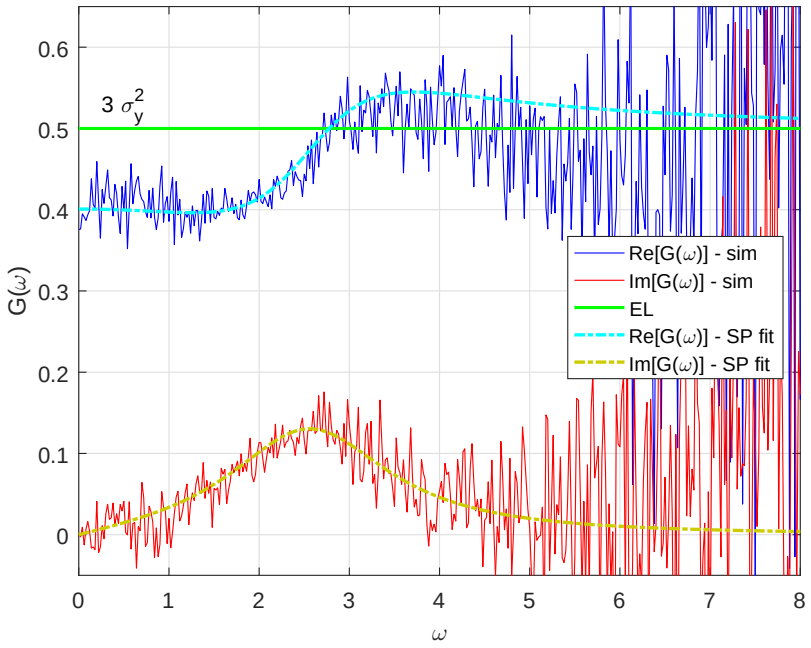

(a) $G(\omega)$

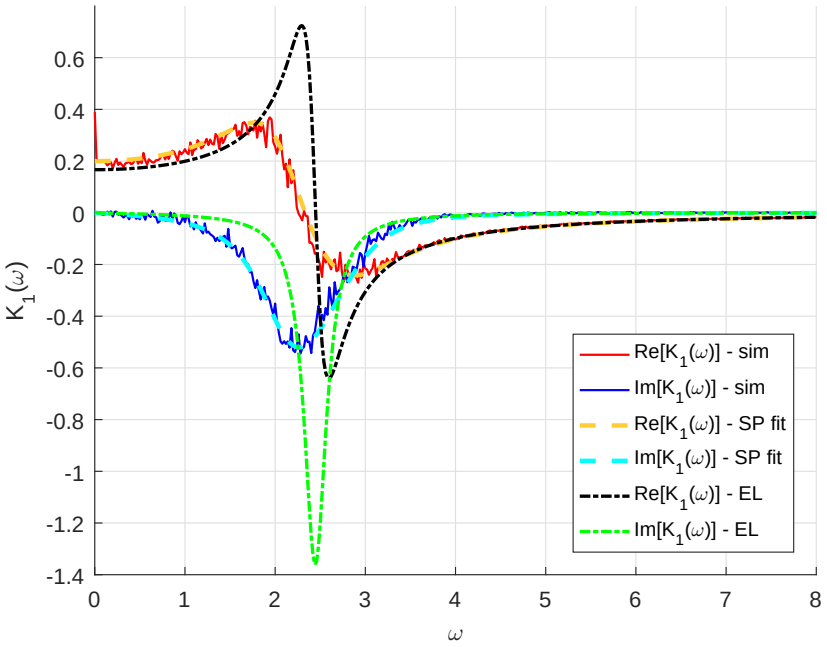

(b) $K_1(\omega)$

Fig. 3.2 Example of the SPF application to a system with cubic nonlinearity and nonlinear constant $\varepsilon_3 = 10$.

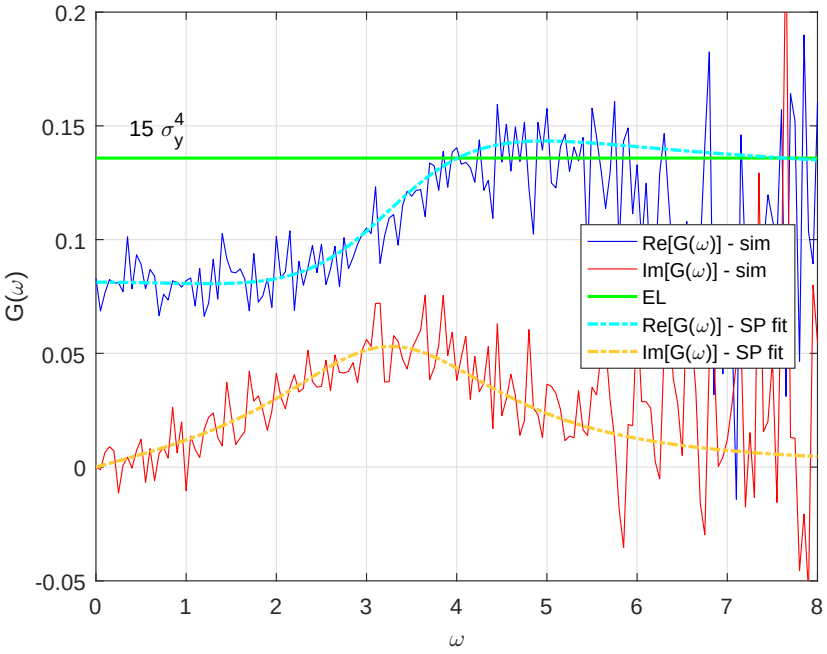

(a) $G(\omega)$

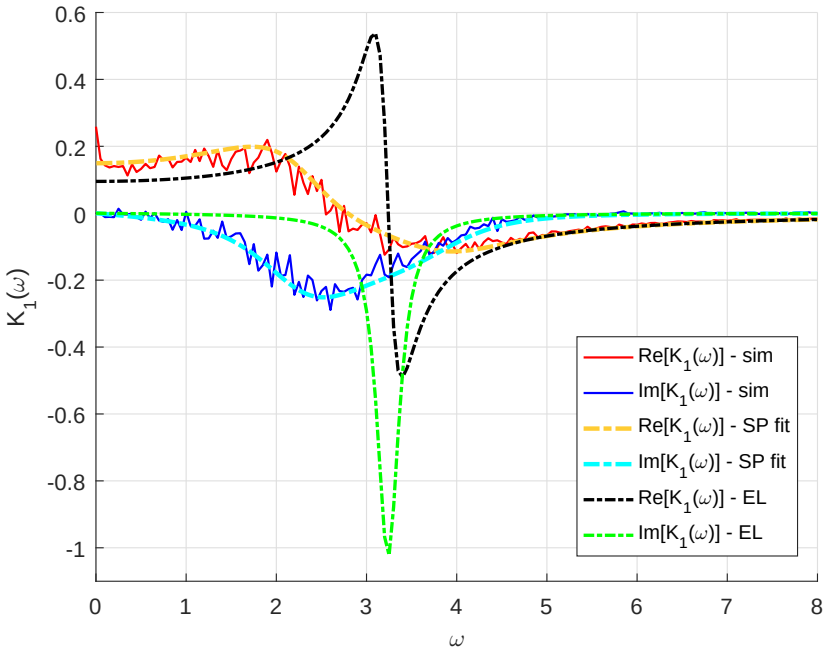

(b) $K_1(\omega)$

Fig. 3.3 Example of the SPF application to a system with quintic (x^5) nonlinearity and nonlinear constant $\varepsilon_5 = 70$.

3.3.1.2 Nonlinear stiffness and nonlinear damping

In the previous section, the application of the SPF method was demonstrated on a system whose nonlinearity is purely stiffening. Here, the SPF is to be tested on a system with both nonlinear stiffness and nonlinear damping. Such a system is described by Eq.(3.21). A version of that system is to be used in this section where the stiffening nonlinearity is cubic as well as the damping nonlinearity and where $\varepsilon_2 \neq 0$ and $\varepsilon_3 \neq 0$,

$$\ddot{y} + 2\beta\dot{y}(1 + \varepsilon_2\dot{y}^2) + y(1 + \varepsilon_3 y^2) = \xi(t). \tag{3.23}$$

The equivalent linear version of the above system is,

$$\ddot{y} + 2\beta\dot{y}(1 + 3\sigma_{\dot{y}}^2\varepsilon_2) + y(1 + 3\sigma_y^2\varepsilon_3) = \xi(t) \tag{3.24}$$

The question that arises next is how to apply to SPF method in this system. It has already been demonstrated how the nonlinear stiffness adds damping to the system and how the SPF models this. How is the additional nonlinear damping is to be considered when applying the SPF?

In chapter 2, it was shown that EL works very well for nonlinear damping as demonstrated in Fig.2.9. Based on this, the first step will be to calculate the equivalent linear damping of the system demonstrated in section 2.4.2 resulting into a nonlinear system with only stiffening nonlinearity,

$$\ddot{y} + 2\beta\dot{y}(1 + 3\sigma_{\dot{y}}^2\varepsilon_2) + y(1 + \varepsilon_3 y^2) = \xi(t) \tag{3.25}$$

This system is identical to the system in Eq.(3.21) and the SPF method can be applied as in the previous section.

Before applying the SPF, the RMS value predicted by EL in the case of the systems described by Eq.(3.24) and Eq.(3.25) is calculated for various values of nonlinear damping. For the reason explained above, the RMS values of the system with linearised damping are calculated first. These are illustrated in Fig.3.4 and Fig.3.5 for velocity and displacement respectively. In each case the RMS value of the linearised system is compared with the simulation results of the original system with linear damping coefficient $\beta = 0.15$ and nonlinear stiffness coefficient $\varepsilon_3 = 20$. EL seems to be consistently accurate in predicting the velocity and displacement RMS of the system as shown earlier in chapter 2 since, the three plots in both figures are very close to each other.

The SPF method requires the calculation of the TF between first Wiener kernel of the nonlinear force and the first Wiener kernel of the response of the system in Eq.(3.23). This is illustrated in Fig.3.6a where the expected non-constant complex function is shown together

the SPF calculation. The parameters used for the fitting function are given in Table C3 in Appendix C. Finally, the prediction of the SPF method for the first Wiener kernel of the original system is calculated and shown in Fig.3.6b where it is compared with the first Wiener kernel from the simulations of the original system and that suggested by EL. It is obvious from the figure that the SPF works very well once more outperforming EL.

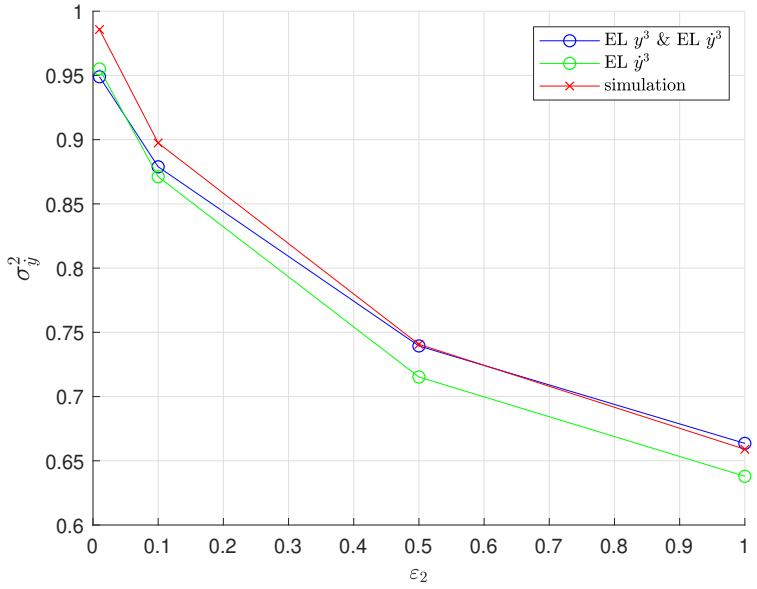

Fig. 3.4 The velocity RMS value versus the damping nonlinearity. For all three plots the linear stiffness is $\varepsilon_3 = 20$. i) The values from the Monte-Carlo simulations (red) ii) The values of the system with linearised damping only (green) iii) The values of the system with linearised damping and linearised stiffness.

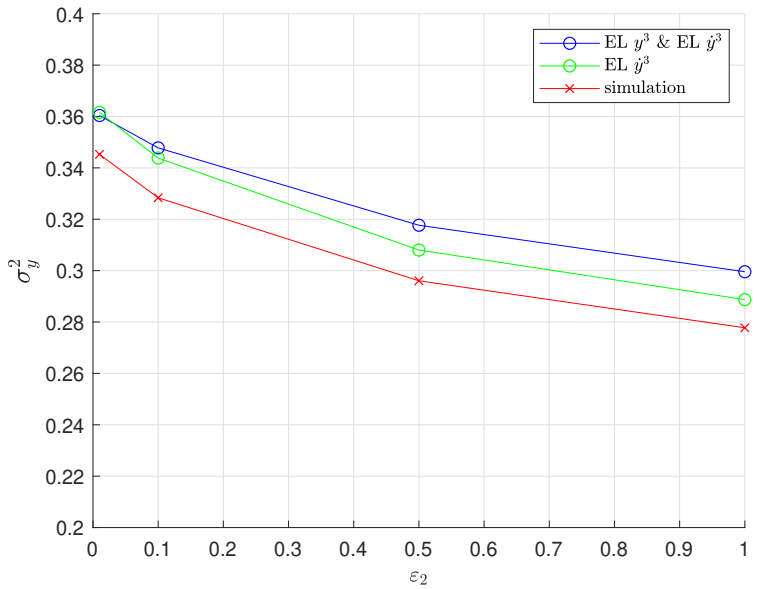

Fig. 3.5 The displacement RMS value versus the damping nonlinearity. For all three plots the linear stiffness is $\varepsilon_3 = 20$. i) The values from the Monte-Carlo simulations (red) ii) The values of the system with linearised damping only (green) iii) The values of the system with linearised damping and linearised stiffness.

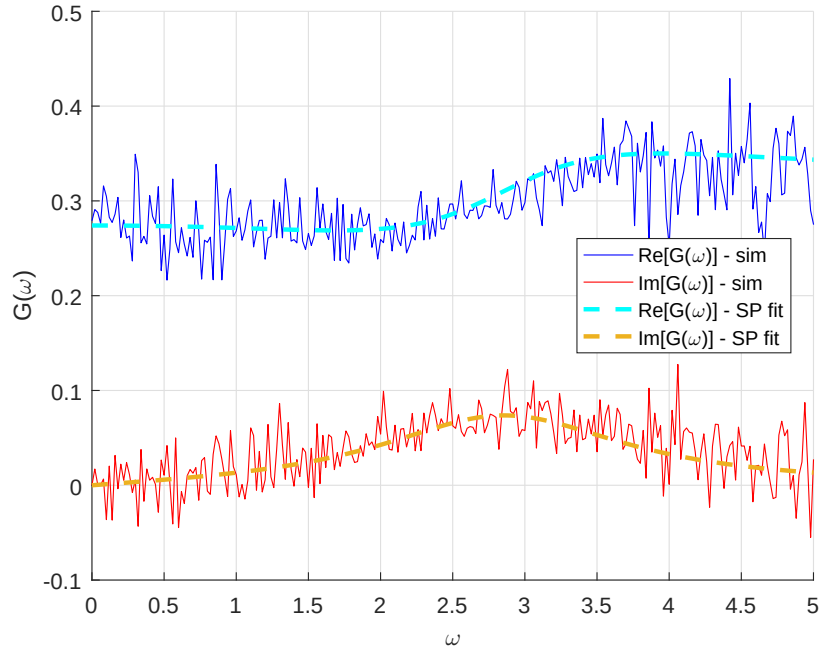

(a) $G(\omega)$

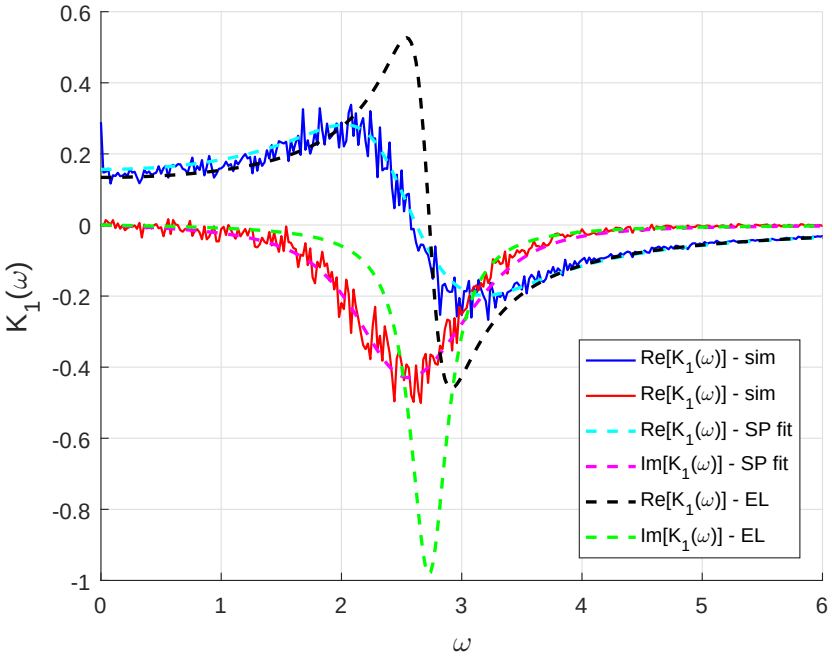

(b) $K_1(\omega)$

Fig. 3.6 Example of the SPF application to a system with cubic nonlinear stiffness and cubic nonlinear damping. The nonlinear constants are $\varepsilon_3 = 20$ and $\varepsilon_2 = 0.1$ for stiffness and damping respectively.

3.4 SPF parameters dependence on nonlinearity

Having developed the SPF method, a natural next step is to investigate the pole parameters involved. Due to time limitations and the decision to focus on other aspects of the project this part has not been explored in depth despite some initial investigations. These investigations mainly concentrated on finding correlations between the SPF parameters and the system parameters and checked whether any relationships such as power laws were present between them .

No general relationship was discovered, but in this section an example of this investigation showing how the SPF parameters depend on the nonlinearity coefficient is presented. In Fig.3.7 the three SPF parameter values are plotted against the nonlinear coefficient for seven different values cases each indicated by a cross. Note that for scaling purposes the plot for the α parameter is scaled by a factor of -30.

From this figure however, not much can be said about the way the parameters depend on the nonlinearity apart from the fact that all three parameters increase in a uniform manner with increasing nonlinearity. This was expected in the case of the ω_p which is related to the natural frequency of the pole -and the first kernel- since frequency increases with increasing nonlinearity. This trend was also expected in the case of the γ which governs the damping in the system. For increasing nonlinearity the effective damping increases, widening the first kernel, as a result the value of γ should also increase. The role of α is to adjust the amplitude of the pole and the trend it should follow is less obvious than the other two parameters.

A more useful way to study these relationships is plotting the parameters against the natural logarithm of the nonlinear coefficient as illustrated in Fig.3.8. The dotted lines are the best-fit lines for each parameter. The effectiveness of the best-fit lines may suggest some sort of power law between the parameters and the logarithmic nonlinearity. The quantification of this power law which involves expressing the best-fit lines in terms of the systems parameters is not straight forward and further research outside the scope of this thesis needs to be carried out.

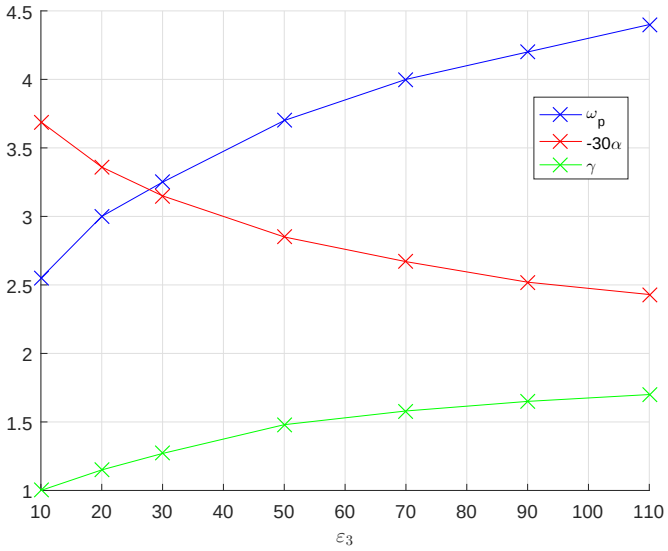

Fig. 3.7 Nonlinear versus SPF parameters.

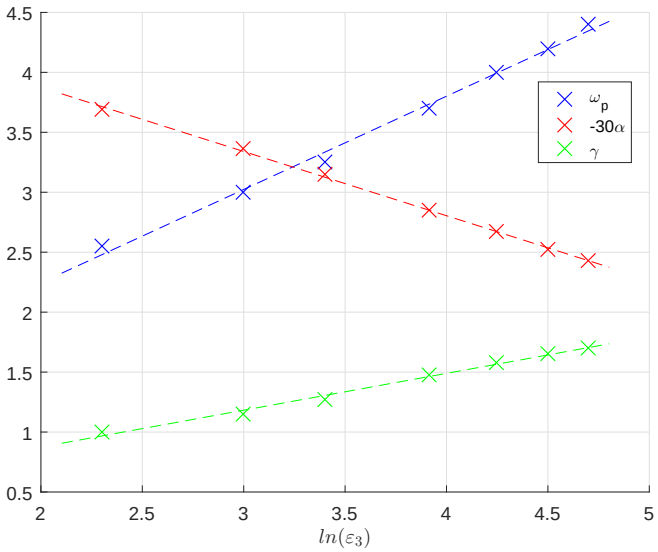

Fig. 3.8 Logarithmic nonlinear coefficient versus SPF parameters.

3.5 Conclusion

From the characteristic function representation of a distribution it is known that all cumulants of order 3 or higher are required to be zero for the Gaussian distribution. EL assumes that the nonlinear stiffening force is characterised by Gaussian dynamics. This is not the case since, the first Wiener kernel of the nonlinear force has a non-zero fourth cumulant explaining the failure of EL to capture the true shape of the first Wiener kernel.

The cumulant approach for the first kernel of the nonlinear force resulted in an expression (Eq.(3.8)) for a TF relating the first Wiener kernel of the nonlinear force to the first Wiener kernel of the response by a non-constant function $G(\omega)$. This is contrary to the constant value of $3\sigma_y^2$ suggested by EL. What this function suggests is some sort of phase shifting behaviour in the system since, it no longer has a zero imaginary part. Therefore, if we could quantify this new function in the right way, it should result in an accurate representation of the first Wiener kernel of the system.

After a simple rearrangement of the original EoM in the frequency domain, it was shown that this function $G(\omega)$ is the TF between the first Wiener kernel of the nonlinear force and the first Wiener kernel of the original system response (Eq.3.15). Observing this TF, it was thought that the prospect of a SP function could provide a good fit for it due to the M-L expansion. The parameter for the SPF were chosen manually to follow the trend in the TF, resulting in a very accurate agreement with the first Wiener kernel of the system (Fig.3.2). The robustness of this new method was demonstrated for higher powers of the nonlinear force.

Looking at the physics behind the suitability of this specific function, it has already been mentioned that it would require a positive non-constant imaginary part in order to comply with the additional damping to the system. Following this, it should also have a non-constant real part to satisfy the Kramers-Kronig relations. Both of these requirements hold for this specific function.

The application of the SPF method on a system with both nonlinear damping and nonlinear stiffness was demonstrated. To make this system firstly linearise the nonlinear damping term since it was already shown that EL works perfectly with nonlinear damping. This will result in a system with only nonlinear stiffness. At this point, the semi-linearised system can be treated as the one above over which the SPF was shown to be an accurate method for predicting its first Wiener kernel.

A drawback of the SPF method is the fact that the parameters of the fitting function are found empirically. Further work to investigate this in order to calculate these parameters analytically based on the system's known parameters such as the damping and stiffening

coefficients as well as the white-noise intensity can be performed but this is something not investigated in this thesis.

Chapter 4

Extending the SPF method to 2DOF

4.1 Introduction

Figures 3.2b and 3.3b illustrate how much better the SPF method introduced in the previous chapter performs compared to EL for a cubic and a quintic nonlinear force respectively. The idea of SPF emerged after a proof that indicated the inaccuracy of EL in assuming Gaussian dynamics for the nonlinear force.

The SPF method demonstrated in the previous chapter is a novel way to improve EL. As with any new methodology, it is important to check its robustness and range of application. Thus, its performance over a 2DOF system like the one shown in Fig.4.1 with random base excitation is to be tested in this chapter.

More specifically, the effectiveness of EL to calculate the RMS value of the response will be investigated once more. As it will be demonstrated in the next section, the RMS value cannot be directly calculated for the equivalent linear system, therefore, a recursive method is used to do that.

In addition, the efficiency of the SPF is to be investigated and various amendments to the the methodology are to be suggested and implemented in order to improve its accuracy.

4.2 Constructing and formulating the 2DOF system

The 2DOF system which is illustrated in Fig.4.1 is represented by the generalised equation of motion,

$$\mathbf{M}\ddot{\mathbf{y}} + \mathbf{C}\dot{\mathbf{y}} + \mathbf{K}\mathbf{y} + \mathbf{f}_{nl}(\mathbf{y}) = \boldsymbol{\xi} \tag{4.1}$$

with white noise base excitation $\xi(t)$ where $\mathbf{M}$, $\mathbf{C}$ and $\mathbf{K}$ are all 2×2 matrices corresponding to the mass, linear damping and linear stiffness elements in the system. Explicitly these

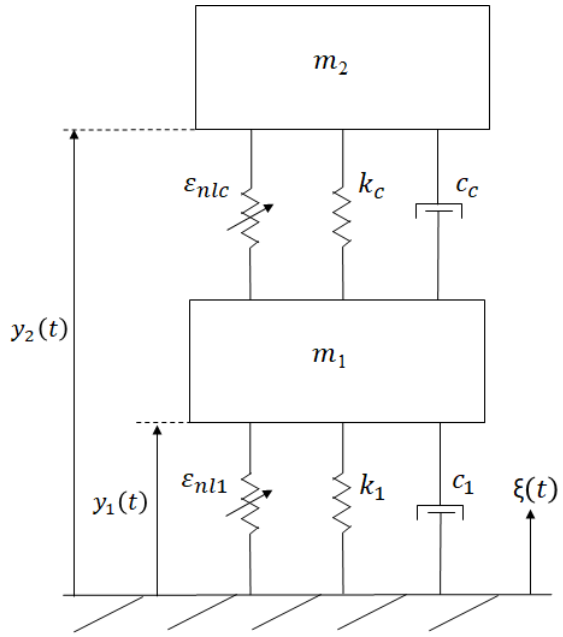

Fig. 4.1 Generalised diagram of the 2DOF system with base motion, $\xi(t)$.

vectors and matrices are,

$$\mathbf{y} = \begin{pmatrix} y_1(t) \\ y_2(t) \end{pmatrix} \tag{4.2}$$

$$\boldsymbol{\xi} = \begin{pmatrix} m_1 \\ m_2 \end{pmatrix} \xi(t) \tag{4.3}$$

$$\mathbf{M} = \begin{pmatrix} m_1 & 0 \\ 0 & m_2 \end{pmatrix} \tag{4.4}$$

$$\mathbf{C} = \begin{pmatrix} c_1 + c_c & -c_c \\ -c_c & c_c \end{pmatrix} \tag{4.5}$$

$$\mathbf{K} = \begin{pmatrix} k_1 + k_c & -k_c \\ -k_c & k_c \end{pmatrix}. \tag{4.6}$$

$f_{nl}(\mathbf{y})$ is vector containing the nonlinear stiffness. Two different system cases based on two different forms of this vector are implemented and discussed in this chapter. As it can be seen from Fig.4.1, one of the cases investigates the response of the masses when only the nonlinear spring between the first mass and the base is present -together with all the other linear elements- while the second case investigates the response of the system when only the nonlinear spring coupling the two masses is present.

Comparisons between the first Wiener kernel and EL are to be performed just like in the previous chapter. The linearised system will now have the form,

$$\mathbf{M}\ddot{\boldsymbol{y}} + \mathbf{C}\dot{\boldsymbol{y}} + \mathbf{K}_{EL}\boldsymbol{y} = \boldsymbol{\xi} \tag{4.7}$$

where the matrix $\mathbf{K}_{EL}$ containing the equivalent linearised stiffness force has to be found in each case.

In both cases of the 2DOF system that follow, the first Wiener kernel of the joined response defined by the $y_T = y_1 + y_2$ variable is considered. In this way the overall energy in the system is contemplated. To show this let,

$$y_T(t) = y_1(t) + y_2(t) \quad \rightarrow \quad Y_T(\omega) = Y_1(\omega) + Y_2(\omega). \tag{4.8}$$

Multiplying both sides by the excitation $\Xi(\omega)$ and getting the expected value, leads to,

$$\begin{aligned} E\left[Y_T(\omega)\Xi(\omega)\right] &= E\left[\left(Y_1(\omega) + Y_2(\omega)\right)\Xi(\omega)\right] \\ \therefore E\left[Y_T(\omega)\Xi(\omega)\right] &= E\left[Y_1(\omega)\Xi(\omega)\right] + E\left[Y_2(\omega)\Xi(\omega)\right]. \end{aligned} \tag{4.9}$$

The above expression can be written in terms of the first Wiener kernel of each term such as,

$$K_{1,y_T}(\omega) = K_{1,y_1}(\omega) + K_{1,y_2}(\omega). \tag{4.10}$$

From the property of the first Wiener kernel also discussed in section 2.6 that the power input is only dependent on the first kernel, $K_{1,y_T}(\omega)$ is equal to the sum on the energy input of the individual masses which is equal to the total energy input in the system. The individual first Wiener kernels of the two masses could have been studied individually in isolation, but for the purposes of this project only the first Wiener kernel of the total response was studied for simplicity and convenience.

Finally, for validation purposes the modal natural frequencies for the linear cases in the examples that follow can be calculated. In both example cases the masses are equal ($m_1 = m_2 = m$) as well as the linear stiffness coefficients ($k_1 = k_c = k$). Therefore, the two modal frequencies can be calculated using the simplified result,

$$\omega_1^2, \omega_2^2 = \frac{1}{2}\frac{k}{m}(3 \mp \sqrt{5}). \tag{4.11}$$

The full analysis of this can be found in chapter 3 of [49].

4.3 Case 1: Nonlinear spring between base and mass

The first case under investigation involves all linear elements in the system as shown in 4.1 as well as the nonlinear spring between the base and the first mass such that $\varepsilon_{nl1} \neq 0$ and $\varepsilon_{nlc} = 0$. The vector describing the nonlinear forces is now given by,

$$\mathbf{f}_{nl}(\mathbf{y}) = \begin{bmatrix} \varepsilon_{nl1} y_1^3 \\ 0 \end{bmatrix}. \tag{4.12}$$

The nonlinear force is a function of the response of the first mass, y_1, hence, the RMS value of this quantity to be used in EL is defined as $\sigma_{y_1}^2$. Consequently, the stiffness matrix of the equivalent linear stiffness is now,

$$\mathbf{K}_{EL} = \begin{pmatrix} k_1 + k_c + 3\varepsilon_{nl1}\sigma_{y_1}^2 & -k_c \\ -k_c & k_c \end{pmatrix}. \tag{4.13}$$

The values of the linear elements used for this case are $k_1 = k_c = 1$, $c_1 = c_c = 0.15$ and $m_1 = m_2 = 1$.

4.3.1 Case 1: EL performance

One of the main comparisons between EL and the actual system for the SDOF case in Chapter 3 was that of the RMS of the response. The same comparison will be performed for both cases of the 2DOF system. In these cases, the calculation of the RMS value of EL is performed by a recursive method for minimising the error, E_r, of the RMS. An algorithmic expression of this is given below where the initial condition (I.C.) for the RMS value has to

be positive.

$$\min_{\sigma^2_{y_1}} \quad E_r = |\sigma^2_{y_1,n} - \sigma^2_{y_1,n-1}| \tag{4.14}$$

I.C. $\quad \sigma_{y_1,0} > 0 \quad \text{and} \quad n = 0$

while $\quad E_r \neq 0$

$$1)\ \mathbf{A}(\omega, \sigma^2_{y_1,n-1}) = -\omega^2\mathbf{M} + i\omega\mathbf{C} + \mathbf{K}_{EL}$$

$$\begin{pmatrix} y_{1,n} \\ y_{2,n} \end{pmatrix} = \mathbf{A}^{-1}(\omega, \sigma^2_{y_1,n-1})\boldsymbol{\xi} = \mathbf{A}^{-1}(\omega, \sigma^2_{y_1,n-1}) \begin{pmatrix} 1 \\ 1 \end{pmatrix} \xi(t)$$

$$y_{1,n} = \left(\mathbf{A}^{-1}(\omega, \sigma^2_{y_1,n-1})_{11} + \mathbf{A}^{-1}(\omega, \sigma^2_{y_1,n-1})_{12}\right) \xi(t) = \mathbf{J}_{y_{1,n}} \xi(t)$$

$$2)\ S_{y_{1,n}} = |\mathbf{J}_{y_{1,n}}|^2 S_{\xi\xi} = |\mathbf{J}_{y_{1,n}}|^2 S_0$$

$$\Rightarrow \sigma^2_{y_{1,n}} = \int S_{y_{1,n}}(\omega)\mathrm{d}\omega = 2S_0 \int (|\mathbf{J}_{y_{1,n}}|^2)\mathrm{d}\omega$$

$$3)\ E_r = |\sigma^2_{y_1,n} - \sigma^2_{y_1,n-1}|$$

$$4)\ n = n + 1.$$

Note that the nonlinear spring is only affected by the response of the first mass, y_1. Hence, when performing EL the nonlinear force is replaced by a term involving σ_{y1} which is to be compared with the analogous RMS value from the simulations. This comparison is illustrated in Fig.4.2. Just like in the SDOF system EL performs well in capturing the RMS value of the system as the close matching of the two plots suggests.

However, once again EL fails to capture the true shape of first Wiener kernel of the system. In Fig.4.3 the real part of the first Wiener kernel for the two modes of the total velocity response, $K_{1,\dot{y}_1+\dot{y}_2}(\omega)$, both for the simulated system and that suggested by EL is plotted for different values of the nonlinear stiffness ε_{nl1}. The two modal frequencies of the linear system as suggested by Eq.(4.11) are $\omega_1^2, \omega_2^2 = \frac{1}{2}\frac{1}{1}(3 \mp \sqrt{5})$ resulting to $\omega_1 = 0.62$ and $\omega_2 = 1.62$. Mode 1 describes the in-phase motion between the two masses while mode 2 describes the out-of-phase motion. For low nonlinear stiffness (red line), EL fails to capture both of the modes.

As the nonlinear coefficient increases, the nonlinear spring becomes very stiff connecting the base with the first mass. As a result, it reduces the problem to effectively a SDOF system where the first mass becomes the new 'base' and the resonant frequencies of the two modes tend to their limits as suggested by the small difference between the black and cyan plots. In addition, the resonant frequency of the first mode for high nonlinearity tends to 1 agreeing with the theoretical prediction since, $\omega_1 = \frac{k_c}{m_2} = \frac{1}{1} = 1\text{rad/s}$. EL can capture the shape of

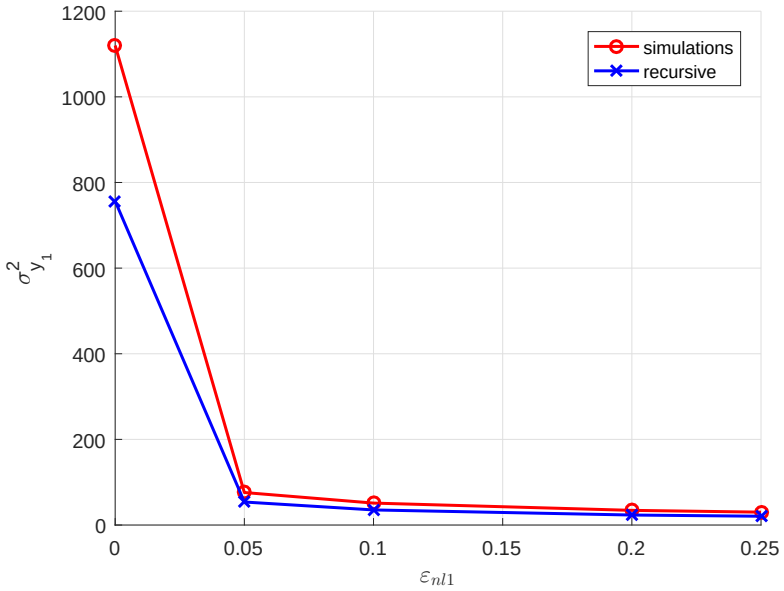

Fig. 4.2 Case 1: Comparison of the RMS of the nonlinear spring between the simulations and the recursive minimisation approach from Eq.4.14 for varying nonlinear stiffness ε_{nl1}.

mode 1 for high nonlinearities where the linear effect from the coupling spring is more dominant but fails to follow the trend in mode 2.

4.3.2 Case 1: Pole fitting

In Fig.4.3, the failure of EL to capture the true shape of the first Wiener kernel of the combined response of the two masses is illustrated. Naturally, at this point, the same question that was asked for the SDOF system in the previous section is to be asked. This is whether EL can be improved? Would the single-pole fitting method suggested and demonstrated in the previous section work for this 2DOF problem? To answer these question, the example case where the the nonlinear spring coefficient is equal to 0.1 ($\varepsilon_{nl1} = 0.1$) is to be used.

As illustrated in section 3.3 the first step to try this is to calculate the transfer function between the first Wiener kernel of the nonlinear force and that of the system's response as illustrated in Eq.(3.17). This new TF, $G(\omega)$ is plotted (blue and red lines) in Fig.4.4 along with the single-pole fit function (orange and cyan) whose parameters values are given in table C4. The resulting first Wiener kernel together with the SPF suggestion as well as the EL are compared in the right plot of Fig.4.4 while a cleared illustration of the results at the two modes is shown in Fig.4.5. From Fig.4.5, it is clear that for mode 2 (right plot) the SPF matches very well the real and imaginary parts of the first Wiener kernel outperforming

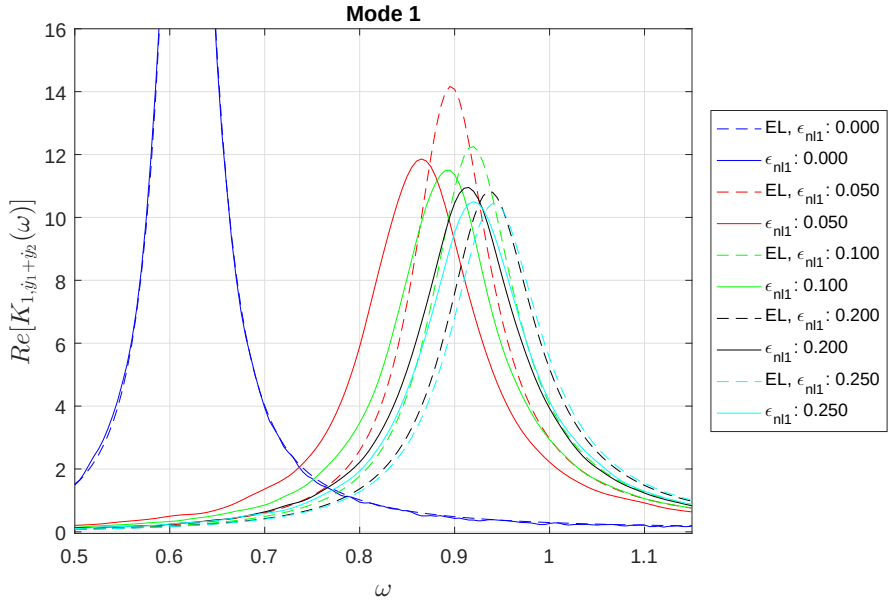

(a)

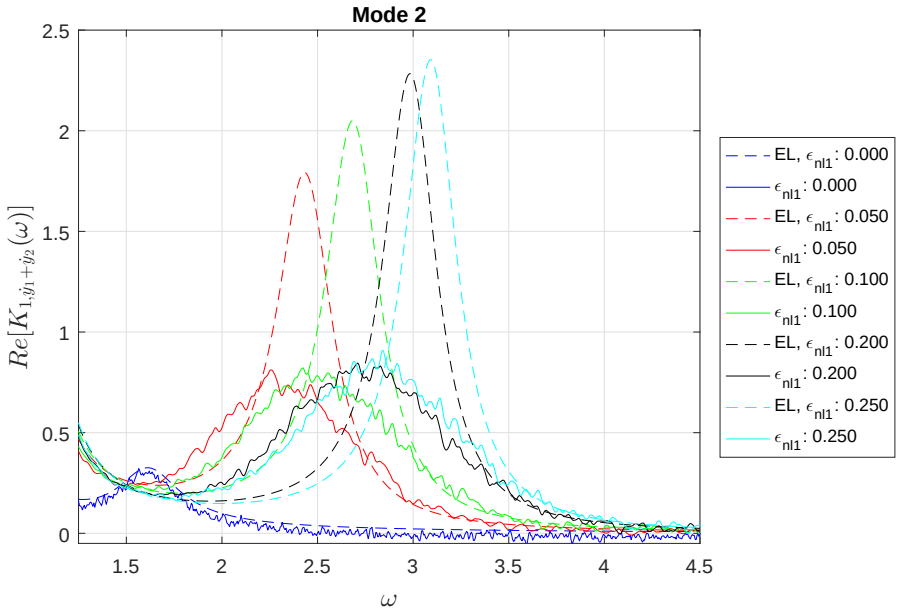

(b)

Fig. 4.3 Case 1: The comparison at the two modes of the first Wiener kernel of the combined response $(\dot{y}_1 + \dot{y}_2)$ of the two masses between EL and simulations for varying nonlinear stiffness ε_{nl1}.

EL. For the first mode (left plot) the SPF still does a much better job than EL but is not as accurate as in the second mode. Is there a way to improve this?

Going back to Fig.4.4 the SPF plot does follow the general trend of the transfer function but not the detailed skewed curved around the domain $1 \leq \omega \leq 2$. Can this be the reason for the disagreement between the two plots in the first mode? In order to check this, a second pole is added to the fitting model so that,

$$\begin{aligned} G(\omega) &= \frac{K_{1,z}(\omega)}{K_{1,y_T}(\omega)} \\ &= \frac{-2\alpha_1\omega_{p1}}{-\omega^2+\omega_{p1}^2+{\gamma_1}^2+2i\gamma_1\omega} + \frac{-2\alpha_2\omega_{p2}}{-\omega^2+\omega_{p2}^2+{\gamma_2}^2+2i\gamma_2\omega} + 3\sigma_{y_1}^2 \end{aligned} \tag{4.15}$$

The parameter values used in this new double-pole fit model presented in Fig.4.6 are given in table C5. As it can be seen in Fig.4.6 the double-pole fit function follows the transfer function calculated from the simulations much closer than the SPF. Furthermore, this extension of the fitting function has an additional improvement on predicting the first mode of the first Wiener kernel as shown in Fig.4.7 while keeping the accuracy of the second mode too.

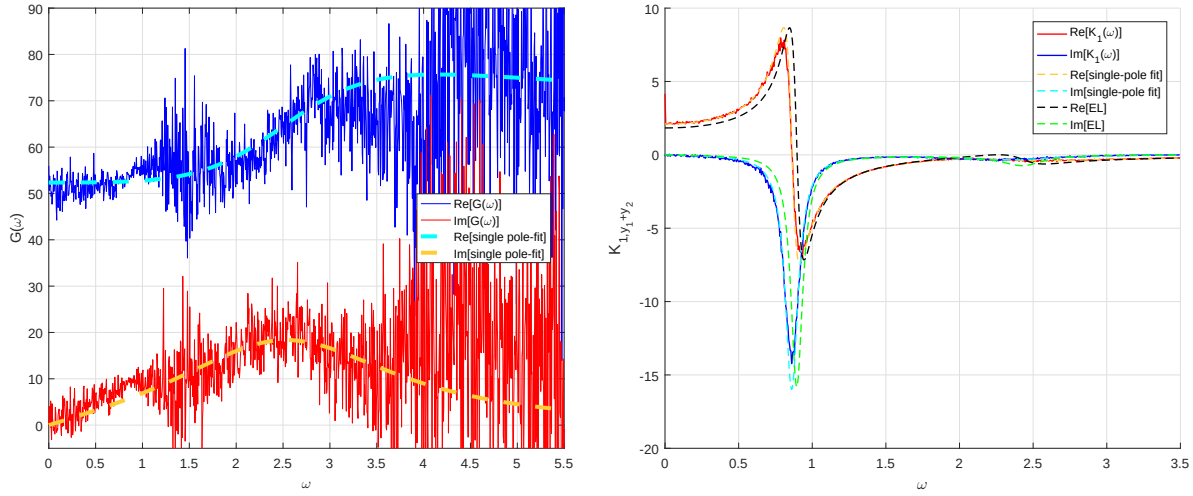

Fig. 4.4 Case 1: The TF between the first Wiener kernel between the nonlinear force and that of the system response along with the single-pole fit (left). The resulting first Wiener kernel of the joined velocity response from simulations, EL and the PF (right). Parameter values for this fitting function are given in table C4.

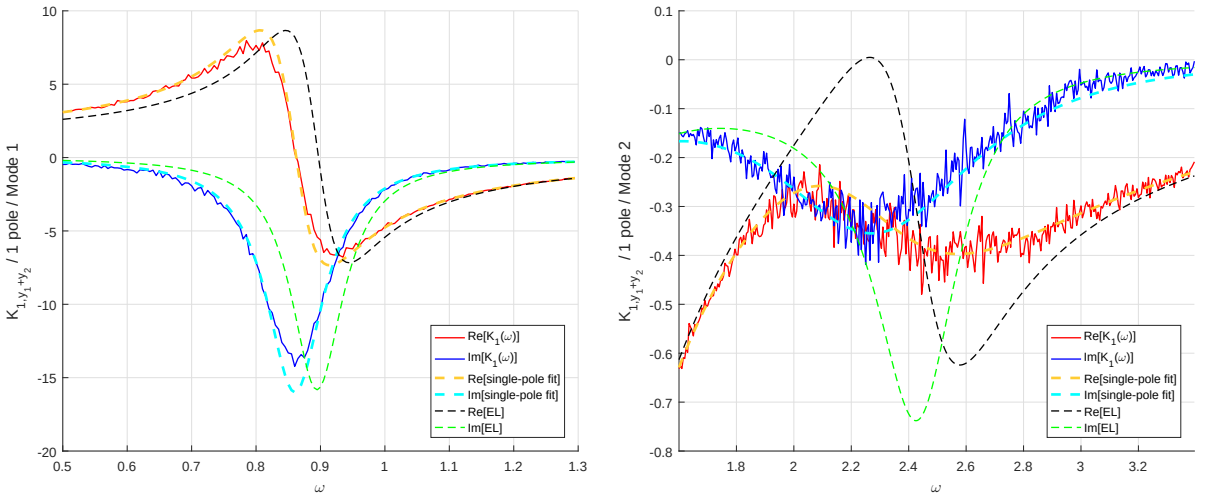

Fig. 4.5 Case 1: The two modes from the resulting first Wiener kernel of the joined response also shown in the figure above (Fig.4.4) on the right. Mode 1 is the in-phase mode between the two masses while Mode 2 is the out-of-phase mode. A single-pole fitting function is used.

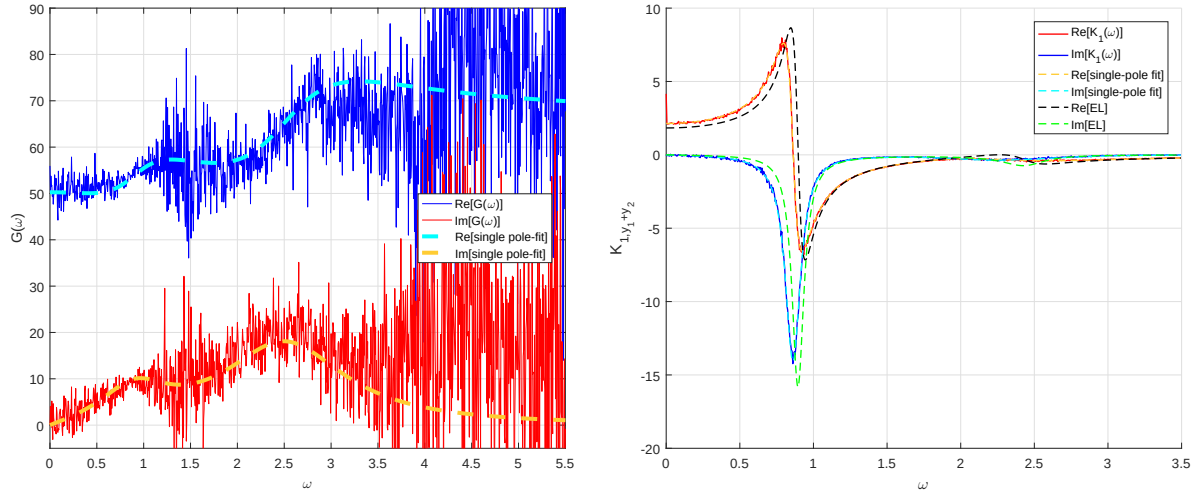

Fig. 4.6 Case 1: The TF between the first Wiener kernel between the nonlinear force and that of the system response along with the double-pole fit (left). The resulting first Wiener kernel of the joined velocity response from simulations, EL and the PF (right). Parameter values for this fitting function are given in table C5.

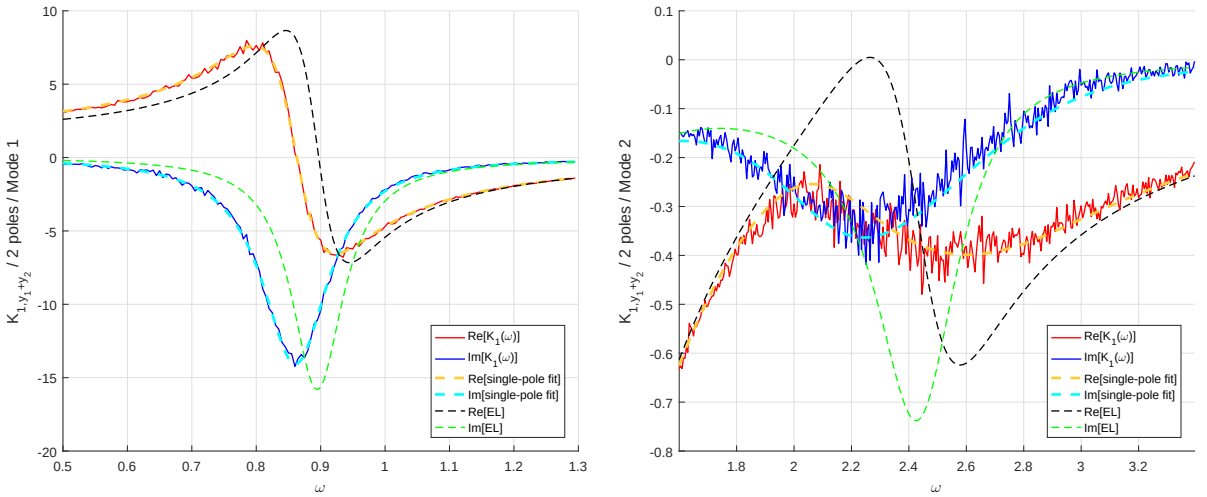

Fig. 4.7 Case 1: The two modes from the resulting first Wiener kernel of the joined response also shown in the figure above (Fig.4.6) on the right. Mode 1 is the in-phase mode between the two masses while Mode 2 is the out-of-phase mode. A double-pole fitting function is used.

4.4 Case 2: Nonlinear spring coupling the two masses

As mentioned in section 4.2 of this chapter, the second case of the 2DOF system to be investigated is having a nonlinear spring coupling the two masses such that $\varepsilon_{nlc} \neq 0$ and $\varepsilon_{nl1} = 0$. Hence, the vector describing the nonlinear forces is now given by,

$$\mathbf{f}_{nl}(\mathbf{y}) = \begin{bmatrix} -\varepsilon_{nlc}(y_2 - y_1)^3 \\ \varepsilon_{nlc}(y_2 - y_1)^3 \end{bmatrix} \tag{4.16}$$

The nonlinear force is a function of the difference of the response of the two masses $(y_2 - y_1)$ hence, the RMS value of this quantity to be used in EL is defined as $\sigma^2_{y_{21}}$. Consequently, the stiffness matrix of the equivalent linear stiffness is now,

$$\mathbf{K}_{EL} = \begin{pmatrix} k_1 + k_c + 3\varepsilon_{nlc}\sigma^2_{y_{21}} & -k_c - 3\varepsilon_{nlc}\sigma^2_{y_{21}} \\ -k_c - 3\varepsilon_{nlc}\sigma^2_{y_{21}} & k_c + 3\varepsilon_{nlc}\sigma^2_{y_{21}} \end{pmatrix} \tag{4.17}$$

Finally, the values of the linear elements used for this case are $k_1 = k_c = 7$, $c_1 = c_c = 0.05$ and $m_1 = m_2 = 1$.

4.4.1 Case 2: EL performance

Similarly to section 4.3.1, the RMS value to be included in the linear term substituting the nonlinear force in EL is found by a minimising procedure. An algorithmic expression of this recursive minimisation over the error of $\sigma_{y_{21}}$ is given below. It requires the initial condition

(I.C.) of the RMS value to be positive.

$$\min_{\sigma^2_{y_{21}}} \quad E_r = |\sigma^2_{y_{21},n} - \sigma^2_{y_{21},n-1}| \tag{4.18}$$

$$\text{I.C.} \quad \sigma_{y_{21},0} > 0 \quad \text{and} \quad n = 0$$

$$\text{while} \quad E_r \neq 0$$

$$1)\ \mathbf{A}(\omega, \sigma^2_{y_{21},n-1}) = -\omega^2\mathbf{M} + i\omega\mathbf{C} + \mathbf{K}_{EL}$$

$$\begin{pmatrix} y_{1,n} \\ y_{2,n} \end{pmatrix} = \mathbf{A}^{-1}(\omega, \sigma^2_{y_{21},n-1})\boldsymbol{\xi} = \mathbf{A}^{-1}(\omega, \sigma^2_{y_{21},n-1}) \begin{pmatrix} 1 \\ 1 \end{pmatrix} \xi(t)$$

$$\begin{aligned} y_{2,n} - y_{1,n} &= \left(\mathbf{A}^{-1}(\omega, \sigma^2_{y_1,n-1})_{22} + \mathbf{A}^{-1}(\omega, \sigma^2_{y_1,n-1})_{21}\right)\xi(t) \\ &\quad - \left(\mathbf{A}^{-1}(\omega, \sigma^2_{y_1,n-1})_{11} + \mathbf{A}^{-1}(\omega, \sigma^2_{y_1,n-1})_{12}\right)\xi(t) \\ &= \mathbf{J}_{y_{21,n}}\xi(t) \end{aligned}$$

$$2)\ S_{y_{21,n}} = |\mathbf{J}_{y_{21,n}}|^2 S_{\xi\xi} = |\mathbf{J}_{y_{21,n}}|^2 S_0$$

$$\Rightarrow \sigma^2_{y_{21,n}} = \int S_{y_{21,n}}(\omega)\mathrm{d}\omega = 2S_0 \int (|\mathbf{J}_{y_{21,n}}|^2)\mathrm{d}\omega$$

$$3)\ E_r = |\sigma^2_{y_{21},n} - \sigma^2_{y_{21},n-1}|$$

$$4)\ n = n + 1.$$

Once more, EL performs well in capturing the RMS value of the system as the agreement between the two plots in Fig.4.8 suggests.

In Fig.4.9 EL is compared to the actual first Wiener kernel of the joined response of the two masses in the same way it was demonstrated in case 1 before. Again, the two modes of the response kernel are shown separately with mode 1 to be the in-phase and mode 2 to be the out-of-phase mode. The two modal frequencies of the linear system as suggested by Eq.(4.11) are $\omega_1^2, \omega_2^2 = \frac{7}{2}\frac{1}{1}(3 \mp \sqrt{5})$ resulting to $\omega_1 = 1.64$ and $\omega_2 = 4.28$.

As nonlinear stiffness increases the second mode dies out will mode 1 approaches its limiting case. This is due to the fact that the system eventually becomes a SDOF system of total mass of 2 on linear stiffness of 7 (nondimensionality in the system so unitless quantities) giving a limiting natural frequency of $\omega_n = \sqrt{m/k} = \sqrt{2/7} = 1.87$. The natural frequency peak in mode 1 is shifted to the right and gets wider with increasing nonlinearity for the same reason as expected and as it was demonstrated in section 2.3.2 and analytically explained in section 2.6. As a reminder, this is because of the energy transfer from the first Wiener kernel to higher order kernel for system with nonlinear stiffness. This sort of behaviour from the first Wiener kernel is true up until the point when the nonlinear spring becomes very stiff and

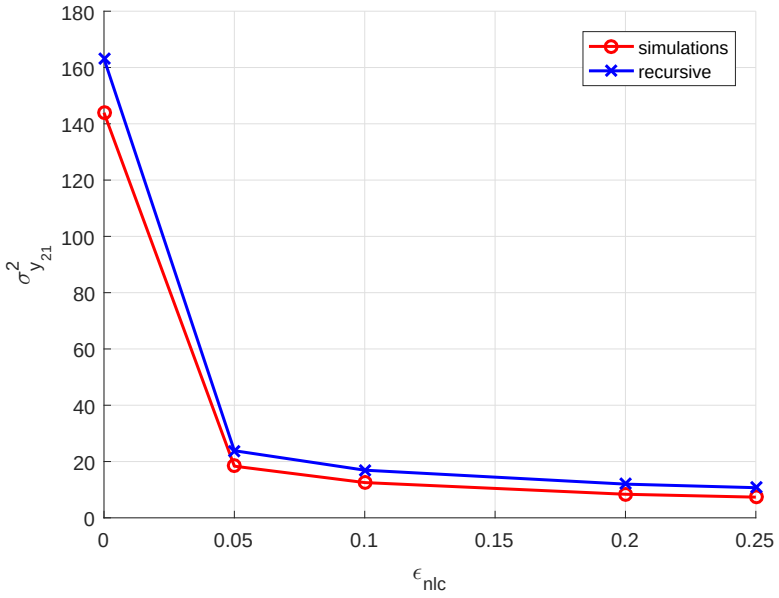

Fig. 4.8 Case 2: Comparison of the RMS of the nonlinear spring between the simulations and the recursive minimisation approach from Eq.4.18 for varying nonlinear stiffness ε_{nlc}.

effectively the system becomes a SDOF system. From that point onwards, the linear effects start becoming more dominant causing the peak to get narrower again. This is visible on the cyan plot ($\varepsilon_{nlc} = 0.1$) in the figure when compared with the black plot ($\varepsilon_{nlc} = 0.05$).

Overall, EL can not follow any of this behaviour reflected by the first Wiener kernel since it fails to capture the true shapes of mode 1 or mode 2 of this particular case.

4.4.2 Case 2: Pole fitting

In this section, an improvement on EL is to performed in the same way it was done for the SDOF systems as well as for case 1 in this chapter. To demonstrated this, the example where the nonlinear spring coefficient is equal to 0.01 ($\varepsilon_{nlc} = 0.01$) is to be used.

The TF between the first kernels of the nonlinear force and that of the original system response is calculated and plotted in Fig.4.10 on the left. On top of this TF a SPF is plotted and the two modes of the resulting first Wiener kernel are shown in Fig.4.11. This fitting function does not result into a satisfactory agreement between the kernels for the different methods.

Consequently, just like in case 1, a second pole with a resonance frequency $\omega_{p2} = 4.65$ is added as illustrated in Fig.4.12 in order to improve the accuracy. The resulting first Wiener kernel from this additional pole function is shown in Fig.4.13. It is clear that this additional

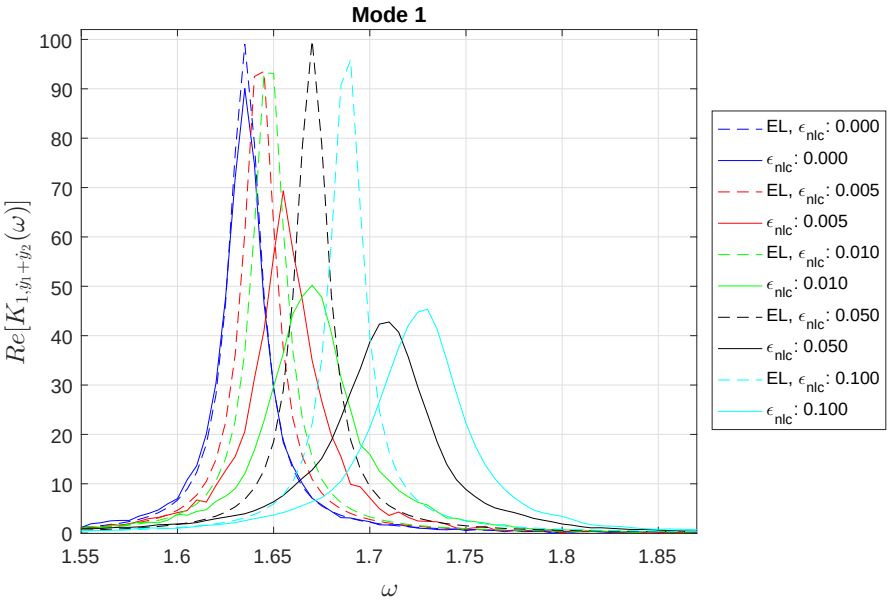

(a)

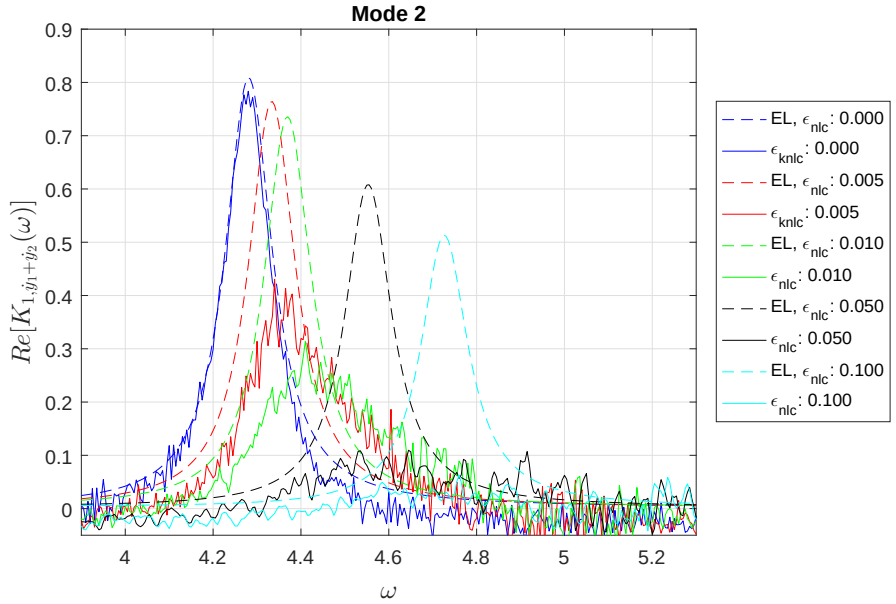

(b)

Fig. 4.9 Case 2: The comparison at the two modes of the first Wiener kernel of the combined response $(\dot{y}_1 + \dot{y}_2)$ of the two masses between EL and simulations for varying nonlinear stiffness ε_{nlc}.

pole has improved considerably the agreement between the kernels for mode 2. However, no improvement is visible for mode 1.

A look back to the TF $G(\omega)$ in Fig.4.10, a clear non-smooth irregularity is visible around $\omega = 1.6$. It seems that another pole may be hidden there. Consequently, a natural thing to try, is adding another pole to our fitting function such that now it looks like,

$$\begin{aligned} G(\omega) &= \frac{K_{1,z}(\omega)}{K_{1,y_T}(\omega)} \\ &= \frac{-2\alpha_1\omega_{p1}}{-\omega^2+\omega_{p1}^2+{\gamma_1}^2+2i\gamma_1\omega} + \frac{-2\alpha_2\omega_{p2}}{-\omega^2+\omega_{p2}^2+{\gamma_2}^2+2i\gamma_2\omega} + \\ &\quad \frac{-2\alpha_3\omega_{p3}}{-\omega^2+\omega_{p3}^2+{\gamma_3}^2+2i\gamma_3\omega} + 3\sigma_{y_{21}}^2. \end{aligned} \tag{4.19}$$

This additional third pole term corrects the disagreement between the plots in Fig.4.11 and Fig.4.13 for mode 1 resulting in a very good match for the first Wiener kernel between this new multi-pole fitting (MPF) function and the simulations outperforming EL. The PF parameters used in each plots are given in the Appendix C.

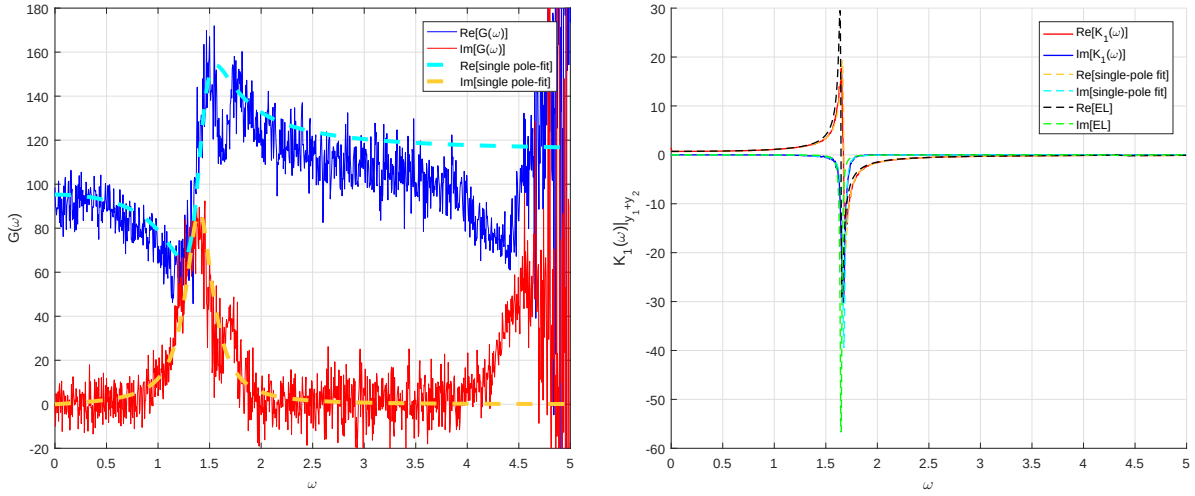

Fig. 4.10 Case 2: The TF between the first Wiener kernel between the nonlinear force and that of the system response along with the single-pole fit (left). The resulting first Wiener kernel of the joined velocity response from simulations, EL and the PF (right). Parameter values for this fitting function are given in table C6.

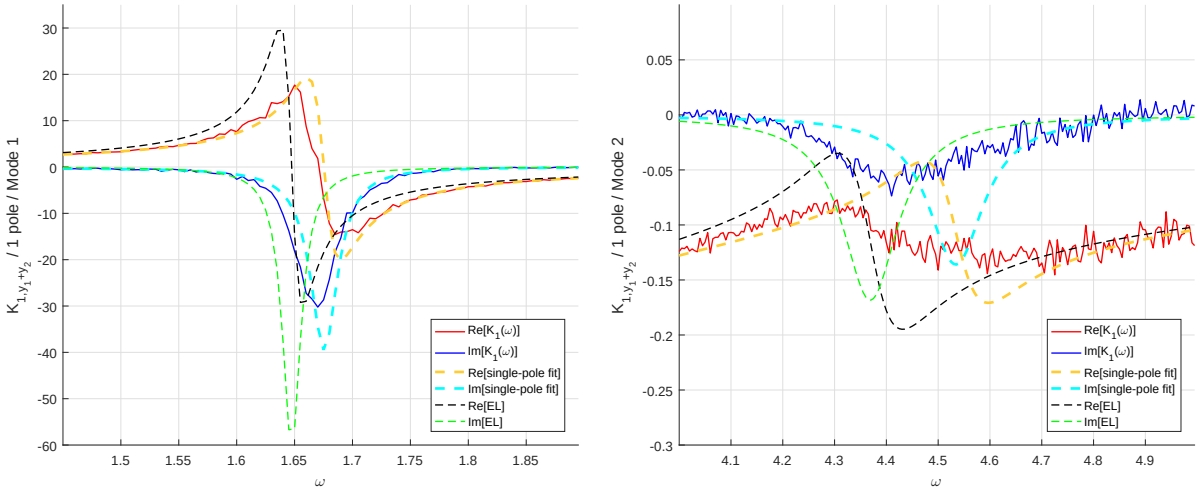

Fig. 4.11 Case 2: The two modes from the resulting Wiener kernel of the joined response also shown in the figure above (Fig.4.10) on the right. Mode 1 is the in-phase mode between the two masses while Mode 2 is the out-of-phase mode. A single-pole fitting function is used.

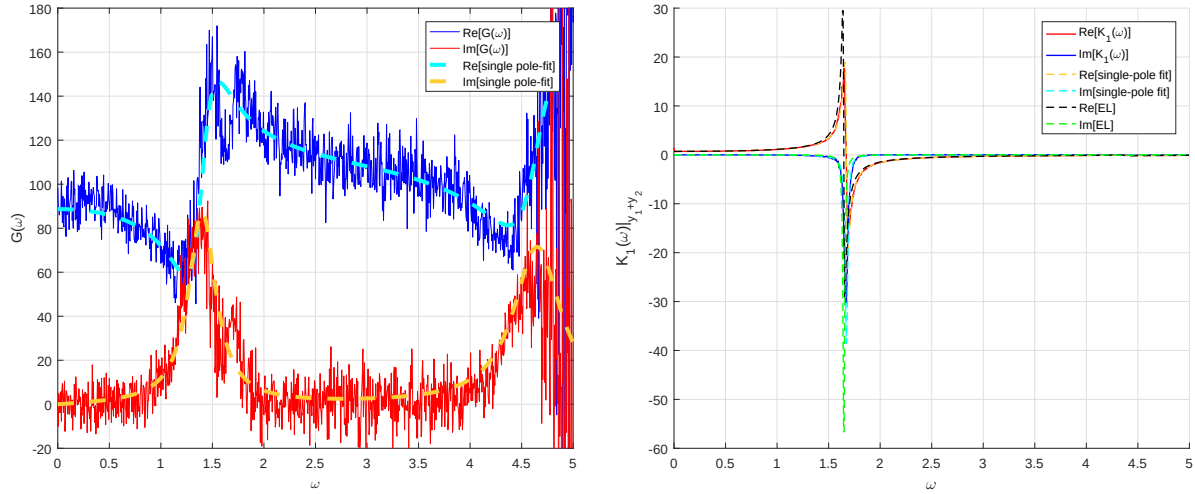

Fig. 4.12 Case 2: The TF between the first Wiener kernel between the nonlinear force and that of the system response along with the double-pole fit (left). The resulting first Wiener kernel of the joined velocity response from simulations, EL and the PF (right). Parameter values for this fitting function are given in table C7.

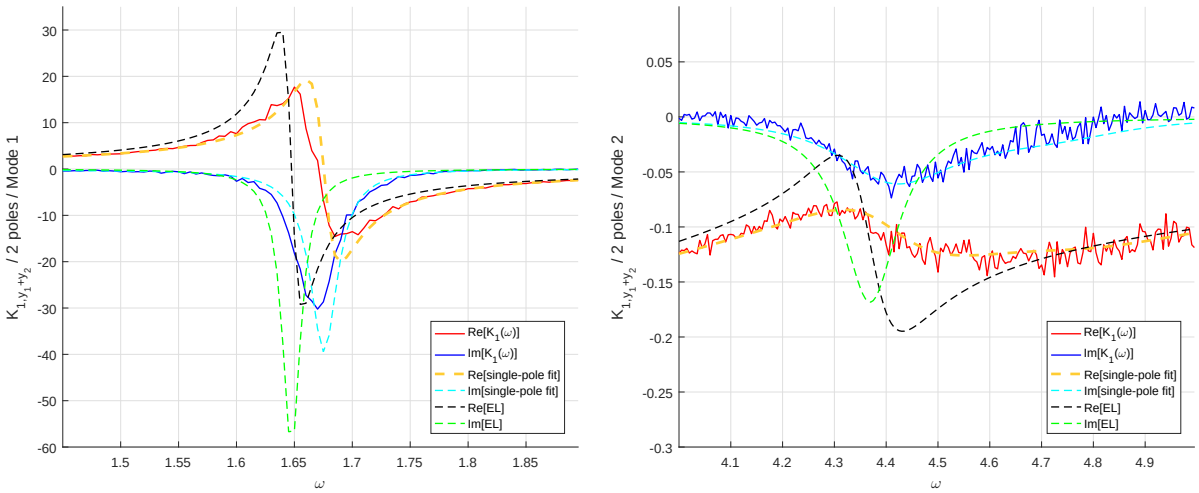

Fig. 4.13 Case 2: The two modes from the resulting Wiener kernel of the joined response also shown in the figure above (Fig.4.12) on the right. Mode 1 is the in-phase mode between the two masses while Mode 2 is the out-of-phase mode. A double-pole fitting function is used.

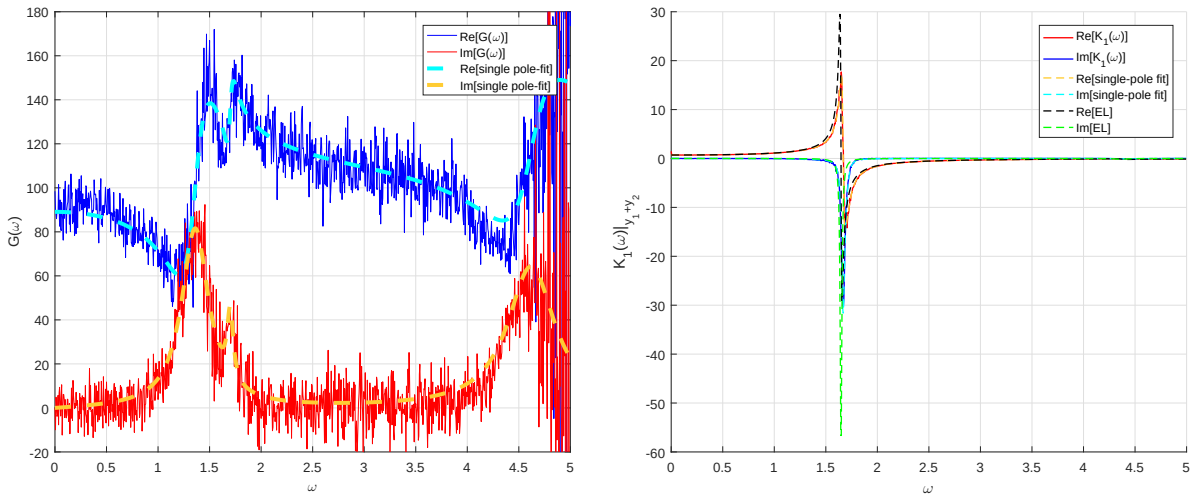

Fig. 4.14 Case 2: The TF between the first Wiener kernel between the nonlinear force and that of the system response along with the triple-pole fit (left). The resulting first Wiener kernel of the joined velocity response from simulations, EL and the PF (right). Parameter values for this fitting function are given in table C8.

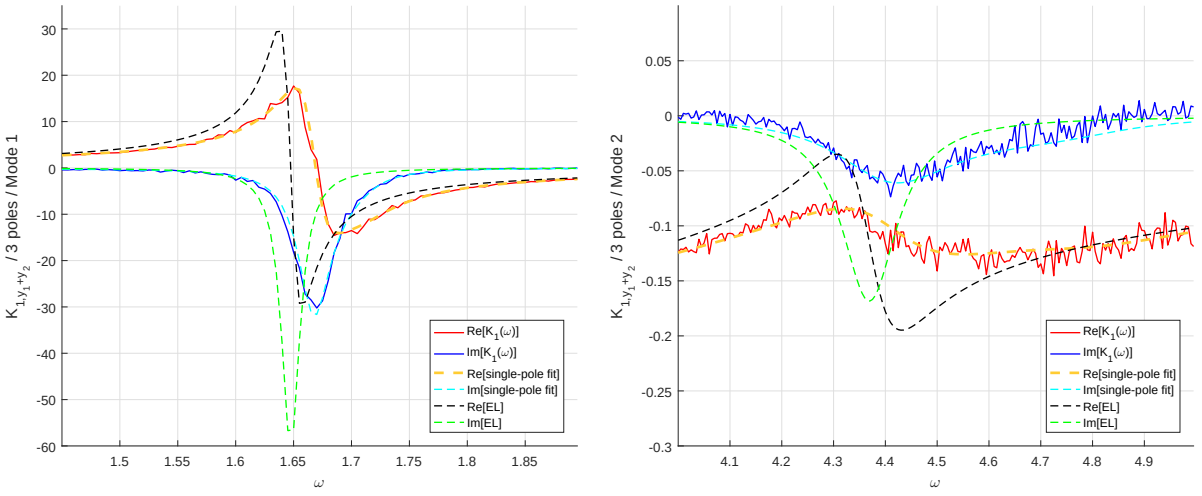

Fig. 4.15 Case 2: The two modes from the resulting Wiener kernel of the joined response also shown in the figure above (Fig.4.14) on the right. Mode 1 is the in-phase mode between the two masses while Mode 2 is the out-of-phase mode. A triple-pole fitting function is used.

4.5 Conclusion

The purpose of this chapter was to test the robustness of the SPF method introduced in Chapter 3. For this task, the nonlinear system was extended from a SDOF system to a 2DOF system of which to different cases were investigated.

Firstly, it was shown that EL can accurately capture the RMS value of the system response (Fig.4.2 and Fig.4.8) as in the case of the SDOF system. This was performed by a recursive algorithm over the minimisation of the error of the RMS value.

However, similarly to the SDOF case EL fails to capture the true shape of the first Wiener kernel and therefore the power spectrum of the response. In order to improve EL, the SPF method was used but its agreement with the original response kernel was not as accurate as in the case of the SDOF system.

As a result, additional poles were added to the fitting function describing the TF between the nonlinear force in each case with that of the system response which improved dramatically the performance of the fitting method. It was shown that the number of additional poles required in each case to fully take advantage of the SPF method depends on the specific system and the position of the nonlinear force. In the first case where the nonlinear force was between the base and the first mass a double-pole fit (Fig.4.7) was shown to be enough while in the case where the nonlinear force was coupling the two masses a triple-pole fit (Fig.4.15) was required.

Chapter 5

Modelling the behaviour of a nonlinear spring

5.1 Introduction

Previously in chapter 3, the efficiency and robustness of the SPF method to capture to true shape of the first Wiener kernel of a SDOF system with nonlinear stiffness outperforming EL was illustrated. An extension of this approach for a 2DOF system was shown in the previous chapter where it was demonstrated that additional poles can improve the accuracy of the fitting function.

The aim of this chapter is to get some insight on what may causes the phase shift observed in the TF between the first Wiener kernel of the nonlinear force and that of the system response giving rise to the single-pole shaped TF between the two kernels. Understanding the mechanics behind this behaviour may be proven helpful in the long run in analytically finding the SP parameters by relating them to a potential simplified model that will be mimicking this behaviour.

To do this, we will be isolating the nonlinear spring from the system and try to build a model for it which exhibits similar behaviour to the nonlinear system. Four different model cases will be investigated each of which involves a series of linear filtering procedures of the spring's response.

The principles of the successful model of an isolated nonlinear spring will then be extended to the original nonlinear system (Duffing oscillator) in order to explain the complex behaviour observed in the previous chapters.

5.2 The isolated nonlinear spring

An investigation of an isolated nonlinear spring like the one illustrated in Fig.5.1 is performed in this chapter. To begin with, we prescribe the motion of the spring $\hat{y}$ by a functional of white-noise, $\hat{y}(t) = \Psi[\xi(t)]$. Therefore, the nonlinear force $z(t)$ of the spring is $z(t) = \hat{y}^3(t)$.

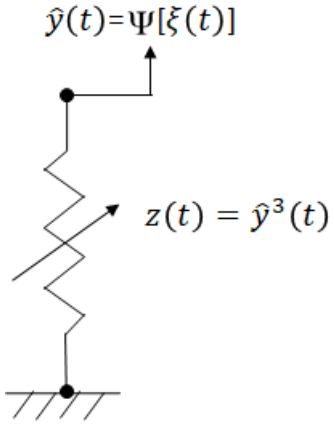

Fig. 5.1 Isolated nonlinear spring with white-noise input.

Following the simplified system of the isolated spring above, is the question: What is the the least effort or minimum operations required to be applied on the white-noise input, $\xi(t)$ to produce a response $\hat{y}(t)$, such that the nonlinear force $z(t)$ shows similar behaviour to the one observed in the previous chapters? More precisely, a behaviour that will diverge from the EL suggestion of a constant TF between the first Wiener kernel of the nonlinear force and the first Wiener kernel of the system's response into something closer to the SP function demonstrated in Fig.3.2a in Section 3.3. A different way to express this is by finding the simplest form of the functional $\Psi[\xi(t)]$ which will result in the desired behaviour of the nonlinear spring.

For example, the new TF, $Q(\omega)$, between the nonlinear force of the isolated spring and the system's response which in this case equals the white-noise input since the spring is massless, should be,

$$Q(\omega) = \frac{Z_1(\omega)}{Y_1(\omega)} = \frac{Z_1(\omega)}{\Xi(\omega)} = \frac{K_{1,z}(\omega)}{K_{1,y}(\omega)} \neq 3\sigma_\xi^2 \tag{5.1}$$

where $K_{1,z}(\omega) = \frac{Z_1(\omega)}{\Xi(\omega)}$ and $K_{1,y}(\omega) = \frac{Y_1(\omega)}{\Xi(\omega)}$ are the first Wiener kernel of the nonlinear force and the original response respectively and $\Xi(\omega) = \mathscr{F}\{\xi(t)\}$. The nonlinear force and the system's response have the subscript '1' to denote the component of the respective quantity

resulting from the first term of the Wiener series of each quantity characterised by the first Wiener kernel for each one.

5.3 The four cases under investigation

The kernel of the nonlinear force is to be calculated after the model of the nonlinear spring is constructed by a series of linear operations on the original response $\xi(t)$ which is the input in the system. Overall, four different cases of the spring model are to be tested. The functions characterising the linear filters involved in each case are to be discussed in the next section.

Case 1:
The first case involves the filtering of the input by a linear filter $h(t)$ to give a linear output $g(t)$ which is equal to the system's response $\hat{y}(t)$. Therefore, the nonlinear force is now $z(t) = \hat{y}^3(t) = (g(t))^3$. Explicitly,

$$\begin{aligned} \hat{y}(t) &= \int h(t-\tau)\xi(\tau)d\tau \\ z(t) &= \hat{y}^3(t) \end{aligned} \tag{5.2}$$

Case 2:
The first step for the second case is the same as the one in case 1 above. However, in this case, the linear response $g(t)$ is passed through another linear filter $w(t)$ to give a new linear output $\hat{y}(t)$ which will be used to calculate the nonlinear force. As it can be seen, case 2 is the same as applying case 1 twice since it involves a double linear filtering. This is demonstrated by,

$$\begin{aligned} g(t) &= \int h(t-\tau)\xi(\tau)d\tau \\ \hat{y}(t) &= \int w(t-\tau)g(\tau)d\tau \\ z(t) &= \hat{y}^3(t) \end{aligned} \tag{5.3}$$

Case 3:
Case 3 starts with the initial linear filtering already seen for cases 1 and 2. For the second step though, a nonlinear operation is performed which requires rising the linear response $g(t)$ over a certain power n to give a new output $\hat{y}(t)$. Here, a cubic power $n = 3$ is used for

simplicity but other odd powers can be used. Specifically,

$$\begin{aligned} g(t) &= \int h(t-\tau)\xi(\tau)d\tau \\ \hat{y}(t) &= g^n(t) \\ z(t) &= \hat{y}^3(t) \end{aligned} \tag{5.4}$$

Case 4:
Finally, the fourth case combines the filtering and the operations already used in the previous three cases. To begin with, it shares the same first step as with all previous cases to give a linear output $g(t)$. Next, a nonlinear operation takes place where the cubic response of the new linear output is calculated in the same way as in the second step of case 3. This nonlinear response is then filtered by a linear filter $w(t)$ just like in the second step of case 2 to give the final system response $\hat{y}(t)$ which has to be raised to the power of three once more in order to calculate the nonlinear force.

$$\begin{aligned} g(t) &= \int h(t-\tau)\xi(\tau)d\tau \\ \hat{y}(t) &= \int w(t-\tau)g^n(\tau)d\tau \\ z(t) &= \hat{y}^3(t) \end{aligned} \tag{5.5}$$

Time domain filtering involves the integral of the product between the filter and and the signal function. In order to make work simpler, all this analysis is performed in the frequency domain where the convolution theorem suggest that,

$$G(\omega) = \mathscr{F}\{g(t)\} = \mathscr{F}\{h(t)\} \cdot \mathscr{F}\{\xi(t)\} = H(\omega)\Xi(\omega) \tag{5.6}$$

The convolution theorem is applied in all the filtering operations presented in this section. This way enables the direct calculation of the first Wiener kernel in each case since it is also calculated and analysed in the frequency domain.

5.4 The different filters

The four models described in the section above involve the linear filters, $h(t)$ and $w(t)$. An experiment was carried out trying different functions for these filters all of which had to satisfy the reality condition already mentioned in section 3.3 which requires $H^*(\omega) = H(-\omega)$ -same stands for $W(\omega)$- so that the two filters are purely real in the time domain and hence, physical.

The functions that were tried for these filters are the single-pole (Fig.5.2a), the rectangular pulse function[67] (Fig.5.2b) and the sinc function[8][65] (Fig.5.2c). The later two functions are the Fourier transform of each other such as,

$$\mathscr{F}\{\text{rect}(at)\} = \frac{1}{\sqrt{2\pi}}\int_{-\infty}^{\infty}\text{rect}(at)e^{-i\omega t}dt = \frac{1}{\sqrt{2\pi a^2}}sinc(\frac{\omega}{\pi a}) \tag{5.7}$$

and

$$\mathscr{F}\{\text{sinc}(at)\} = \frac{1}{\sqrt{2\pi}}\int_{-\infty}^{\infty}\text{sinc}(at)e^{-i\omega t}dt = \frac{1}{\sqrt{2\pi a^2}}rect(\frac{\omega}{\pi a}) \tag{5.8}$$

allowing to work with these two functions without worrying about the reality condition since their inverse Fourier transform give a purely real function directly.

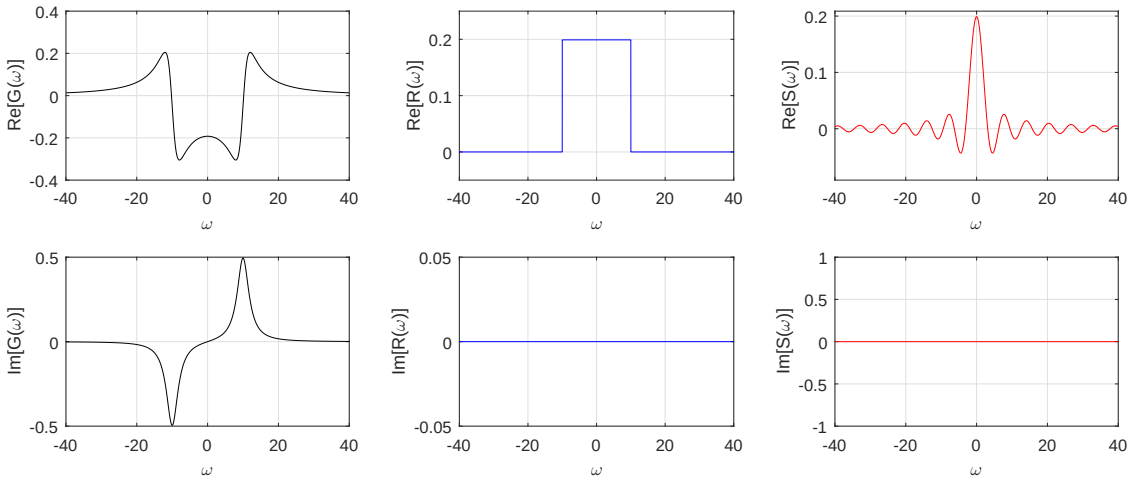

(a) Single-pole filter (b) Rectangular pulse filter (c) Sinc-function filter

Fig. 5.2 Three general examples of the filter functions used in the nonlinear spring models.

5.5 The Successful model

The purpose of investigating the models described by the four cases in section 5.3 is to estimate the true behaviour of the TF between the first Wiener kernel of the nonlinear force and that of the system's response contrary to the EL suggestion and with the least effort possible. It should be noted that at this point, we are not interested in finding the true TF function $Q(\omega)$ (Eq.(5.1)) but only identify the model which results in a TF with the qualitative features observed for the TF $G(\omega)$ (Eq.(3.15)) in the previouse chapters. These will require the real part of the TF to be a non-constant purely positive function and the imaginary part to be a positive non-zero function.

In Fig.5.3, the results of these four cases under investigation are shown. The shape of the two filters is illustrated in each case as well as the real and imaginary parts of the TF $Q(\omega)$ in Eq.(5.1). Moreover, for this initial invetigation, the two filters $H(\omega)$ and $W(\omega)$ both have a single-pole function shape in all cases apart from when they are not used in which case are equal to the Heaviside function[1].

For cases 1 to 3, the outcome suggests a relation to EL. This is due to the fact that for these three cases, the TF $Q(\omega)$ as it can be seen in Fig.5.3 has a constant real part and a zero imaginary part just like EL. These outcomes are not surprising though. The first case is a simple linear operation acting on the white-noise and hence a linear out come is expected. Case 2 is a effectively involving the same linear filtering as in case 1 with the linear filter being $V(\omega) = H(\omega)W(\omega)$ and therefore expecting the same behaviour as with the first model. The nonlinear operation in case 3 does not add any further complexity to the model than the final step in cases 1 and 2. It simply takes the first filtered output to produce a nonlinear force $z(t) = g^{3n}(t)$ which as we saw in the previous cases exhibits the EL pattern.

The only case where EL behaviour is not generated according to the results in Fig.5.3 is case 4. The TF illustrated in Fig.5.3d no longer has constant real part nor a zero imaginary part. What is more, the shapes of the real and imaginary part look similar to the ones of the TF $G(\omega)$ for the SDOF system illustrated in Fig.3.2a. This result suggests that the least effort required to model a nonlinear spring by a combination of linear operations is the one demonstrated by case 4. This is to filter the input by a single-pole filter to get a new linear output which is then undertakes a nonlinear operation before it goes through another linear filter.

The investigation on this problem does not finish here since a similar result already described above for case 4 can be achieved when the first filter $H(\omega)$ is substituted with a

[1] $H(n) = \begin{cases} 0 & \text{if } n < 0 \\ 1 & \text{if } n \geq 0 \end{cases}$

wide enough step function (Fig.5.2b). This will allow all the non-zeros frequencies around the resonant frequency specified by the second filter to pass through the first filter. This behaviour is illustrated in Fig.5.4 where the results between a narrow and a wider $H(\omega)$ filter are compared. Similar results can also be obtained for exactly the same reason when the first filter is a wide enough sinc function. This is demonstrated in Fig.5.5 where again a narrow sinc function is compared to a wider one. In both cases, it can be seen how numerical errors are generated by the zero valued range of the filters; when $\omega > 10$ for the rectangular function and around the minimum values $\omega = 10$ and $\omega = 20$ for the sinc function.

The flexibility on the choice of function used for the very first filter was demonstrated and commented on in the previous paragraph. However, the same does not hold true for the second filter $W(\omega)$. Any other combination of filters involving a non-single pole function for the second filter does not result into a meaningful $Q(\omega)$ TF and which could relate to the equivalent TF of the SDOF system in chapter 3.

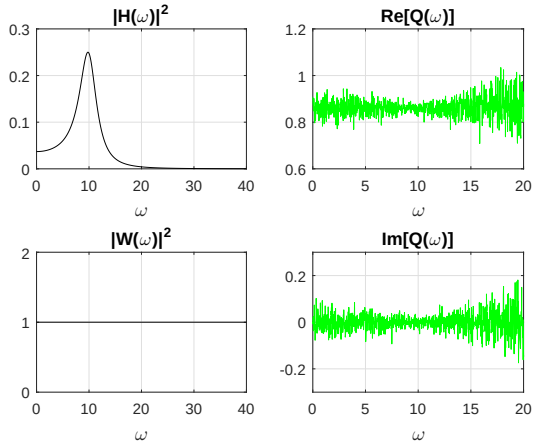

(a) Case 1

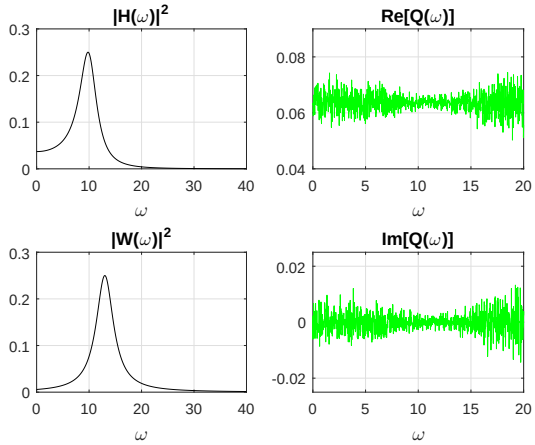

(b) Case 2

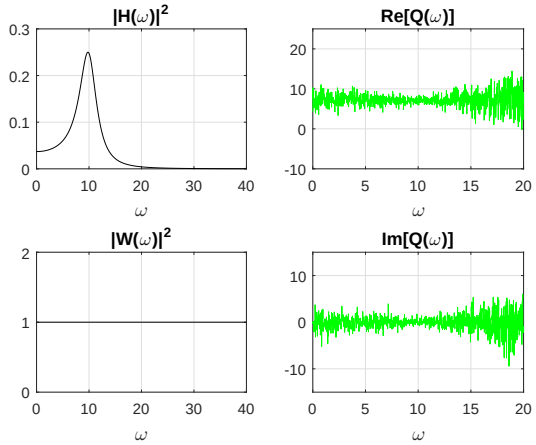

(c) Case 3

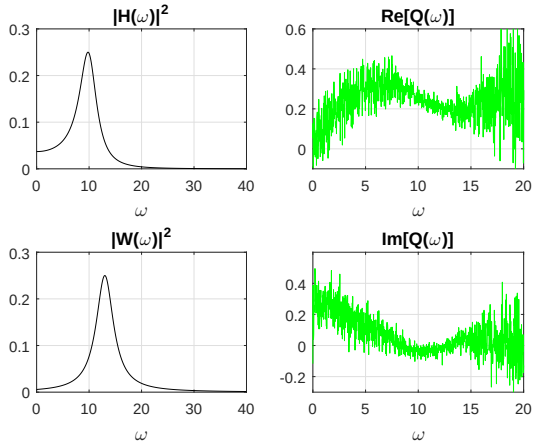

(d) Case 4

Fig. 5.3 The results for all four cases of the nonlinear spring model.

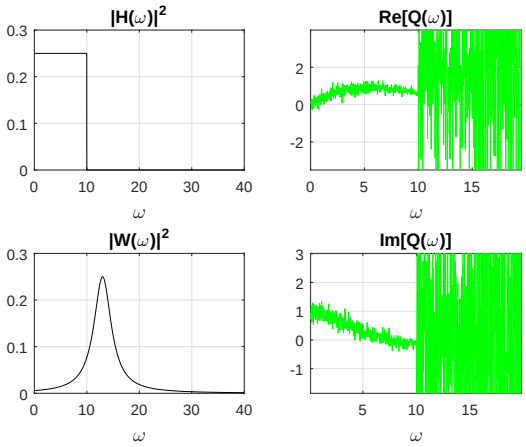

(a) Case 4 results with narrow rectangular pulse function for the first filter.

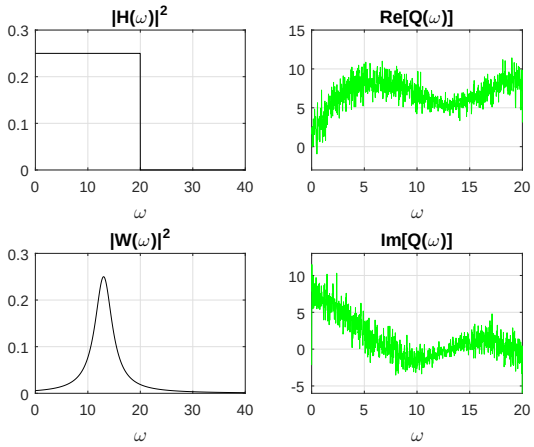

(b) Case 4 results with wide rectangular pulse function for the first filter.

Fig. 5.4 Case 4 plots with the first filter being a rectangular pulse function.

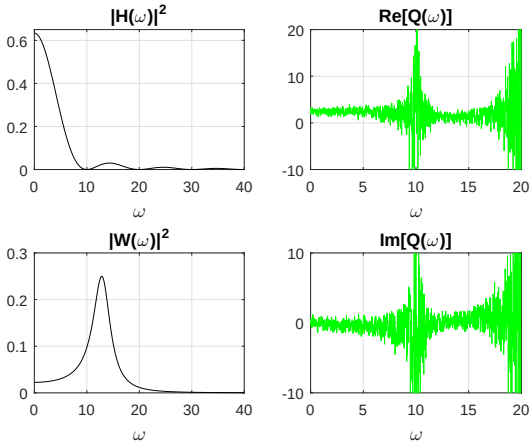

(a) Case 4 results with narrow sinc function for the first filter.

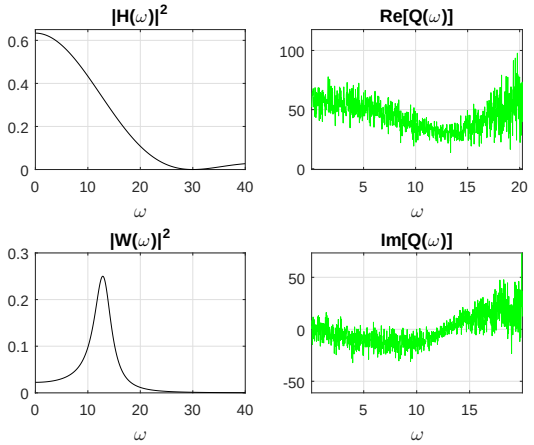

(b) Case 4 results with wide sinc function for the first filter.

Fig. 5.5 Case 4 plots with the first filter being a sinc function.

5.6 Conclusion

The goal in this chapter was to model a nonlinear spring to show similar behaviour to the one observed in Fig.3.2a where the TF between the first Wiener kernel of the nonlinear force and that of the original nonlinear system is not just a purely real constant value like EL suggests. In order to do this, an isolated spring under white-noise input is used. A combination of linear filtering and nonlinear operations over the input is used to obtain the desired behaviour.

The minimum number of operations required to achieve this behaviour was found to be described by the model in case 4, Eq.(5.5). Specifically, this involves the linear filtering of the input which is then raised to an odd power n before it is filtered again by another linear filter. This result is illustrated in Fig.5.3d where the TF $Q(\omega)$ in no longer a positive constant.

On the choice of the type of filters, the second linear filter needs to be a single-pole function similar to a frequency response while the first filter can be any function which will allow all the important frequencies around the resonance of the second filter to pass through. The flexibility over the choice of the first filter is demonstrated in figures Fig.5.4 and Fig.5.5.

Chapter 6

Extending the model of a nonlinear spring to a nonlinear system

6.1 Introduction

In the previous chapter, it was demonstrated how the behaviour of a nonlinear spring can be modelled through a series of linear filtering and nonlinear operations over a white-noise input. Specifically, it was shown that the minimum effort required to do that was to pass the white-noise signal through a linear filter and then raise the new signal to a odd power before filtering it again through another linear filter. It was also mentioned that the second filter needs to be a single-pole function in order for the modelled response to give rise to the desired shape of the TF between the first Wiener kernel of the nonlinear force and that of the system response required to implement the SPF method described in chapter 3.

Can the main principles behind the modelling of the isolated nonlinear spring being related to the original nonlinear system under investigation? This is the question this chapter investigates. To give an answer to this question, an iterative method is to be use to solve an alternative version of the Duffing equation which requires the minimisation of an error term arising from a specific rearrangement of the terms in the differential equation. It should be stressed that this iteration method is not an efficient way to solve the nonlinear system under investigation. Nevertheless, the purpose of its use is purely based on the prospect of giving us some insight into the mechanism behind the behaviour of the nonlinear system, as well as the possibility to relate it to earlier findings demonstrated in chapter 5. As it has been already said earlier in chapter 5, understanding the mechanics giving rise to the single-pole shaped TF observed in the previous chapters may be proven helpful in the future in analytically finding the SP parameters by relating them to a simplified model of the system.

The initial iteration procedure will be shown not to have a smooth convergence solution. The origin of this problem will be introduced and a suggestion of how to fix this in order to get the desirable result will be suggested and implemented. To close the chapter, the relation between the performance of the iteration method for the nonlinear system and that of the isolated nonlinear spring model is discussed in order to explain the results and give a further understanding on how the nonlinear system behaves.

6.2 Formulating the iteration method

Starting with the original Duffing equation with a nonlinear stiffening nonlinearity,

$$\ddot{y}+2\beta\dot{y}+y(1+\varepsilon_3 y^2)=\xi(t) \tag{6.1}$$

an attempt to modify it into a form that will allow a numerical approach like the iteration method to solve is made.

The first step is to add on both sides of the equation above the constant term $3\varepsilon_3\sigma_y^2$ arising from EL and at the same time move the nonlinear term to the right-hand side such that

$$\ddot{y}+2\beta\dot{y}+y(1+3\varepsilon_3\sigma_y^2)=\xi(t)-\varepsilon_3 y^3+3\varepsilon_3\sigma_y^2 y. \tag{6.2}$$

This rearranged form of the equation now consists of a linear equation on the LHS with linear stiffening constant

$$k_{EL}=1+3\varepsilon_3\sigma_y^2 \tag{6.3}$$

and an error term $R(y)$ on the RHS where

$$R(y)=-\varepsilon_3 y^3+3\varepsilon_3\sigma_y^2 y. \tag{6.4}$$

This linear system can now be defined by a linear differential operator,

$$L(y)=\ddot{y}+2\beta\dot{y}+y(1+3\varepsilon_3\sigma_y^2) \tag{6.5}$$

so that

$$L(y)=\xi(t)+R(y) \tag{6.6}$$

The solution for $L(y)$ can now be found numerically using the iteration method,

$$\begin{aligned} L(y_0) &= \xi(t) \\ L(y_1) &= \xi(t) + R(y_0) \\ &\dots \\ L(y_n) &= \xi(t) + R(y_{n-1}). \end{aligned} \tag{6.7}$$

Instead of solving the iterative steps individually a system of linear differential equations is created which can be put into a matrix form that can be solved efficiently using a MATLAB ODE solver [71][50][3]. The generalised form of this is described by the state-space form of each iteration by,

$$\dot{\boldsymbol{y}}_n = \bar{\bar{M}}_L \boldsymbol{y}_{1\dots n} + \boldsymbol{b}(\xi(t), R(\boldsymbol{y}_{1\dots n-1})) \tag{6.8}$$

where $\bar{\bar{M}}_L$ is a $2n \times 2n$ matrix known as the iteration matrix where n is the number of iterations. The $2n$ size column vector $\boldsymbol{b}(\xi(t), R(\boldsymbol{y}_{1\dots n-1}))$ is a function of the input $\xi(t)$ and the error function $R(\boldsymbol{y}_{1}\dots_{n-1})$ which is evaluated using the results from the previous iteration. Explicitly, the generalised version of the above iteration scheme for n iterations is given by

$$\frac{d}{dt}\begin{pmatrix} y_0 \\ \dot{y}_0 \\ y_1 \\ \dot{y}_1 \\ y_2 \\ \dot{y}_2 \\ \dots \\ y_n \\ \dot{y}_n \end{pmatrix} = \begin{pmatrix} 0 & 1 & 0 & 0 & 0 & 0 & \dots & 0 & 0 \\ k_{EL} & 2\beta & 0 & 0 & 0 & 0 & \dots & 0 & 0 \\ 0 & 0 & 0 & 1 & 0 & 0 & \dots & 0 & 0 \\ 0 & 0 & k_{EL} & 2\beta & 0 & 0 & \dots & 0 & 0 \\ 0 & 0 & 0 & 0 & 0 & 1 & \dots & 0 & 0 \\ 0 & 0 & 0 & 0 & k_{EL} & 2\beta & \dots & 0 & 0 \\ \dots & \dots & \dots & \dots & \dots & \dots & \dots & \dots & \dots \\ 0 & 0 & 0 & 0 & 0 & 0 & \dots & 0 & 1 \\ 0 & 0 & 0 & 0 & 0 & 0 & \dots & k_{EL} & 2\beta \end{pmatrix} \begin{pmatrix} y_0 \\ \dot{y}_0 \\ y_1 \\ \dot{y}_1 \\ y_2 \\ \dot{y}_2 \\ \dots \\ y_n \\ \dot{y}_n \end{pmatrix} + \begin{pmatrix} 0 \\ \xi(t) \\ 0 \\ \xi(t) + R(y_0) \\ 0 \\ \xi(t) + R(y_1) \\ \dots \\ 0 \\ \xi(t) + R(y_{n-1}) \end{pmatrix}. \tag{6.9}$$

Unfortunately, the above iteration scheme when used to solve a dynamic system with significant nonlinear stiffness using a MATLAB solver does not result in a converging solution. In Fig.6.1 an example simulation of the iterative procedure with four iterations is presented for a system with $\beta = 0.15$ and $\varepsilon_3 = 0.5$. The time history of the system is presented after every iteration. It is clear that around $t = 120$ and $t = 195$ the response of the system shoots in every iteration resulting in a non-convergent solution.

In the next section, the reason causing this failure is explained and a way to go surpass it is presented and implemented.

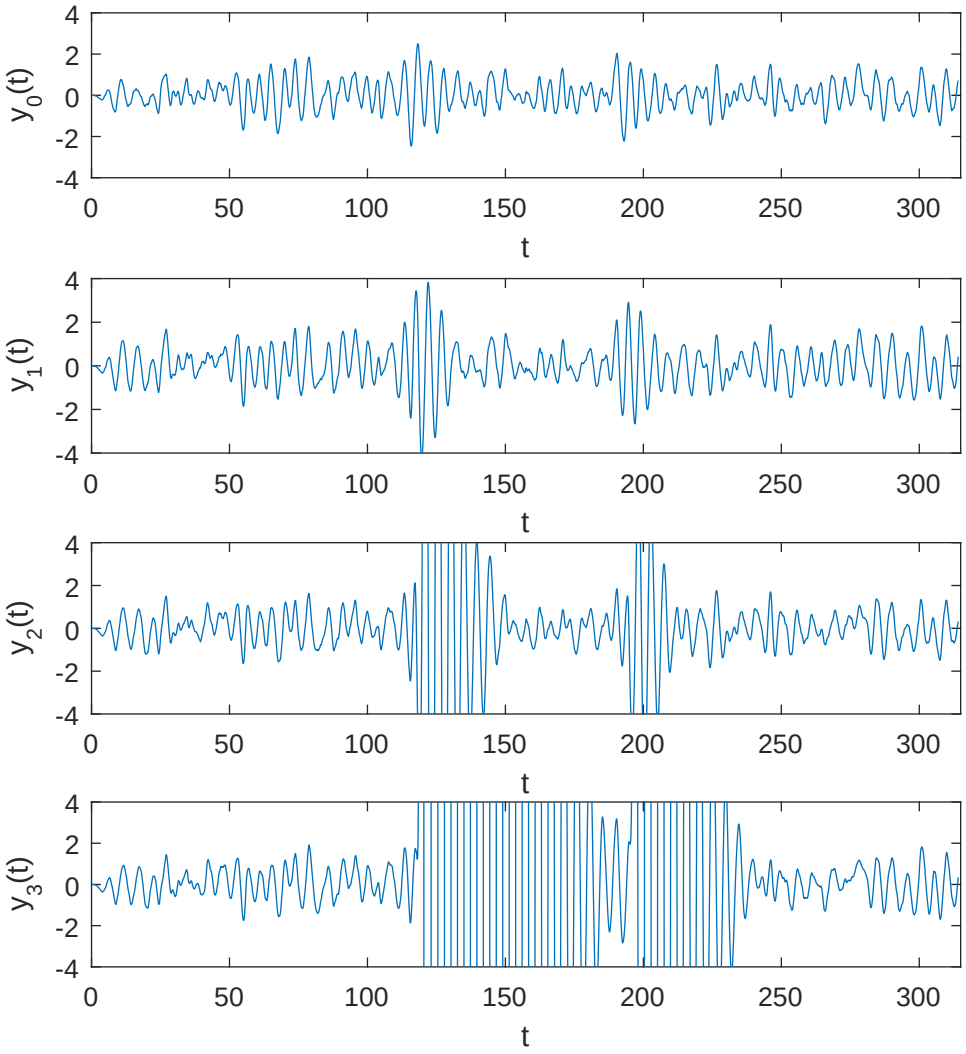

Fig. 6.1 Time history of the response of a nonlinear system response for each of the four iterative steps.

6.3 The error function and the problem of non-convergence

It was shown that the iteration method does not converge and solution estimations get worse for later iterations. The purpose of this section is to identify the cause of this non-convergent behaviour and fix it if possible.

Starting with Fig.6.2 where a general example of the error function, $R(y)$ introduced in Eq.(6.4) is plotted and for which a few points need to be noted. The two turning points at $y_{max} = \sigma_y$ and $y_{min} = -\sigma_y$ have a magnitude of $|R(y_{max})| = |R(y_{min})| = 2\varepsilon_3\sigma^3$. The error function is bounded within this limit for the displacement range of $-2\sigma_y \leq y \geq 2\sigma_y$ (light

blue lines). Once, the displacement is out of this range the error term shoots to very high values causing numerical instability in the solver leading to non-convergence solutions. Physically, it can be thought as if an impulse is applied to the system. The impulse which can be modelled by a delta function at the point where the boundary is exceeded produces some high amplitude transient response which takes some time to die out and go back again within the acceptable bounds. During this transient, the solver, as mentioned before, can not converge to a reasonable solution.

This is demonstrated by a simulation example in Fig.6.3 where the time history of the response displacement is shown in the top plot along with the light blue lines indicating the upper and lower bounds within two standard deviations. In the bottom plot of the same figure, the corresponding error of the response is shown along with the red lines indicating the upper and lower bounds of the limit $2\varepsilon_3\sigma^3$. For the points in the top plot which exit the $\pm 2\sigma_y$ bounds (light blue lines) the corresponding error value is amplified massively due to the cubic term in the error function making these points surpass the bounds of the error term by a large amount leading to the non-converging solution due to the incapability of the numerical solver to deal with these kind of extreme values.

Due to the complexity of the iteration method over a random process such as the one above, the processing time required for a reasonable number of ensemble time histories is too long. This makes the investigation of this method and particularly the effort in resolving the non-convergence issue illustrated and explained above time-consuming. Another limitation is the fact that the individual parameters which influence the solution, such as the number of iterations, the strength of the nonlinearity and the way the error function is calculated can not be isolated easily in order to study their individual effect. As a result, in the next section, we will try and understand the fundamentals of the iteration method by investigating the nonlinear system under a simpler and much more straight forward input, the harmonic. This will not require a large number of simulations for calculating the system's response. As a result, the solutions of the numerical solver will be calculated faster allowing a more efficient investigation over the iteration method introduced in this chapter.

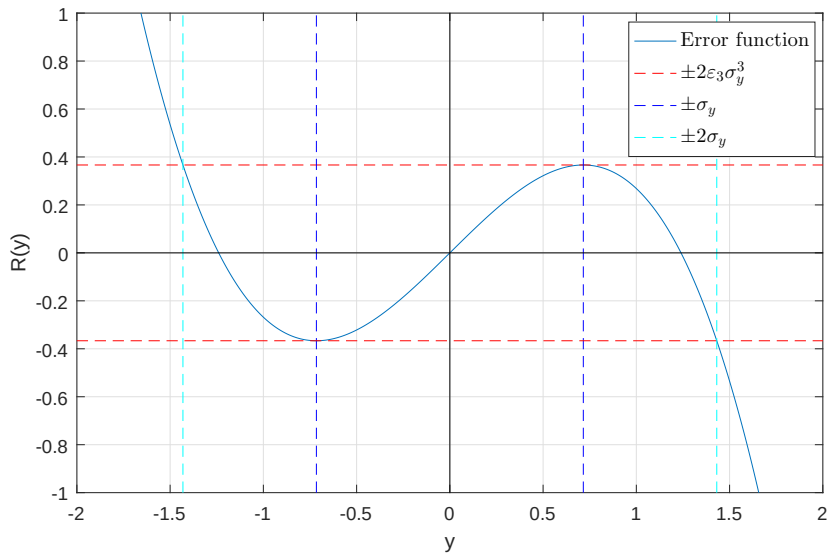

Fig. 6.2 The error function $R(y) = -\varepsilon_3 y^3 + 3\varepsilon_3\sigma_y^2 y$.

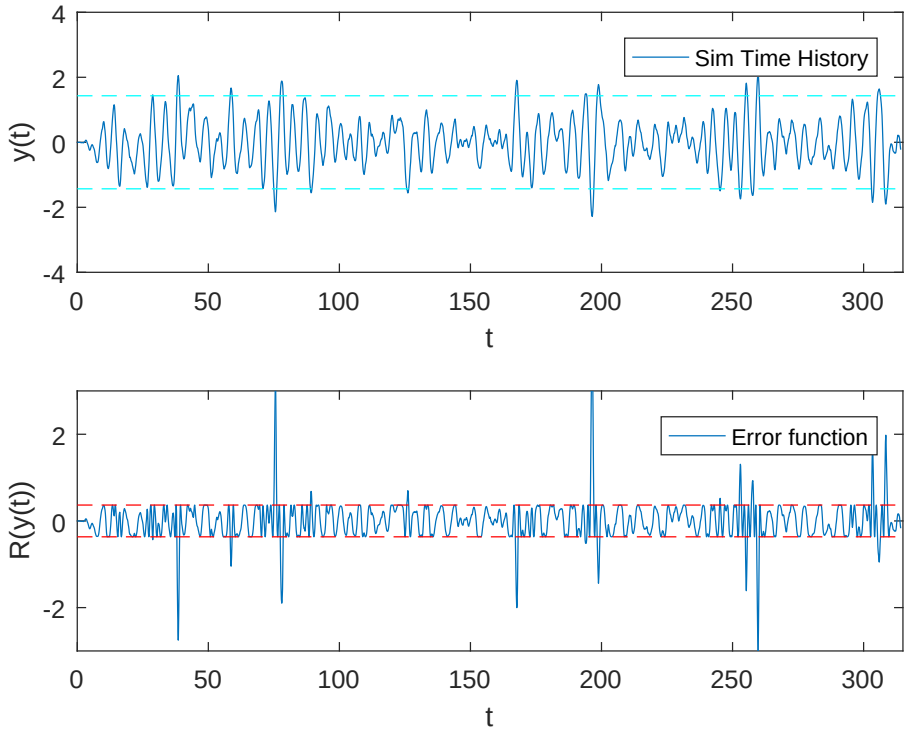

Fig. 6.3 Time history of system response (top) and the equivalent error produced by the error function $R(y)$ (bottom).

6.4 Investigating the iteration method with harmonic excitation

As mentioned in the previous paragraph a harmonically excited Duffing oscillator is to be used to investigate the convergence problem arises by the iteration method demonstrated in the previous section.

The new differential equation describes the Duffing oscillator with a harmonic force,

$$\ddot{y} + 2\beta\omega_n\dot{y} + \omega_n^2 y + \varepsilon_3 y^2 = F_H(t). \tag{6.10}$$

The harmonic force is $F_H(t) = F\cos(\omega_F t)$ where F is the amplitude and ω_F is the frequency of the harmonic input. For this kind of input, the linearised nonlinear spring takes the form,

$$\ddot{y} + 2\beta\omega_n\dot{y} + y(\omega_n^2 + \frac{3}{4}\varepsilon_3 A^2) = F_H(t) \tag{6.11}$$

where $A = |Y(\omega)|$ is the linearisation constant to be calculated by solving,

$$A = |Y(\omega)| = \frac{|F|\delta(\omega_F)}{|\omega^2 + 2i\beta\omega_n\omega + \omega_n^2 + \frac{3}{4}\varepsilon_3 A^2|} = \frac{|F|}{[(\omega_F^2 + \omega_n^2 + \frac{3}{4}\varepsilon_3 A^2)^2 + (2\beta\omega_n\omega_F)^2]^{\frac{1}{2}}} \tag{6.12}$$

using a root-finding method such as the Newton-Raphson[1][18].

Once the equivalent linear stiffness term is calculated by finding A from the previous equation, the same steps from Eq.(6.8) onwards need to be carried out in order to formulate the iteration method for the new system. This is to add the new linear term to both sides of the original nonlinear equation, Eq.(6.10), and take the nonlinear term to the RHS such that,

$$\ddot{y} + 2\beta\omega_n\dot{y} + y\omega_n^2 + \frac{3}{4}\varepsilon_3 A^2 y = \xi(t) - \varepsilon_3 y^3 + \frac{3}{4}\varepsilon_3 A^2 y. \tag{6.13}$$

This rearranged form of the equation is now consisting of a linear equation on the LHS with linear stiffening constant

$$k_{ELH} = \omega_n^2 + \frac{3}{4}\varepsilon_3 A^2 \tag{6.14}$$

and an error term $R_H(y)$ on the RHS where

$$R_H(y) = -\varepsilon_3 y^3 + \frac{3}{4}\varepsilon_3 A^2 y. \tag{6.15}$$

The new linear system can now be defined by a linear differential operator,

$$L_H(y) = \ddot{y} + 2\beta\dot{y} + y(\omega_n^2 + \frac{3}{4}\varepsilon_3 A^2) \tag{6.16}$$

so that

$$L_H(y) = F_H(t) + R_H(y). \tag{6.17}$$

In the same way as in Eq.(6.7), the solution for $L_H(y)$ can now be found numerically using the iteration method,

$$\begin{aligned} L_H(y_0) &= F_H(t) \\ L_H(y_1) &= F_H(t) + R_H(y_0) \\ &\dots \\ L_H(y_n) &= F_H(t) + R_H(y_{n-1}). \end{aligned} \tag{6.18}$$

Similarly to Eq.(6.9), the iteration steps above can be formulated in a matrix form,

$$\frac{d}{dt}\begin{pmatrix} y_0 \\ \dot{y}_0 \\ y_1 \\ \dot{y}_1 \\ y_2 \\ \dot{y}_2 \\ \dots \\ y_n \\ \dot{y}_n \end{pmatrix} = \begin{pmatrix} 0 & 1 & 0 & 0 & 0 & 0 & \dots & 0 & 0 \\ k_{ELH} & 2\beta & 0 & 0 & 0 & 0 & \dots & 0 & 0 \\ 0 & 0 & 0 & 1 & 0 & 0 & \dots & 0 & 0 \\ 0 & 0 & k_{ELH} & 2\beta & 0 & 0 & \dots & 0 & 0 \\ 0 & 0 & 0 & 0 & 0 & 1 & \dots & 0 & 0 \\ 0 & 0 & 0 & 0 & k_{ELH} & 2\beta & \dots & 0 & 0 \\ \dots & \dots & \dots & \dots & \dots & \dots & \dots & \dots & \dots \\ 0 & 0 & 0 & 0 & 0 & 0 & \dots & 0 & 1 \\ 0 & 0 & 0 & 0 & 0 & 0 & \dots & k_{ELH} & 2\beta \end{pmatrix} \begin{pmatrix} y_0 \\ \dot{y}_0 \\ y_1 \\ \dot{y}_1 \\ y_2 \\ \dot{y}_2 \\ \dots \\ y_n \\ \dot{y}_n \end{pmatrix} + \begin{pmatrix} 0 \\ F_H(t) \\ 0 \\ F_H(t) + R_H(y_0) \\ 0 \\ F_H(t) + R_H(y_1) \\ \dots \\ 0 \\ F_H(t) + R_H(y_{n-1}) \end{pmatrix}. \tag{6.19}$$

Just like with the original system under white-noise input, the harmonically excited system formulated in this section does not converge to a solution even for weak nonlinearities. Below, a few ways to force convergence on the system by manipulating the error are suggested. The efficiency of each method is tested and the role different parameters such as the number of iteration and the force amplitude play in each case are investigated.

6.5 Methods to ensure convergence for the harmonically excited system

Various ways to calculate the error term or manipulate the error function to ensure convergence to the harmonically excited system will be introduced in this section. The effectiveness

of each method will be demonstrated to enable comparison and evaluation of the methods. The parameters of the system used whose general formulation is expressed by Eq.(6.10) and which are held the same throughout this section unless stated otherwise, are: $\beta = 0.15$Nm/s, $\omega_n = 1$rad/s, $\varepsilon_3 = 2$, $F = 10$N and $\omega_F = 2$rad/s.

6.5.1 Averaging the error term

Two ways to average the error term in each iteration based on more than just the result from the previous iteration but a number of the previous iterations are considered. This is due to the fact that the error term of early iterations is smaller than later iterations which is the reason causing the non-convergence. As a result, it aims to smooth out the effect of the error in each iteration so that it does not result in very high amplitude solutions which eventually lead to a non-converging solution.

Average the error term using the two previous iterations.
In the first case the average of the error from the two previous iterations is considered such as the iteration steps are now,

$$\begin{aligned} L_H(y_0) &= F_H(t) \\ L_H(y_1) &= F_H(t) + R_H(y_0) \\ L_H(y_2) &= F_H(t) + \frac{1}{2}(R_H(y_1) + R_H(y_0)) \\ &\cdots \\ L_H(y_n) &= F_H(t) + \frac{1}{2}(R_H(y_{n-1}) + R_H(y_{n-2})). \end{aligned} \tag{6.20}$$

Average the error term using all previous iterations.
In the second case the average of the error from all the previous iterations is considered such

as the iteration steps are now,

$$\begin{aligned}
L_H(y_0) &= F_H(t) \\
L_H(y_1) &= F_H(t) + R_H(y_0) \\
L_H(y_2) &= F_H(t) + \frac{1}{2}(R_H(y_1) + R_H(y_0)) \\
L_H(y_3) &= F_H(t) + \frac{1}{3}(R_H(y_2) + R_H(y_1) + R_H(y_0)) \\
&\dots \\
L_H(y_n) &= F_H(t) + \frac{1}{n}\left(\sum_{i=0}^{n-1} R_H(y_i)\right).
\end{aligned} \tag{6.21}$$

The results from these the averaging methods are illustrated in Fig.6.4. Fig.6.4a shows the case where the average is calculated using the two previous iterations while Fig.6.4b shows the results of the second case where the average is calculated using all the previous iterations.

From the whole time history (top plots for both cases), it is clear that the first case does not allow for the high amplitude oscillations for higher iterations during the first time steps; something happening in the second case. This make sense because in the second case, the error converges at a lower rate compared to the first case since all the previous iterations are always considered when calculating the error. However, at the steady-state solution, it is clear that the second case convergence to the solution by the fifth iteration compared the eighth for the first case. Again, this is due to the smoother calculation of the error term in successive iterations. In general though, both methods are effective in calculating the steady-state solution.

6.5.2 Weighting the error term

A different way to manipulate the error term is by putting a weight on it for every iteration based on the number of iterations to be performed. The aim here is to put a low weight on the error for the early iterations in order to avoid high amplitude results which will amplify for higher iterations leading to non-converging solutions. An arithmetic progression is used to generate the weight factor for each iteration. The number of iterations are defined in the beginning of the procedure hence in each iteration the weighting factor is increased by the same amount. For the general example where the number of iterations is n, the first time the error term appears which is in the second iteration, the weighting factor on the error term is $\frac{1}{n}$. This factor will be increasing by an arithmetic progression with common difference $\frac{1}{n}$ such

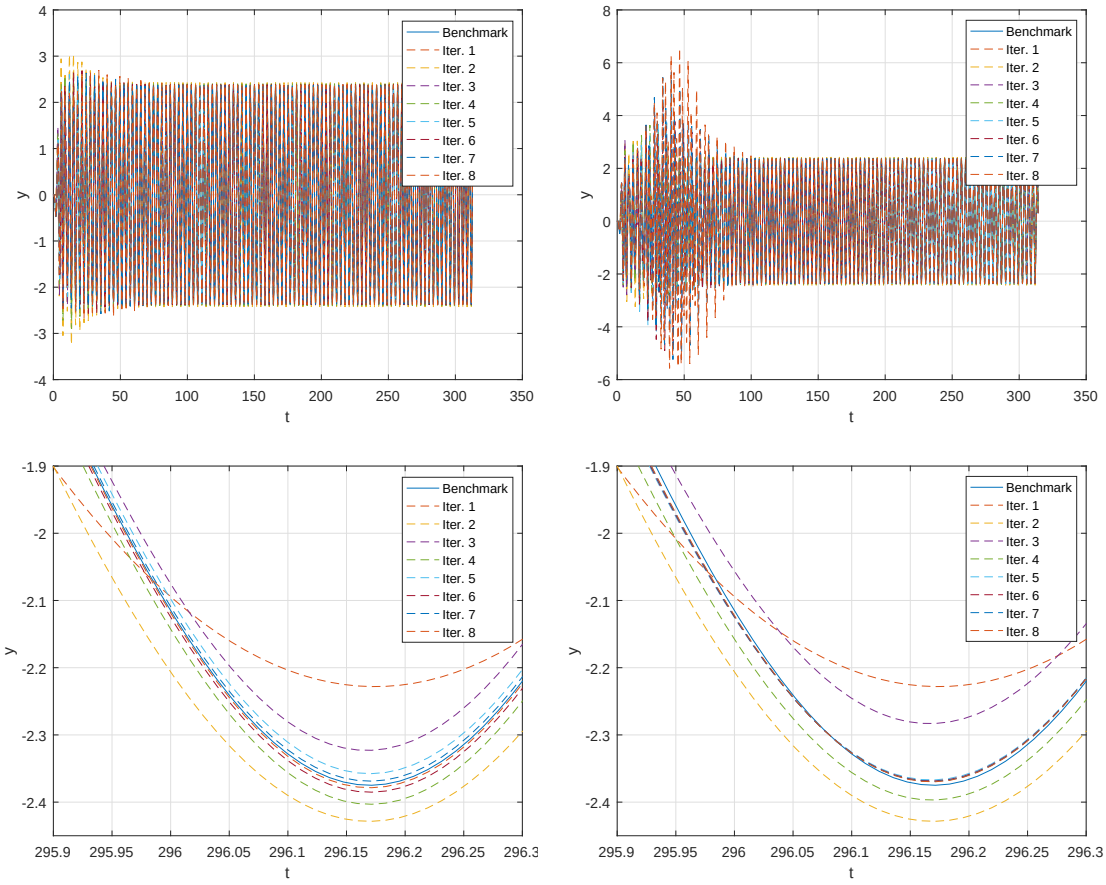

(a) Use the two previous iterations.

(b) Case 2: Use all the previous iterations.

Fig. 6.4 Averaging the error term.

as the last weighting factor is 1 to fully enclose the right solution. Explicitly, the iteration steps for this method are,

$$\begin{aligned} L_H(y_0) &= F_H(t) \\ L_H(y_1) &= F_H(t) + \frac{1}{n} \cdot R_H(y_0) \\ L_H(y_2) &= F_H(t) + \frac{2}{n} \cdot R_H(y_1) \\ &\dots \\ L_H(y_n) &= F_H(t) + 1 \cdot R_H(y_{n-1}). \end{aligned} \tag{6.22}$$

The result of the iteration method for this case is illustrated in Fig.6.5a for four iterations. This is compared to a more successful case explained in the the next section where the error term is weighted and averaged at the same time. The iteration method in this case does not manage to capture the exact solution at least for this number of iterations. This is one of the disadvantages of the weighting method when used by itself which requires to know approximately the number of iterations needed for the solution to converge.

6.5.3 Averaging and Weighting the error term

The two methods -averaging and weighting- in 6.5.1 and 6.5.2 can also be combined so that the iteration steps look like,

$$\begin{aligned} L_H(y_0) &= F_H(t) \\ L_H(y_1) &= F_H(t) + \frac{1}{n} \cdot R_H(y_0) \\ L_H(y_2) &= F_H(t) + \frac{2}{n} \cdot \left(\frac{1}{2} (R_H(y_1) + R_H(y_0) \right) \\ &\dots \\ L_H(y_n) &= F_H(t) + 1 \cdot \left(\frac{1}{2} R_H(y_{n-1}) + R_H(y_{n-2}) \right). \end{aligned} \tag{6.23}$$

The result of this case is given in Fig.6.5b. It captures the full solution by the fourth iteration outperforming the cases in the previous sections illustrated in Fig.6.5a and Fig.6.4.

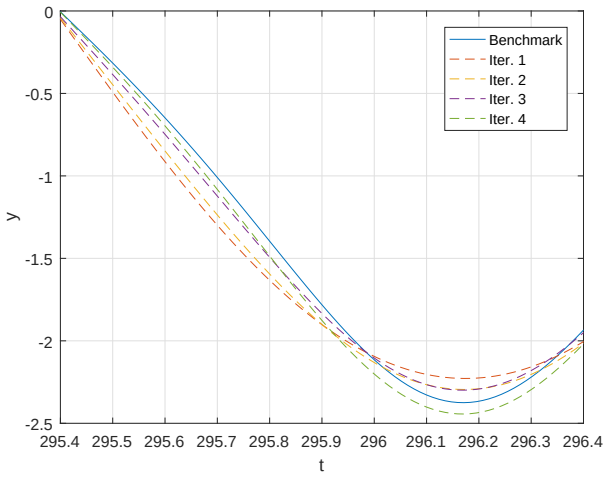

(a) No averaging.

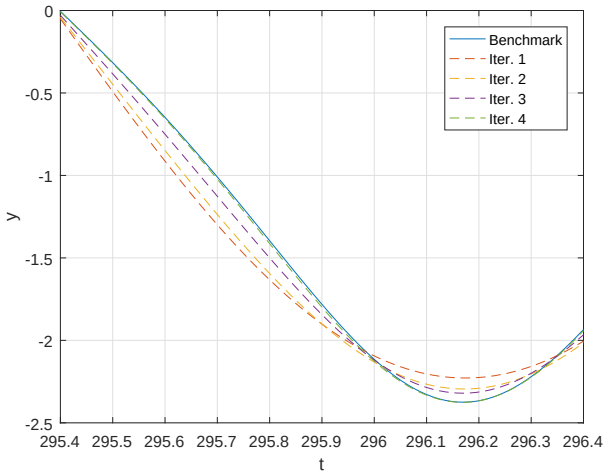

(b) With averaging.

Fig. 6.5 Weighting the error term.

6.5.4 Manipulating the error function

In Fig.6.2 the error function of the system under white-noise input is illustrated. Similarly, in Fig.6.6 the error function $R_H(y)$ (continuous navy blue line) of the harmonically excited system is shown which is

$$R_H(y) = -\varepsilon_3 y^3 + \frac{3}{4}\varepsilon_3 A^2 y \tag{6.24}$$

Just like with the original system the error gets too big when the response y gets out of the range, $y < -\frac{1}{2}A$ and $y > \frac{1}{2}A$. This is where the absolute value of the error function excites the bound (red lines) of $R_H(y) = \frac{1}{4}\varepsilon_3 A^3$.

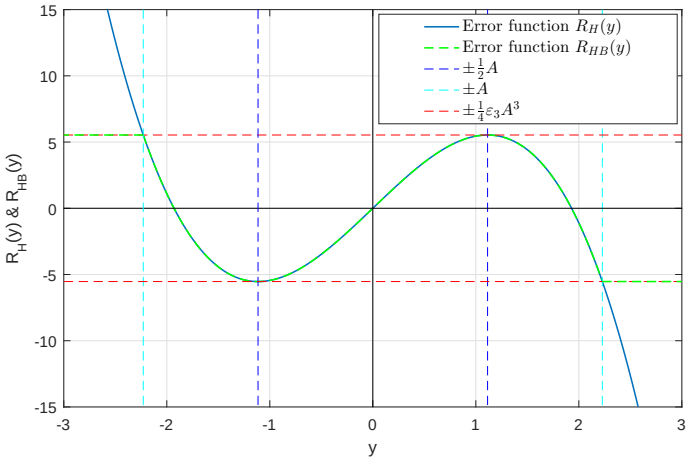

Fig. 6.6 The error functions $R_H(y)$ and $R_{HB}(y)$.

As a result, a new error function $R_{HB}(y)$ is defined which is bounded within the desired bounds. This is a piecewise function where for $-A \geq y \leq A$, the new error function is the same as the original one. However, for $y < -A$, $R_{HB}(y) = \frac{1}{4}\varepsilon_3 A^3$ and $y > A$, $R_{HB}(y) = -\frac{1}{4}\varepsilon_3 A^3$. Specifically, this new error function is defined as

$$R_{HB}(y) = \begin{cases} \frac{1}{4}\varepsilon_3 A^3 & \text{for} \quad y < -A \\ -\varepsilon_3 y^3 + \frac{3}{4}\varepsilon_3 A^2 y & \text{for} \quad -A \geq y \leq A \\ -\frac{1}{4}\varepsilon_3 A^3 & \text{for} \quad y > A. \end{cases} \tag{6.25}$$

and is illustrated in Fig.6.6 by the discontinuous green line along with the original error function (continuous navy blue line) and the boundary lines (horizontal discontinuous red lines). In this way, the error function will be clipped at the boundaries not allowing for high amplitude input impulses into the system which could eventually had lead to a non-converging solution.

The results of this case with no averaging and with averaging of the error term are illustrated in Fig.6.7a and Fig.6.7b respectively. In both cases together with the system response, the evolution of the error term is also demonstrated for eight iterations. The clipping of the error function resulting from the new piece-wise error function converges to its correct value faster when the averaging of the error term is applied. Hence, the systems also converges to correct solution faster in this case.

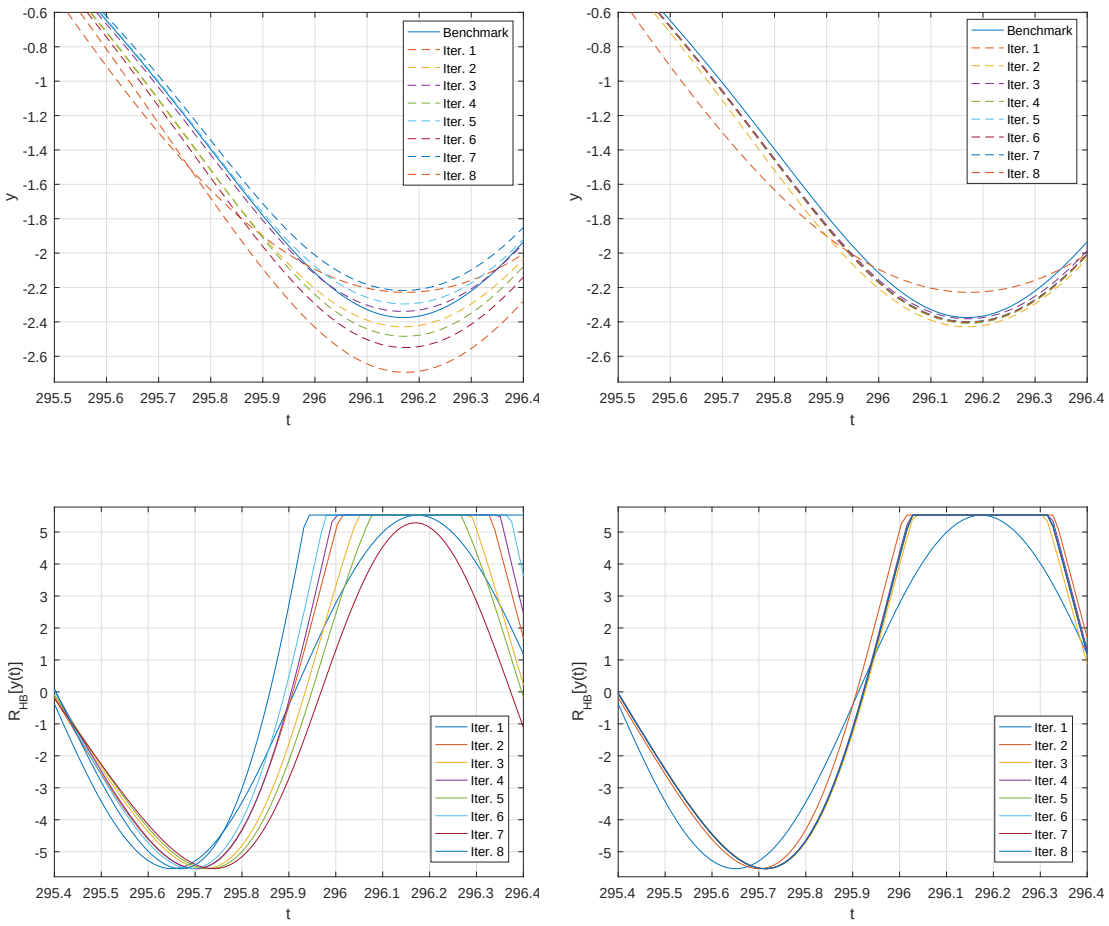

(a) No averaging.

(b) With averaging.

Fig. 6.7 Manipulating the error function. Top: Steady-state solution from time history. Bottom: The error function corresponding to the steady-state solution above.

6.6 Methods to ensure convergence for the original system

In this section, we go back to the original nonlinear random system described by Eq.(6.1). The iteration method was shown in section 6.3 not to be working for this system since it could not find a convergent solution. The reasons leading to this failure were explained in section 6.3 where the behaviour and the effect of the error function, Eq.(6.24), were explained and illustrated in figures Fig.6.2 and Fig.6.3. In short, it was shown that the non-convergence is due to the value of the error function which gets amplified because of its cubic nature when the response is greater than a threshold value equal to $2\varepsilon_3\sigma_y^3$; where ε_3 is the nonlinear coefficient and σ_y is the variance of the linearised response.

Three methods to overcome the problem of non-convergence are presented in this section. The first two methods work well only for weak nonlinearities and have nothing to do with correcting the iteration method itself. The third method is more sophisticated and works for stronger nonlinearities. This method is an extension of the work in section 6.4 and 6.5 where the iteration method was performed on a harmonically excited system. Various alternations and manipulations of the error function were investigated that allow for a convergent solution for this system.

6.6.1 Method 1: Selecting simulations with correct time history

For weak nonlinearities (i.e. small values of ε_3) not all time-history simulations lead to a non-convergent solution like the one in Fig.6.3. As a result, the ones that do converge are chosen to form the ensemble of simulations used to calculate the first Wiener kernel for each iteration.

An example of this shown in Fig.6.8b for a system with $\varepsilon_3 = 0.2$ and $\beta = 0.15$ where five iterations were performed and compared with a benchmark solution of the original system. As it can be seen the first two iterations are close to each other and far from the solution. This is an expected behaviour since the first iteration describes a linear system and the second one uses the error of the first iteration which is very small. Further iterations approach the the benchmark solution suggesting a conversion towards the solution.

Apart from the restriction on the strength of nonlinearity, a drawback of this method is the number of simulations that need to be performed in order to get a good sample of 'good' or converging simulations. The percentage of accepted simulations drops as the strength of the nonlinearity increases hence, more simulations are required to be performed.

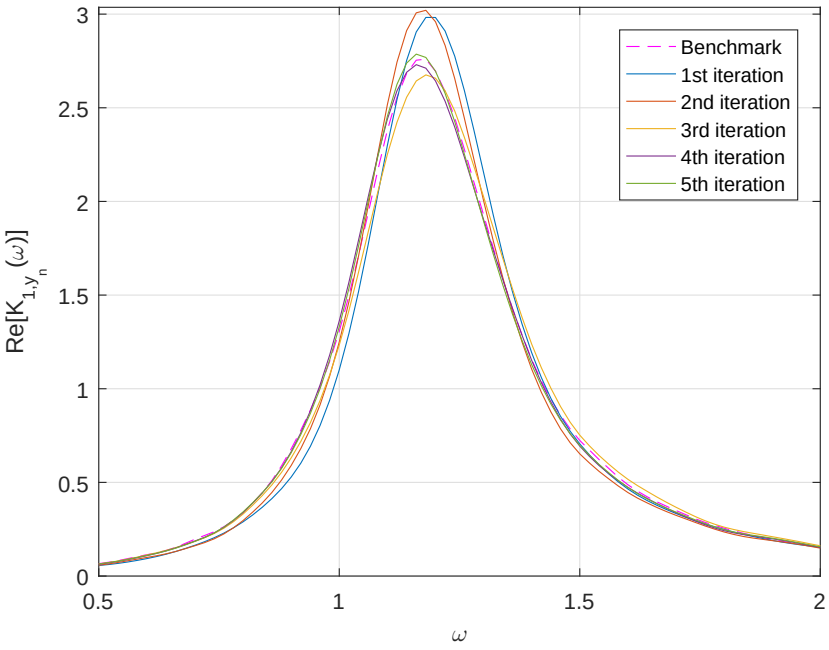

(a)

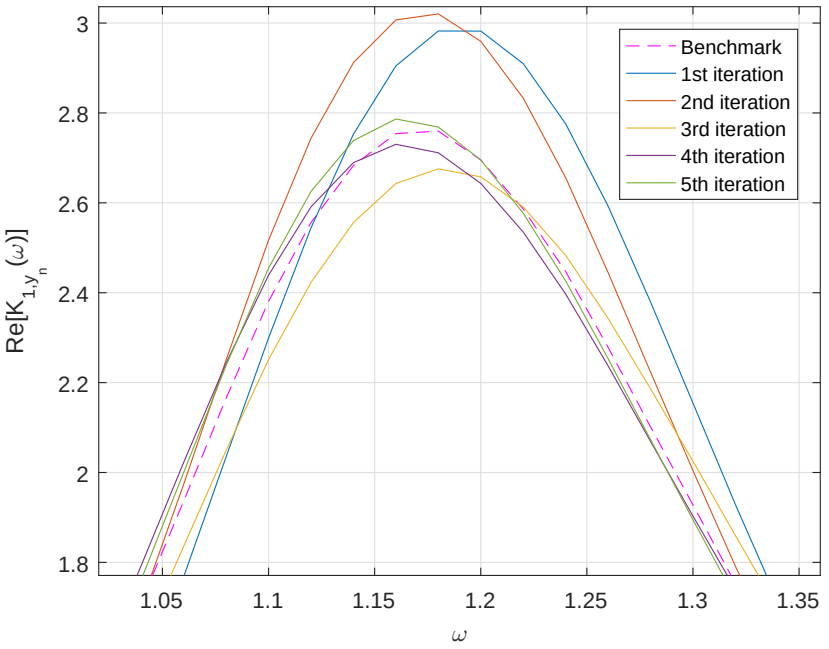

(b)

Fig. 6.8 Example of a corrected iteration procedure which allows for convergence when choosing simulations with correct time history. Parameters used: $\varepsilon_3 = 0.2$, $\beta = 0.15$.

6.6.2 Method 2: Local correction of the time-history

The second method used to ensure a convergent solution for the iteration method works for a systems with slightly stronger nonlinearity compared to the one for systems where the first methodology described above works. Regardless, the strength of nonlinearity is still considered to be weak.

In this case, we do not seek the cases were a convergent solution takes place. Instead, a small non-convergent window is allowed for the response's time-history at later iterations. This window is identified and corrected by replacing it with the response of the first iteration which ensures a convergent solution since it describes a linear system.

For a system with $\varepsilon_3 = 0.5$ and $\beta = 0.15$ the first four iterations are plotted in Fig.6.9. On the fourth iteration $y_3(t)$, between $t = 125$ and $t = 175$ the response does not stay within the desired bounds which eventually lead to a non-converging solution. Therefore, the response within this range is replaced by the response of the first iteration step, $y_0(t)$.

The result of this local correction on the response of the fourth iteration step results in a converging solution illustrated in Fig.6.10. Similarly to the first method in section 6.6.1, the first two iterations are far away from the benchmark solution due to the fact that the first iteration describes a linear system and the second one uses the error of the first iteration which is very small. By the fourth iteration a satisfied solution has been achieved that closely matches the benchmark solution.

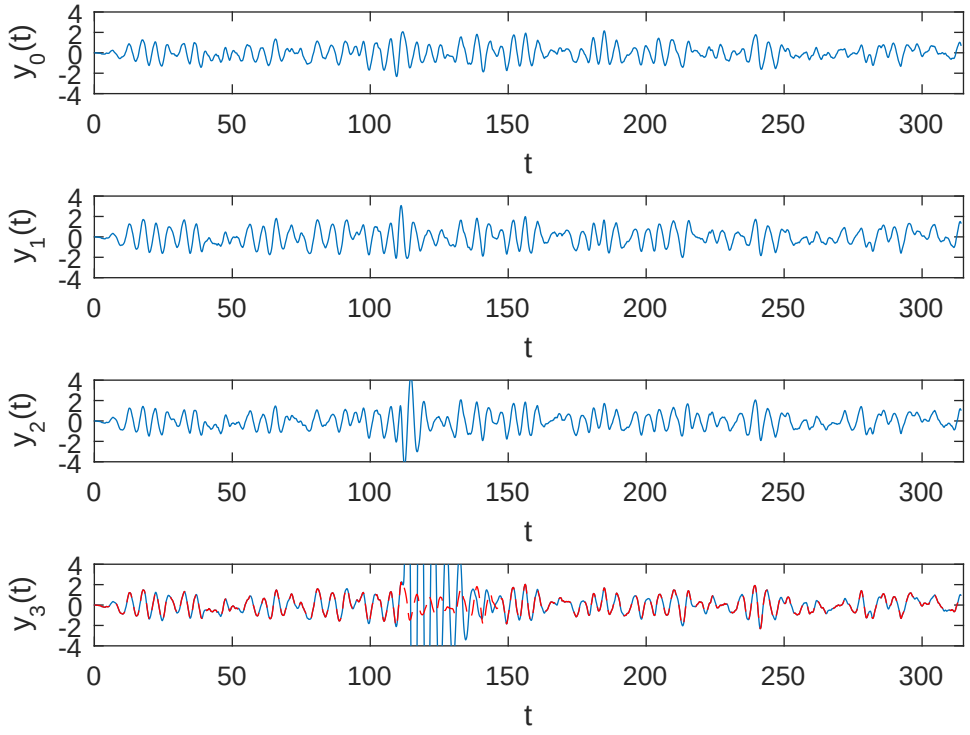

Fig. 6.9 The response at each of the four iterations. Blue is the original response. In the fourth iteration the red line corresponds to the corrected response. Between $t = 125$ and $t = 175$ the response of the forth iteration does not stay within the desired bounds so it is replaced by the response of the first iteration at that specific window. Parameters used: $\varepsilon_3 = 0.5$, $\beta = 0.15$.

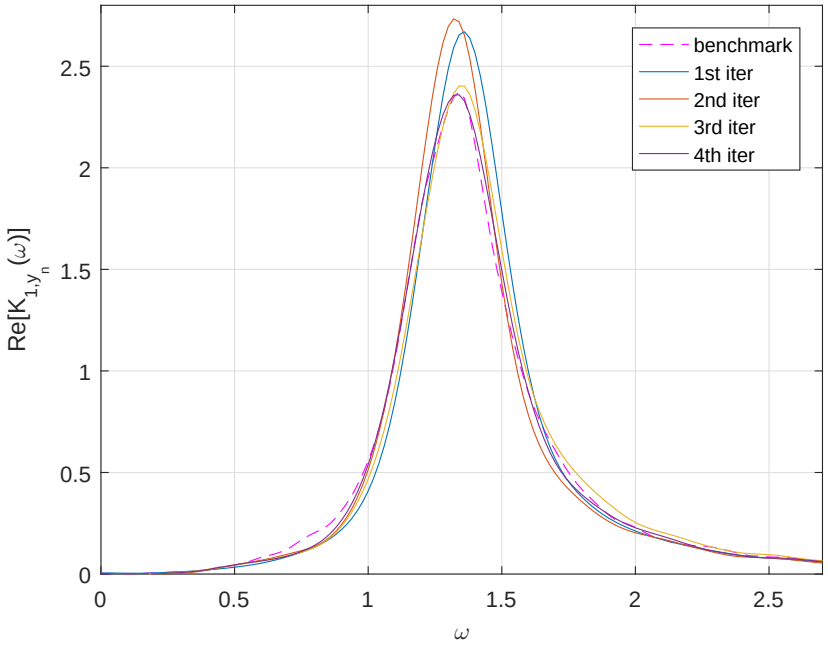

(a)

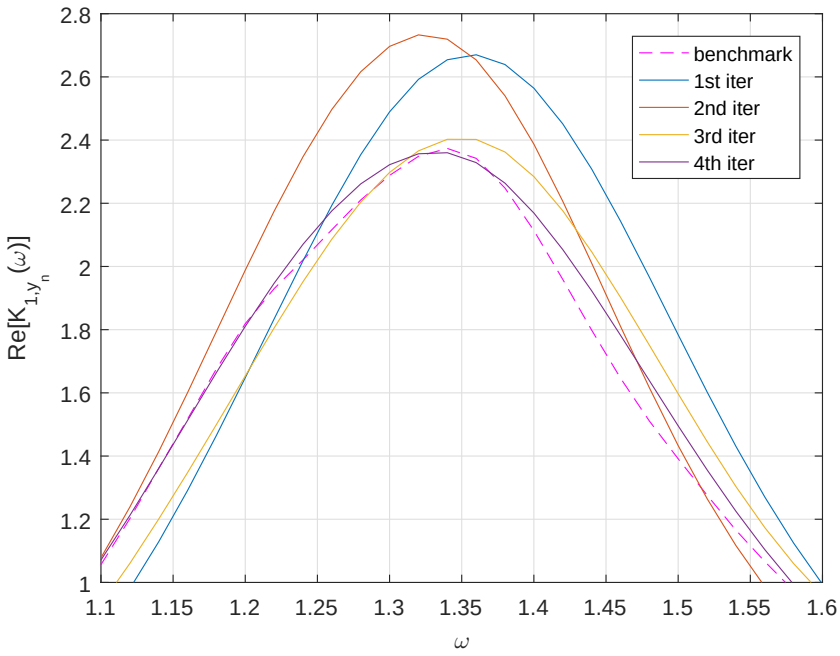

(b)

Fig. 6.10 Example of a corrected iteration procedure which allows for convergence when locally correcting the time-history of the response. The Parameters used: $\varepsilon_3 = 0.5$, $\beta = 0.15$.

6.6.3 Method 3: Averaging, Weighting and Manipulating the error function

This third method extends the techniques described in section 6.4 to the original nonlinear system under white-noise excitation. Because of the nature of this method which deals with the calculation of the error term, it can be applied to a system with stronger nonlinearity compared to the the two previous methods. As a results, it will applied on the same system as before, Eq.6.1, with $\beta = 0.15$ but nonlinear coefficient $\varepsilon_3 = 2$. Here, it should be noted that for all the following results in this chapter for the calculation of the first Wiener kernel in each iteration a smoothing algorithm was applied to eliminate the effect of noise on the kernels. Finally, a total of 50 simulations were used in each case to make up the ensemble for the calculation of the first kernel.

Averaging and weighting the error term.
The first techniques introduced in section 6.5 were the averaging and weighting of the error term. Their combined performance on the harmonically excited system was formulated and applied in section 6.5.3. The same idea is now applied to the original system. Any of the two ways -use two previous iterations or use all previous iterations- of averaging the error term can be used. The results for both are very similar, thus, for simplicity we only demonstrate the case where the averaging is calculated by using the results by two previous iterations only. Stating this, the iteration method for the original system is now,

$$\begin{aligned} L(y_0) &= \xi(t) \\ L(y_1) &= \xi(t) + \frac{1}{n} \cdot R(y_0) \\ L(y_2) &= \xi(t) + \frac{2}{n} \cdot \left(\frac{1}{2}(R(y_1) + R(y_0) \right) \\ &\dots \\ L(y_n) &= \xi(t) + 1 \cdot \left(\frac{1}{2} R(y_{n-1}) + R(y_{n-2}) \right). \end{aligned} \tag{6.26}$$

The results of this procedure are illustrated in Fig.6.11 where the first Wiener kernel of the response at each iteration is plotted for four and seven iterations respectively. Fig.6.11a suggests that four iterations can get us close to the desire solution. However, an increased number of iterations can improve the agreement between the kernel of the final iteration and that of the desired solution as shown in the bottom figure.

The progress from a kernel representing a linear response (first iteration) to a kernel representing a nonlinear system (latter iterations) is clear in both of the figures. In the case of the seven iterations this progress is smoother due to the smaller difference between the weighting of the error term for consecutive iterations. Finally, the disagreement appearing in both plots between the iteration kernels and that of the original system between $1.3 < \omega < 1.5$ can be attributed to numerical limitations and can be improved with increasing the ensemble of simulations and by increasing the resolution of the solution in each simulation.

Averaging and weighting the error term plus a new error function.

In section 6.3 the error gets too big when the response y gets out of the range, $y < -2\sigma_y$ and $y > 2\sigma_y$. This is where the absolute value of the error function excites the bound of $2\varepsilon_3\sigma_y^3$.

As a result, a new error function $R_B(y)$ is defined which is bounded within the desired bounds, similarly to the one in Fig.6.6 for the harmonic case. This is a piecewise function where for $-2\sigma_y \geq y \leq 2\sigma_y$, the new error function is the same as the original one. However, for $y < -2\sigma_y$, $R_B(y) = 2\varepsilon_3\sigma_y^3$ and $y > 2\sigma_y$, $R_B(y) = -2\varepsilon_3\sigma_y^3$. Specifically, this new error function is defined as

$$R_B(y) = \begin{cases} 2\varepsilon_3\sigma_y^3 & \text{for} \quad y < -\sigma_y \\ -\varepsilon_3 y^3 + 3\varepsilon_3\sigma_y^2 y & \text{for} \quad -2\sigma_y \geq y \leq 2\sigma_y \\ -2\varepsilon_3\sigma_y^3 & \text{for} \quad y > 2\sigma_y. \end{cases} \tag{6.27}$$

and is illustrated in Fig.6.12 by the discontinuous green line along with the original error function (continuous navy blue line) and the boundary lines (horizontal discontinuous red lines). For the specific system, Eq.2.30 is used to calculate the RMS value of the equivalent linear response which is $\sigma_y \approx 0.58$ for $\beta = 0.15$ and $\varepsilon_3 = 2$. Hence, the bounds will have an absolute value of $2\varepsilon_3\sigma_y^3 \approx 2 \cdot 2 \cdot (0.58)^3 \approx 0.77$. This agrees with the value indicated by the bounds (red lines) in Fig.6.12.

Changing the error function alone seems not to be enough in getting the first Wiener kernel with a satisfactory accuracy. This is shown in Fig.6.13 where the convergence to the solution is not uniform to start with and secondly, it is not accurate since by the 5^{th} iteration the solution does not get to agree with the benchmark solution.

Because of the above unsatisfactory results, in addition to the new error function, the averaging and weighting of the error term are also implemented just like in the previous subsection. The results of the iteration method after all these modifications are shown in Fig.6.14. The same method is applied for four (Fig.6.14a) and five (Fig.6.14b) iterations. It is shown that the iteration method achieves a good agreement with the desired solution with the use of only four iterations. In the case of the five iterations (bottom plot) the solution of

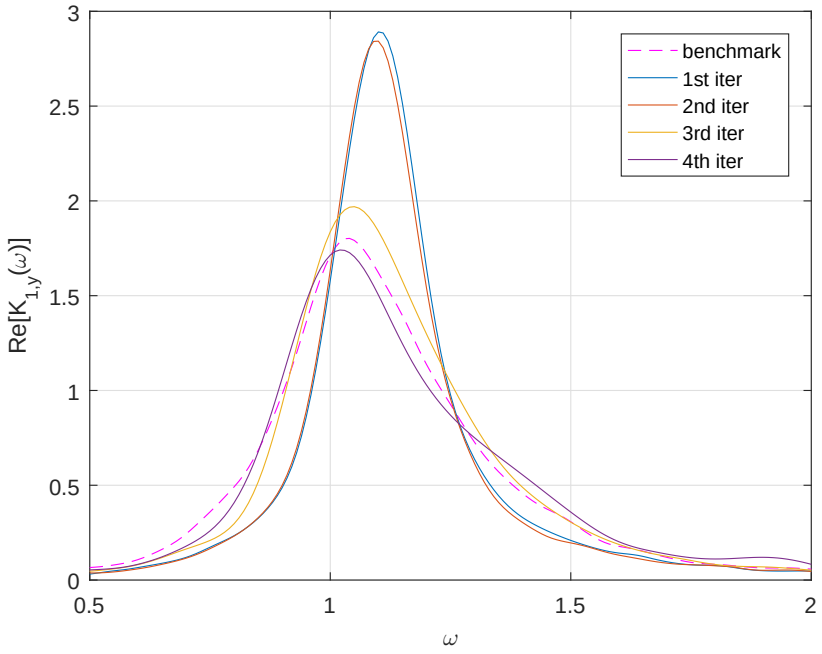

(a) 4 iterations

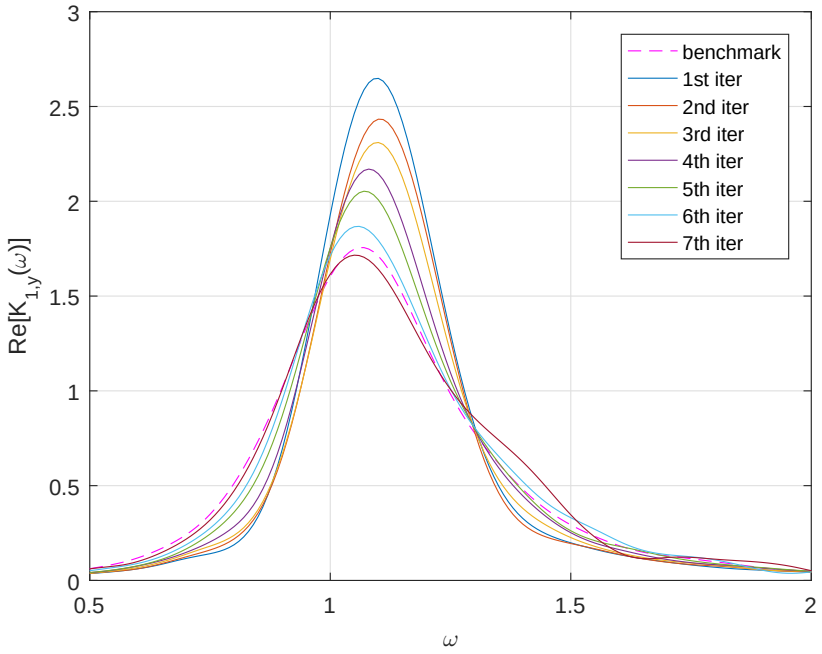

(b) 7 iterations.

Fig. 6.11 Applying the averaging and weighting techniques on the error term. The error function takes its original form as expressed in Eq.6.24 and illustrated in Fig.6.2. Parameters used: $\varepsilon_3 = 2$, $\beta = 0.15$.

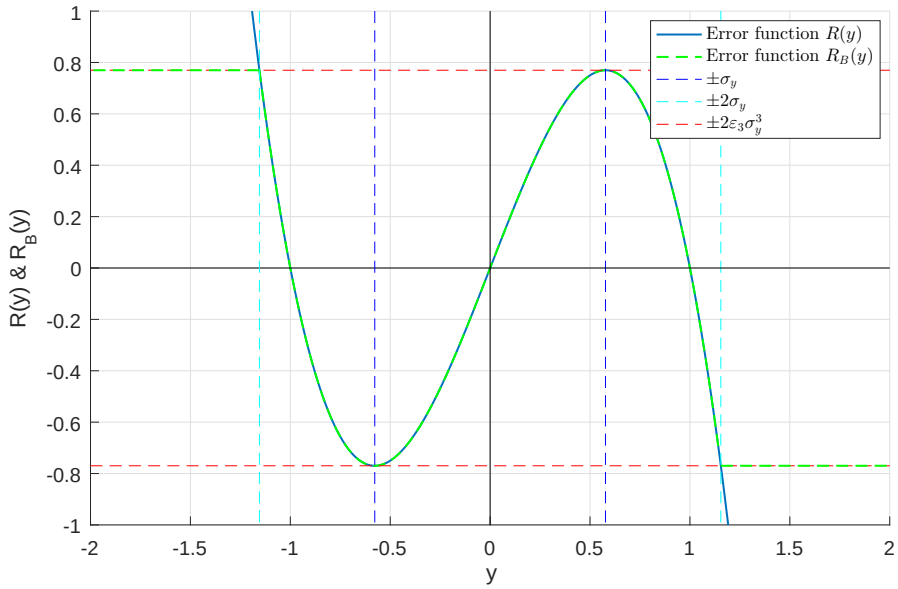

Fig. 6.12 The error functions $R(y)$ and $R_B(y)$. Parameters used: $\beta = 0.15$ and $\varepsilon_3 = 2$.

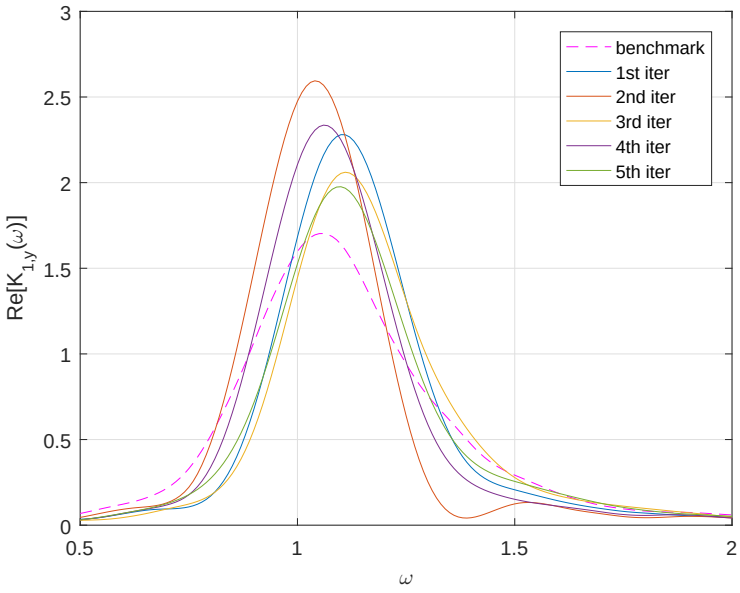

Fig. 6.13 The first Wiener kernel for each of the five iterations in the case where the new error function (Eq.(6.27) and Fig.6.12) is used. Parameters used: $\beta = 0.15$ and $\varepsilon_3 = 2$.

the latter iteration has a very small improvement compared to the the latter iteration in the case of the four iterations (top plot).

Finally, we should check how the TF $G(\omega)$ behaves during the iteration procedure and how it is shaped for each iteration. We recall that $G(\omega)$ is a TF between the first Wiener kernel of the nonlinear force and that of the system's response. Hence, the TF between the first kernel of the nonlinear force $z_n = y_n^3$ where n denotes the n^{th} iteration and that of the respective iteration response y_n will be calculated such that,

$$G_n(\omega) = \frac{K_{1,z_n}(\omega)}{K_{1,y_n}(\omega)} \tag{6.28}$$

Fig.6.15 shows the TF for the first, third and fifth iterations each of which is compared to the TF of the benchmark system. As expected, the first iteration, Fig.6.15a, is describing a linear response hence the TF $G_1(\omega)$ is having a flat real component and a zero imaginary component. By the third iteration the response incorporates nonlinear behaviour with the phase lag on the TF taking place which results to $G_3(\omega)$ having a positive non-constant imaginary part and a non-constant real part. This TF though does not perfectly match the TF of the benchmark system since the first kernels of the two in Fig.6.14 do not match either. This mismatch is perfected by the fifth iteration where $G_5(\omega)$ in Fig.6.15c matches the TF of the benchmark system well. By that point, the iteration method captures the full effect of the phase lag taking place on the TF improving the agreement between the two plots which also explains the agreement between their kernels in Fiq.6.14.

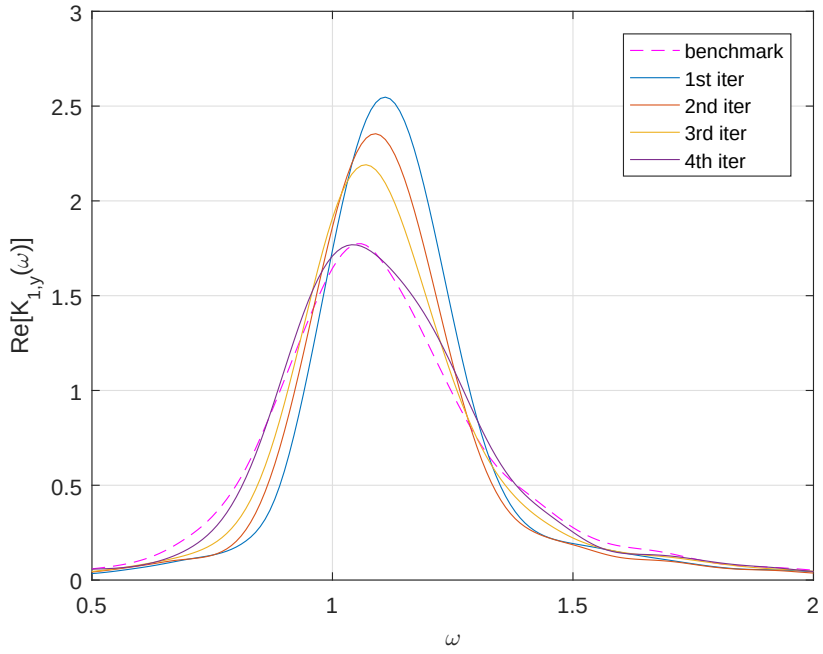

(a) 4 iterations

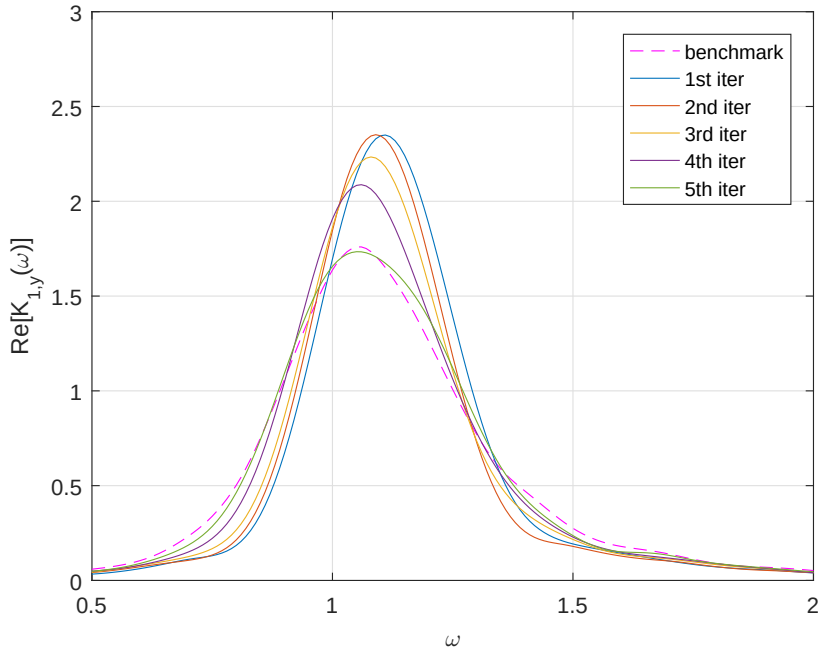

(b) 5 iterations.

Fig. 6.14 Applying the averaging and weighting techniques on the error term. The error function also takes the new form expressed in Eq.(6.27). Parameters used: $\varepsilon_3 = 2$, $\beta = 0.15$.

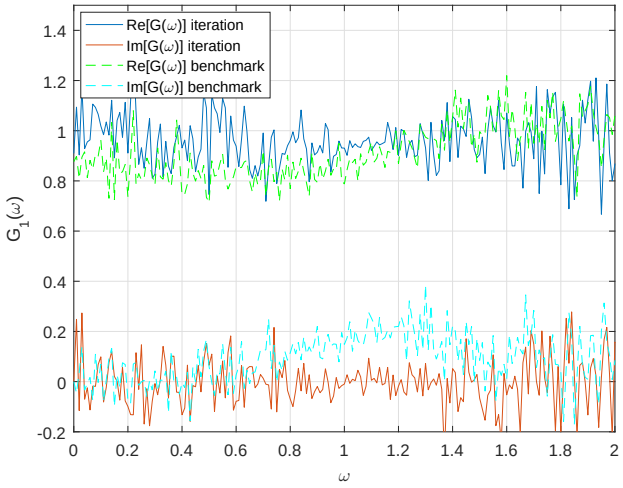

(a) first iteration.

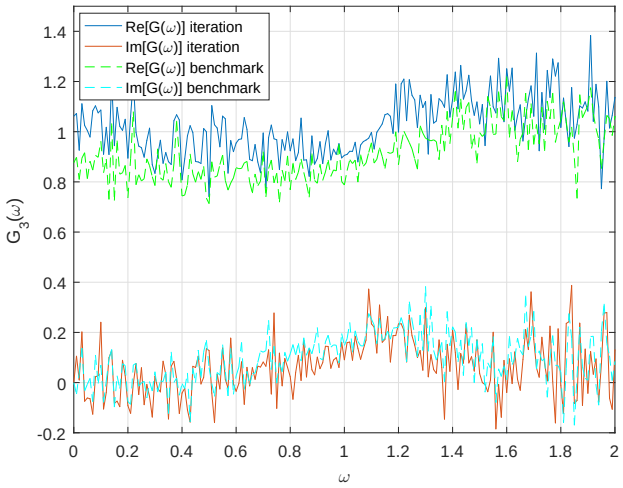

(b) 3^{rd} iteration.

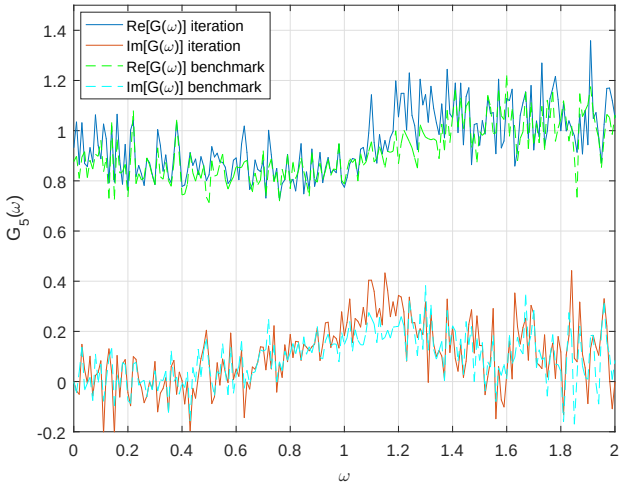

(c) 5^{th} iteration.

Fig. 6.15 The TF $G(\omega)$ for three of the iterations of the case in Fig.6.14b.

6.7 Relating the iteration method to the model of the isolated nonlinear spring

In the previous sections, it was demonstrated how the iteration method can be used to solve the nonlinear Duffing oscillator with white-noise input. The importance of the error in getting a converging solution was explained and modifications for its estimation were applied to get the results in section6.6.

In this section, an attempt will be made to 'marry' the results of the iteration method on the nonlinear systems with the ones presented in section 5.5 where a method to model the behaviour of an isolated nonlinear spring was presented.

The successful model of the isolated spring is described by the set of equations in Eq.(5.5). The first step in this model is to pass the input (white-noise) through a linear filter. Then, we raise the output from the first step into an odd power before passing it through another linear filter. The cube of the later output can model the response of an isolated nonlinear spring. In contrast to a linear response, this inherits the interesting property of a non-constant TF between the first Wiener kernel of the nonlinear force and that of the system's response as illustrated in Fig.5.3d and Fig.3.2a which forms the basis for the SP method introduced in Chapter 3.3.

The model for describing the isolated nonlinear spring acted as a motivation in using the iteration method to solve the nonlinear system in this chapter. Looking closer at the iteration method, one can observe a similar process followed by the model of the nonlinear spring described above. From Eq.(6.7) where the iteration procedure is summarised the following can be said for each of the steps comprising it.

In the first iteration, the solution of a linear operator describing a dynamical system under white-noise is found just like with the first step in the isolated spring:

$$\begin{aligned} &\text{Nonlinear spring step 1: } g(t) = \int h(t-\tau)\xi(\tau)d\tau \\ &L(y_0) = \xi(t) \quad \mapsto \quad y_1(t) \sim \int L(y_0(t-\tau))\xi(\tau)d\tau. \end{aligned} \tag{6.29}$$

For the second iteration, the error term $R(y)$, Eq.(6.24), appears for the first time. This is composed by a linear, $3\varepsilon_3\sigma_y^2 y$, and a nonlinear term, $-\varepsilon_3 y^3$. The fact that the response from the previous iteration is now taken to a cubic power through the error term ($y_0(t) \rightarrow R(y_0(t)) \sim y_0^3(t)$) can be paralleled to the nonlinear operation performed on the output of the first response in Eq.(5.5) in the case of the nonlinear spring. After this nonlinear operation the same linear operator which now acts on a nonlinear input (the nonlinear term and the

white-noise) just like the second step in the spring's case where the nonlinear input ($g^n(t)$) is filtered by another linear filter, $w(t)$. The parallel between the two cases can be demonstrated by,

$$\begin{aligned} &\text{Nonlinear spring step 2: } x(t) = \int w(t-\tau) g^n(\tau) d\tau \\ L(y_1) = \xi(t) + R(y_0) \quad &\mapsto \quad y_2(t) \sim \int L(y_1(t-\tau))(\xi(\tau) + R(y_1)) d\tau \\ &\mapsto \quad y_2(t) \sim \int L(y_1(t-\tau))(\xi(\tau) - \varepsilon_3 y_1^3(\tau) + 3\varepsilon_3 \sigma_y^2 y_1(\tau)) d\tau. \end{aligned} \tag{6.30}$$

This new output, $y_2(t)$ when raised to an odd power (i.e. cubic) to represent a nonlinear force, $z(t) = y_2^3(t)$, inherits some of the nonlinear properties we were expecting to see for our system. These include the non-constant TF $G(\omega)$ as observed and illustrated in Fig.5.3d for the nonlinear spring and Fig.6.15 for the iteration method.

Due to the way the error is calculated in the iteration process where it is smoothed-out using the averaging and weighting techniques to avoid big values for the error in order to ensure convergence, a further number of iterations may be required to get the actual solution of the system. This was observed in Fig.6.15 where despite the fact that by the third iteration the TF $G(\omega)$ exhibits the nonlinear behaviour of the phase lag that causes its imaginary part to be positive non-zero and the real part to be non-constant, the first Wiener kernel of the third iteration, Fig.6.14, has not reached the desired solution. As it can be seen in this same figure, more iterations can improve the accuracy of the result.

6.8 Conclusion

The motivation for this chapter was to relate the findings from chapter 5 from a nonlinear isolated spring to a nonlinear system. This enables us to understand the mechanism causing the phase lag observed in earlier chapters over the TF between the first Wiener kernel of the nonlinear force and that of the system's response referred throughout this thesis as $G(\omega)$.

The iteration method introduced early in this section was formulated to solve a rearranged form of the original nonlinear system, the Duffing oscillator. The method is characterised by an iterative procedure for solving a linear operator under a white-noise and an error term, summarised by the scheme in Eq.(6.7).

Initially, it was shown that the iteration could not lead to a converging solution. An example of this is shown in Fig.6.1 where after a number of iterations the response shoots leading to a diverging solution. The cause of this behaviour was explained through the study of the error function, Eq.(6.4), describing the error term in the iteration. It was shown that

once the error function takes a value higher than the threshold value, $|2\varepsilon\sigma_y^3|$, indicated by the red line in Fig.6.2 the system takes the input from the error as an impact to the system that takes some time to die out. This transient effect on the system is causing the solution to diverge.

In order to enable the iteration method to reach a converging solution a pilot investigation was performed on a harmonically excited nonlinear system. The averaging and weighting techniques on the error term were introduced in section 6.5.3 and in section 6.5.4 a modification on the error function was suggested. All these approaches were shown to have a smooth progression on the calculation of the error term enabling the iteration method to settle in a convergence solution.

The suggested techniques from the harmonically excited system were then applied onto the original Duffing system with white-noise input, section 6.6.3. The approach combining these methods resulted in a converging iteration scheme even for strong nonlinearities and for a small number of iterations. An illustration of a successful case using this approach is plotted in Fig.6.14. For the same example, the evolution of the TF $G(\omega)$ for each iteration was demonstrated in Fig.6.15. From this figure, the clear evolution from a linear response to the exact nonlinear system response matching the benchmark system is illustrated.

In addition to the above approach two other approaches that make the iteration method workable for weak nonlinearities were suggested. The first of these methods required the selection of only the simulations with converging time history to make up the ensemble required to calculated the kernels for each iteration method, section 6.6.1. The second one required the local correction on the time history of latter iterations as demonstrated in Fig.6.9 in order skip out on the high amplitude response that would have cause the error term to shoot leading to a non-converging solution.

After the successful performance of the iteration method for the original nonlinear system, an attempt to explain the mechanism causing the phase lag in the TF $G(\omega)$ was performed in section 6.7. This was done in combination to the results from section 5. A parallel comparison between the successful model of the isolated spring in the previous chapter and the iteration method from this chapter was performed in detail to show that the same principles were applied to both cases. These principles are the cause of the phase lag which gives the particular shape to the TF $G(\omega)$ as observed in previous chapters.

Chapter 7

Conclusions and Future Work

7.1 Conclusions

Nonlinear dynamics is a notoriously difficult subject. In this thesis, the behaviour of nonlinear systems under white-noise input was investigated based on the well established Wiener series theory. The outcomes of this project could potentially be useful to engineers in industry to quickly predict the response statistics of such systems, as well as being of great assistance in understanding the underlying physics of these systems.

More specifically, the objective of this thesis was to use the Wiener theory introduced in Chapter 1 for nonlinear systems under white-noise input in order to improve the well establish method of Equivalent Linearisation (EL). As a first step, the behaviour of the first Wiener kernel -a key element of the Wiener series- was explored and understood. Properties of the first kernel were demonstrated in Chapter 2 for systems with nonlinear stiffness and nonlinear damping. Once the behaviour of the first kernel was compared to EL also in Chapter 2 an alternative approach to improve EL known as single-pole fit (SPF) was suggested in Chapter 3. Some applications of this new method were illustrated in Chapters 3 and 4. Further research on the mechanism underlining this new methodology led to the investigation for the modelling of an isolated nonlinear spring in Chapter 5. Finally, it was shown that the same principles behind the successful model of the nonlinear spring also govern the nonlinear system as demonstrated through the iteration method in Chapter 6. The main conclusions arising from each chapter of this thesis follow in the next three subsections in more detail.

7.1.1 Observing the behaviour of the first Wiener kernel and comparison with EL

The main observation from Chapter 2 was that of the widening effect on the first Wiener kernel of the system when adding nonlinear stiffness in the system. This is illustrated in Fig.2.3a. Consequently, the same effect appears on the power spectrum of the response of a nonlinear system with linear damping since it is known that the power spectrum of the response is linearly proportional to the the real part of the first Wiener kernel. This was proven by Langley [40] and is demonstrated in Fig.2.4. This widening effect which is effectively adding extra damping in the system was analytically explained by a proof in 2.6. The proof is based on an energy approach for the energy transferred between the kernels. It was shown that the input energy which is already known to be absorbed by the first Wiener kernel is then transferred to the higher order kernels for a system with nonlinear stiffness. This loss of energy by the first Wiener kernel which increases when increasing the nonlinear stiffness is observed as 'additional damping' in the first kernel.

Next, the concept of EL was introduced and its performance for systems with nonlinear stiffness and nonlinear damping was demonstrated in Fig.2.7 and Fig.2.9 respectively. For a system with nonlinear damping only, EL is a very accurate for extracting the response power spectrum of the system. On the contrary, it fails to capture the power spectrum of the response for a system with nonlinear stiffness despite the fact that it can perform very well in estimating the RMS value of the response and the shifting in the natural frequency.

In both system cases, the contribution of the first Wiener kernel in the system was calculated. This was done by a direct calculation of the kernel in each case as well as by the calculation of the coherence function. As expected, in the case of the system with nonlinear damping the first Wiener kernel is highly dominant since its contribution in the system is prevailing. This is shown in Fig.2.16 and confirmed by the coherence function results in Fig.2.17. Now, Fig.2.14 and the related results from the coherence function in Fig.2.15 show that for a system with nonlinear stiffness the contribution of the the first Wiener kernel to the system decreases when increasing the nonlinear stiffness. These results were the motivation that led to the energy approach proof mentioned before to explain the behaviour of the first Wiener kernel.

7.1.2 Improving EL: The Single-Pole Fit method

Observing the limitation of EL to accurately estimate the response power spectrum of a system with nonlinear stiffness, a method of enhancing EL was introduced in Chapter 3.

This requires the fitting of an appropriate function over the transfer function (or Frequency Response Function) between the first Wiener kernel of the nonlinear force and the first Wiener kernel of the system response. The TF defined in Eq.(3.15) is set to be a constant value for EL. However, as it can be seen by its calculation from the data simulations in Fig.3.2a this can not be correct. Therefore, a single-pole function (orange line in Fig.3.2a) whose parameters are chosen empirically by trial and error is chosen instead to fit this TF. Using this new fitting approach, results in an accurate calculation of the first Wiener kernel as illustrated in Fig.3.2b especially compared to EL.

The validity of this new approach was tested and demonstrated for higher order of nonlinear stiffness. As with quintic nonlinear stiffness is presented by Fig.3.3 in section 3.3.1.1. Additionally, in section 3.3.1.2 the application of the SPF method was performed for a system with both nonlinear stiffness and nonlinear damping. The way do this is to firstly linearise the nonlinear damping in the equation since it was shown already that EL works well for nonlinear damping. This results into a new system with nonlinear stiffness only where the SPF method can be applied just like before.

Moreover, the extension of the SPF method for a 2DOF system with white-noise base excitation was explored in Chapter 4. Two different cases of this system were investigated which showed that additional poles maybe required for the fitting function -Eq.(4.15) and Eq.(4.19)- in order achieve the desired results. Specifically, it was shown that the number of poles required is dependent on the structure of the system and the position of the nonlinear elements in the system. For the first case in section 4.3 where the nonlinear spring is between the base and the first mass was shown that a double-pole fit is required while for the second case in section 4.4 where the nonlinear spring is between the two masses a triple-pole fit is needed.

The SPF can be of great assistance in solving nonlinear random problems. If we could express the SPF parameters in terms of the system parameters, the creation of an ensemble of simulations or experiments for calculating the first Wiener kernel of a system would not be required for the SPF. As a result, it could be used in the quick prediction of the response statistics for these systems when the system parameters are known. This could potentially be extremely useful in industry where response statistics of structures with known parameters and white-noise input are investigated. An example of this would be a wind turbine where the wind can be assumed to be white-noise input and blade parameters such as the length and material properties are known. If the nonlinearity in the blade could be simplified to be of the form, y^n, the response statistics of the blade could potentially by found using an appropriate SPF model for the blade if blade parameters could be related to the SPF parameters.

SPF can also be useful in the reverse problem where the system parameters are not known but need to be identified. Experiments on these systems can be performed and the first Wiener kernel can be reconstructed from the experimental data. Properties of the SPF such as the natural frequency, the peak value, the real part initial and asymptotic value can be used to identify the parameters of the system. Once more, all these could be achieved effectively if the calculation of the SPF parameters could be analytically expressed in terms of the system parameters. More thoughts on how this can potentially be achieved follow on the last section.

7.1.3 Modelling of an isolated nonlinear spring and relating it to the nonlinear system

After the implementation of the SPF method for various cases which confirmed its validity and robustness, the interest turned to the mechanism that causes the phase lag appearing in the SPF shaped TF $G(\omega)$.

To simplify things, an investigation was carried out on an isolated nonlinear spring. The aim was to model the nonlinear spring in the simplest possible way to exhibit the nonlinear behaviour observed in the previous chapters. This requires the TF $G(\omega)$ not to be a real constant suggesting EL approximations but instead, a complex function with positive imaginary part and non-constant positive part as explained by the Kramers-Kronig relations in section 3.3.1.1.

Four different cases were tested for this model. The successful model requires the linear filtering of the input which is then raised to an odd power before it is filtered again by another linear filter, Eq(5.5). It was also shown that the second linear filter has to be a single-pole shaped function similar to a frequency response while the first filter can be any function that will allow all the important frequencies around the resonance of the second filter to pass through. An example of the successful model is illustrated in Fig.5.3d.

In chapter 6, we applied the principles governing the successful model of the nonlinear spring onto the original nonlinear system. This was done by solving a rearrange form of the original system demonstrated by Eq.(6.13) using the iteration method. Initially, the iterative process formulated into a matrix form by Eq.(6.9) could not yield to a converging solution. This was demonstrated to be due to the nature of the error function incorporated in the procedure which causes an extreme jump in the amplitude of the response when the input from the previous iteration was passing the threshold of $2\varepsilon_3\sigma_y^3$, Fig.6.2.

Different ways to ensure convergence in the iteration method were suggested. One of these methods required the selection of only the simulations with converging time history to make up the ensemble required to calculated the kernels for each iteration method, section

6.6.1. The second one required the local correction on the time history of latter iterations as demonstrated in Fig.6.9 in order to replace the high amplitude response that would have caused the error term to jump abnormally leading to a non-converging solution. The third method had to do the the calculation of the error in the iterative procedure. An averaging and weighting technique was used to smooth out the calculation of the error and a manipulation of the error function to suppress high amplitude responses in the subsequent iterations was implemented. The latter techniques were firstly introduced and tested on a harmonically excited nonlinear system in sections 6.5.3 and 6.5.4 respectively.

Having the iteration method converging, in section 6.7 it was shown how the system shares the same principles with the successful model of the isolated spring. The simplified model of the nonlinear system as it is structured by the iteration method can potentially be of great importance in understanding the underlying physics of nonlinear systems. Additionally, the importance of having a mechanism made up of elementary operations to model the behaviour of a random nonlinear system can be useful in the sense that any analysis can be done more easily on a simplified model. It can even open the potential of duplicating complex behaviour using a series of basic and well understood operations. In the next section a few more points on how this simplified model can be exploited are suggested.

7.2 Suggestions for Future Work

Developing the SPF method to improve EL opens the door to many other potential challenging projects. An obvious one but possibly one of the most challenging too has to do with the parameter values (tabulated in Appendix C for each case) of the SPF. It has already been mentioned that the parameter values of the fitting function for all the cases demonstrated in this thesis are manually chosen by a trial and error method. This is clearly the main drawback of the method and a step in understanding it was briefly investigated in section 3.4 where some of it limitations were expressed. Hence, further research aimed to the analytical determination of these parameters would be very beneficial since it will eliminate human error and automate the process saving time. Ideally, the relationship between the pole function parameters and the system parameters need to be established in a generalised manner.

In doing so, the investigation in section 3.4 can be repeated in a more elegant way. This may help in eliminating the errors and uncertainty involved by the fact the the SP parameters where approximated solutions found using trial and error. As a result, optimisation techniques can be used to find the optimised SP parameters by eliminating the error between the SP function and the data from simulations. Finding the best SP parameters in this way, may help in the research for correlating these parameters with the system's parameters.

Further theoretical work that could emerge from this research is related to the type of system excitation. The original derivation of the Wiener series is for systems under white-noise input. In the literature review in Chapter 1 it was mentioned that Hawes and Langley [30] extended the Wiener theory for non-white inputs. As a result, the possibility of extending the SPF method using Hawes' results to nonlinear systems with non-white input will be an interesting investigation. The TF between the first Wiener kernel of the nonlinear force and the system response for the non-white noise input case can be calculated from the already known equations. However, it does not imply that this will also be a single-pole function. It would be very useful if we could relate this new TF with the single-pole function and see if this relation arises from a simple relationship between the two inputs.

The robustness of the SPF method was tested for a few types of nonlinear systems with cubic and quintic nonlinear stiffening force as well as for a system with nonlinear stiffness and nonlinear damping. Some further research can also be done on other types of nonlinear force such as a trigonometric one or on a Van der Pol [70] type of oscillator where a term in the differential equation contains both the displacement and velocity variables. A whole new investigation can also be performed by expanding the research for systems with band-limited noise. In addition, for the 2DOF system the multi-pole fitting method can be tested for non-base excitation but instead, exciting the masses individually.

Supporting the research around the SPF method the findings in chapters 5 and 6 of the simplified model giving rise to the complex nonlinear behaviour can be exploited. Analytical work can be performed in finding the exact linear filters in the model. These can then be used to calculate the SP function characterising the nonlinear system giving information on the pole parameters. In addition, based on the simplified model mentioned above, experiments -in vibrations or electronics- can be set up where well known elements representing the linear filters can be combined in the right way to produce certain nonlinear behaviour.

On a more practical note, the validity of the SPF method can be tested on real nonlinear systems. Experiments to confirm the theoretical work presented in this thesis can be performed. An appropriate nonlinear system can be used such as a clamped beam with a tip mass excited by an electromagnetic shaker. A pure white-noise input is very difficult to be produced by a shaker so, a way to instrument the experiment in a way to effectively simulate a white-noise input will need to be thought of.

Expanding on the experimental possibilities, the calculation of the first Wiener kernel from an experimental data can be used to identify and quantify nonlinearities in the structure. A way to translate the shape of the calculated kernels into the type of potential nonlinearities must be established. This can be done by combining the suggested work in the first paragraph of this section along with building a database of kernel examples of pre-established systems with already known nonlinearities. Methodologies like machine learning could be used to extract important information from such a database and relating parameters to structural properties.

References

[1] Atkinson, K. E. (1989). *An introduction to numerical analysis*. Wiley.

[2] Barahona, M. and Poon, C.-S. (1996). Detection of nonlinear dynamics in short, noisy time series. *Nature*, 381(6579):215–217.

[3] Barrett, R., Berry, M., Chan, T. F., Demmel, J., Donato, J., Dongarra, J., Eijkhout, V., Pozo, R., Romine, C., and van der Vorst, H. (1994). *Templates for the Solution of Linear Systems: Building Blocks for Iterative Methods*. Society for Industrial and Applied Mathematics.

[4] Barton, D. A. W., Burrow, S. G., and Clare, L. R. (2010). Energy Harvesting From Vibrations With a Nonlinear Oscillator. *Journal of Vibration and Acoustics*, 132(2):021009.

[5] Bendat, J. S. and Piersol, A. G. (1986). *Random Data: Analysis and Measurement Procedures*. John Wiley & Sons, 2nd edition.

[6] Bo, Z., Tiecheng, L., Dong, G., and Xiaolei, D. (2006). Application of Equivalent Linearization Algorithm on Voltage Transformer Protection during Fundamental Resonance in Power System. In *2006 IEEE 8th International Conference on Properties and applications of Dielectric Materials*, pages 361–364. IEEE.

[7] Bothwell, F. E. (1952). The Method of Equivalent Linearization. *Source: Econometrica*, 20(2):269–283.

[8] Bracewell, R. N. (2000). *The Fourier transform and its applications*. McGraw Hill.

[9] Brillinger, D. R. (1965). An Introduction to Polyspectra. *The Annals of Mathematical Statistics*, 36(5):1351–1374.

[10] Caughey, T. K. (1962). Equivalent Linearization Techniques. *The Journal of the Acoustical Society of America*, 34(12):2001.

[11] Charlier, C. (1914). Frequency curves of type A in heterograde statistics. *Ark. Mat. Astr. Fysik*, 9(25):1–17.

[12] Chatterjee, A. and Vyas, N. (2001). Stiffness Non-Linearity Classification Through Structured Response Component Analysis Using Volterra Series. *Mechanical Systems and Signal Processing*, 15(2):323–336.

[13] Collins (2012). Dictionary of Mathematics.

[14] Couliard, PY and Langley, R. (2001). Nonlinear dynamics of deep-water moorings. In *20th International Conference on Offshore Mechanics and Arctic Engineering; OMAE 2001*, pages Vol. 1: Offshore Technology, pp.47–56, Rio de Janeiro, Brazil.

[15] Da Silva, S. (2011). Non-linear model updating of a three-dimensional portal frame based on Wiener series. *International Journal of Non-Linear Mechanics*, 46(1):312–320.

[16] Da Silva, S., Cogan, S., and Foltête, E. (2010). Nonlinear identification in structural dynamics based on Wiener series and Kautz filters. *Mechanical Systems and Signal Processing*, 24(1):52–58.

[17] De L. Kronig, R. (1926). On the Theory of Dispersion of X-Rays. *Journal of the Optical Society of America*, 12(6):547.

[18] Deuflhard, P. P. (2004). *Newton methods for nonlinear problems : affine invariance and adaptive algorithms*. Springer.

[19] Digital Library of Mathematical Funtions (2017). Eighteen Orthogonal Polynomials, Classical Orthogonal Polynomials, Sums.

[20] Dubnov, S., Tishby, N., and Cohen, D. (1997). Polyspectra as measures of sound texture and timbre*. *Journal of New Music Research*, 26(4):277–314.

[21] Esmaeilzadeh Seylabi, E., Jahankhah, H., and Ali Ghannad, M. (2012). Equivalent linearization of non-linear soil-structure systems. *Earthquake Engineering & Structural Dynamics*, 41(13):1775–1792.

[22] Feldman, M. (2011). *Hilbert transform applications in mechanical vibration*. Wiley.

[23] Frechet, M. (1910). Sur les foncionelles continues. *Annales Scientifiques de L'Ecole Normale Superieure*, 27(3):193–216.

[24] Gammaitoni, L., Neri, I., and Vocca, H. (2010). The benefits of noise and nonlinearity: Extracting energy from random vibrations. *Chemical Physics*, 375:435–438.

[25] Garrè, L. and Kiureghian, A. D. (2010). Tail-Equivalent Linearization Method in frequency domain and application to marine structures. *Marine Structures*, 23:322–338.

[26] Goodwin, R. M. (1951). The Nonlinear Accelerator and the Persistence of Business Cycles. *Econometrica*, 19(1):1.

[27] Gram, J. (1883). Ueber die Entwicklung reeller Funktionen in Reihen mittelst der Methode der kleinsten Quadraten (On the Development of Real Functions in Series by the Method of the Least Squares). *J. Reine Angew. Math.*, 94:41–73.

[28] Greb, U. and Rusbridge, M. G. (1988). The interpretation of the bispectrum and bicoherence for non-linear interactions of continuous spectra. *Plasma Physics and Controlled Fusion*, 30(5):537–549.

[29] Hall, P. (1992). *The bootstrap and Edgeworth expansion*. Springer-Verlag.

[30] Hawes, D. (2017). *Nonlinear stochastic vibration analysis for energy harvesting and other applications*. PhD thesis.

[31] Hawes, D. H. and Langley, R. S. (2018). Analysis of the power flow in nonlinear oscillators driven by random excitation using the first Wiener kernel. *Journal of Sound and Vibration*, 412:256–269.

[32] Hinch, E. J. (1991). *Perturbation methods*. Cambridge University Press.

[33] Kautz, W. (1954). Transient synthesis in the time domain. *Transactions of the IRE Professional Group on Circuit Theory*, CT-1(3):29–39.

[34] Kolassa, J. E. (2006). *Series approximation methods in statistics*. Springer.

[35] Kovacic, D. I. and Brennan, M. J. (2011). *The Duffing Equation: Nonlinear Oscillators and their Behaviour*. John Wiley & Sons.

[36] Kramers, H. A. (1927). La diffusion de la lumière par les atomes. *Atti Cong. Intern. Fisici*, (Transactions of Volta Centenary Congress):545–557.

[37] Krot, A. and Tkachova, P. (2000). On approach to speech recognition using nonlinear signal decomposition into Volterra-Wiener functional series. In *2000 10th Mediterranean Electrotechnical Conference. Information Technology and Electrotechnology for the Mediterranean Countries. Proceedings. MeleCon 2000 (Cat. No.00CH37099)*, volume 2, pages 522–525. IEEE.

[38] Kumar, U., Prakash, A., and Jain, V. K. (2008). Characterization of chaos in air pollutants: A Volterra-Wiener-Korenberg series and numerical titration approach. *Atmospheric Environment*, 42(7):1537–1551.

[39] Kuo, H.-H. (1996). *White noise distribution theory*. CRC Press.

[40] Langley, R. (2015). Bounds on the vibrational energy that can be harvested from random base motion. *Journal of Sound and Vibration*, 339:247–261.

[41] Laplace, P.-S. (1812). Théorie analytique des probabilités [Analytic Probability Theory]. *Collected in Œuvres VII*, 2:194–203.

[42] Lee, Y. W. and Schetzen, M. (1965). Measurement of the Wiener kernels of a nonlinear system by cross-correlation. *International Journal of Control*, 2:3:237–254.

[43] Leigh J. R. (1983). The describing function method. In *Essentials of Non-linear Control Theory*, chapter 3, pages 10–22. IET.

[44] Lin, Y. K. (1967). *Probabilistic theory of structural dynamics*. McGrawl-Hill, New York.

[45] Ludeke, C. A. (1949). A Method of Equivalent Linearization for Non-Linear Oscillatory Systems with Large Non-Linearity. *Journal of Applied Physics*, 20(7):694–699.

[46] Marinca, V. and Herisanu, N. (2012a). Perturbation Method: Lindstedt-Poincaré. In *Nonlinear Dynamical Systems in Engineering*, pages 9–29. Springer Berlin Heidelberg, Berlin, Heidelberg.

[47] Marinca, V. and Herisanu, N. (2012b). The Method of Harmonic Balance. In *Nonlinear Dynamical Systems in Engineering*. Springer, Berlin, Heidelberg.

[48] McWilliam, S and Langley, R. (1994). Random response of offshore vessels to nonlinear wave forces. In *The 5th International Conference on Recent Advances in Structural Dynamics*, pages 724–733.

[49] Meirovitch, L. (1975). *Elements of vibration analysis.* McGraw-Hill.

[50] Miller, K. S. (1950). ON ITERATIVE METHODS IN LINEAR DIFFERENTIAL EQUATIONS.

[51] Newland, D. (2005). *An Introduction to Random Vibrations, Spectral & Wavelet Analysis*. Dover Publications, Inc.

[52] Ogunfunmi, T. (2007). *Adaptive Nonlinear System Identification: The Volterra and Wiener Model Approaches*. Springer Science & Business Media.

[53] Palm, G. and Poggio, T. (2006). Stochastic Identification Methods for Nonlinear Systems: An Extension of the Wiener Theory. *SIAM Journal on Applied Mathematics*.

[54] Park, Y. and Hofmayer, C. (1995). Practical application of equivalent linearization approaches to nonlinear piping systems.

[55] Ren, Y. and Yu, Y. (2012). Identification of The Nonlinear Vibration Characteristics Based on the Wiener kernels. *Applied Mechanics and Materials*, 204-208:4668–4672.

[56] Rizzi, S. A. and Muravyov, A. A. (2000). COMPARISON OF NONLINEAR RANDOM RESPONSE USING EQUIVALENT LINEARIZATION AND NUMERICAL SIMULATION. II:833–846.

[57] Rizzi, S. A. and Muravyov, A. A. (2002). Equivalent Linearization Analysis of Geometrically Nonlinear Random Vibrations Using Commercial Finite Element Codes.

[58] Roberts, J. B. and Spanos, P. D. (2003). *Random Vibration and Statistical Linearization*. Courier Corporation.

[59] Robinson, J. H., Muravyov, A. A., Rizzi, S. A., and Turner, T. L. (1998). A New Stochastic Equivalent Linearization Implementation for Prediction of Geometrically Nonlinear Vibrations. Technical report, NASA Technical Reports Server.

[60] Rota, G.-C. and Shen, J. (2000). On the Combinatorics of Cumulants. *Journal of Combinatorial Theory, Series A*, 91(1-2):283–304.

[61] Sansone, G. (1991). *Orthogonal functions*. Dover.

[62] Schetzen, M. (1981). Nonlinear system modeling based on the Wiener theory. *Proceedings of the IEEE*, 69(12):1557–1573.

[63] Schetzen, M. (2006). *The Volterra and Wiener theories of nonlinear systems*. Krienger publishing company, Malabar, Florida.

[64] Socha, L. (2008). *Linearization methods for stochastic dynamic systems*. Springer Verlag.

[65] Stenger, F. (1993). *Numerical methods based on Sinc and analytic functions*. Springer-Verlag.

[66] Strogatz, S. H. (2014). *Nonlinear Dynamics and Chaos: With Applications to Physics, Biology, Chemistry, and Engineering*. Westview Press.

[67] Tang, K. T. (2007). *Mathematical methods for engineers and scientists*. Springer.

[68] Taran, a. N. and Taran, V. N. (2014). Application of Volterra-Wiener spline series for the analysis of nonlinear electric circuits. *Journal of Communications Technology and Electronics*, 59(7):758–766.

[69] Toll, J. S. and S., J. (1956). Causality and the Dispersion Relation: Logical Foundations. *Physical Review*, 104(6):1760–1770.

[70] van der Pol, B. (1920). A theory of the amplitude of free and forced triode vibrations. *Radio Review (later Wireless World)*, 1:701–710.

[71] Varga, R. S. (2009). *Matrix iterative analysis*. Springer.

[72] Volterra, V. (1887). Sopra le funzioni che dipendono de altre funzioni. *Rend. R. Academia dei Lincei*, 2o:Sem.: 97–105, 141–146 and 153–158.

[73] Volterra, V. (1913). *Lecons sur les Fonctions De Lignes*. Paris.

[74] Volterra, V. (2005). *Theory of Functionals and of Integral and Integro-Differential Equations*. Dover Publications.

[75] Walach, E. and Widrow, B. (1984). The least mean fourth (LMF) adaptive algorithm and its family. *IEEE Transactions on Information Theory*, 30(2):275–283.

[76] Wallace, D. L. (1958). Asymptotic Approximations to Distributions. *The Annals of Mathematical Statistics*, 29(3):635–654.

[77] Wiener, N. (1958). *Nonlinear Problems in Random Theory*. Technology Press of Massachusetts Institute of Technology.

[78] Worden, K. and Tomlinson, G. (2000). *Nonlinearity in Structural Dynamics: Detection, Identification and Modelling*. CRC Press.

Appendix A

Nondimensionalisation of the Duffing Oscillator

The nondimsionalisation procedure for Eq.(2.2) to its new form given by Eq.(2.3) is demonstrated here. Starting by copying Eq.(2.2),

$$\ddot{x} + 2\beta\omega_0(1+\hat{\varepsilon}_2\dot{x}^2)\dot{x} + \omega_0^2(1+\hat{\varepsilon}_3 x^2)x = f(t). \tag{A.1}$$

and introducing the new nondimentional variable y such as,

$$y(t) = x(t)/\sigma_0 \;\rightarrow\; x(t) = \sigma_0 y(t) \tag{A.2}$$

where σ_0^2 is the linear displacement RMS value given by,

$$\sigma_0^2 = \frac{\pi S_{ff}}{4\beta\omega_0^3}. \tag{A.3}$$

Substituting Eq.(A.2) into Eq.(A.1) and dividing all the terms by σ_0 leads to,

$$y'' + 2\beta\omega_0(1+\hat{\varepsilon}_2\sigma_0^2 y'^2)y' + y\omega_0^2(1+\hat{\varepsilon}_3\sigma_0^2 y^2) = f(t)/\sigma_0. \tag{A.4}$$

The dependent variable is then described over a new dummy time-variable τ, such as $y(t) \rightarrow y(\tau)$ where $\tau = \omega_0 t$. To get the relationship between the derivatives of $y(t)$ and $y(\tau)$ the chain rule is used so that,

$$y'(t) = \frac{d}{dt}y(t) = \frac{d}{d\tau}y(\frac{d\tau}{dt}) = \omega_0\frac{d}{d\tau}y(\tau) = \omega_0\dot{y}(\tau) \;\rightarrow\; y'(t) = \omega_0\dot{y}(\tau),\; y''(t) = \omega_0^2\ddot{y}(\tau). \tag{A.5}$$

Substituting $t = \tau\ \omega_0$, the results from Eq.(A.5) into Eq.(A.4) and dividing by ω_0^2 gives the final nondimensionalised version of the Duffing equation,

$$\ddot{y} + 2\beta(1 + \varepsilon_2 \dot{y}^2)\dot{y} + y(1 + \varepsilon_3 y^2) = g(\tau). \tag{A.6}$$

where $\varepsilon_2 = \hat{\varepsilon}_2 \sigma_0^2 \omega_0^2$ and $\varepsilon_3 = \hat{\varepsilon}_3 \sigma_0^2$ are the two nondimensionalised nonlinear coefficients for nonlinear damping and nonlinear stiffness respectively. The power spectrum of the new excitation force $g(\tau)$ is dependent on the damping coefficient only such that, $S_{gg} = 4\beta/\pi$ since for the linear system,

$$\sigma_y^2 = \frac{\pi S_{gg}}{4\beta} = 1 \ \rightarrow\ S_{gg} = \frac{4\beta}{\pi}. \tag{A.7}$$

Appendix B

Equivalent linearisation for asymmetric system

The asymmetric Duffing oscillator given in 2.21 with zero damping nonlinearity ($\varepsilon_2 = 0$),

$$\ddot{y} + 2\beta\dot{y} + y(1 + \varepsilon_{2s}y + \varepsilon_3 y^2) = g(\tau). \tag{B.1}$$

where the excitation $g(\tau)$ is white noise. By substituting the nonlinear terms in the equation with a linear term of an arbitrary coefficient n_l and some force F_0 to account for the asymmetry, we get the linearised form of the Duffing oscillator,

$$\ddot{y} + 2\beta\dot{y} + y(1 + n_l) + F_0 = g(\tau). \tag{B.2}$$

To find the optimal value of n_l, we aim to minimise the error between Eq.(B.1) and Eq.(B.2) with respect to n_l. The squared error is found by subtracting the linearised equation from the nonlinear equation and squaring, resulting in,

$$\epsilon^2 = (\varepsilon_{2s}y^2 + \varepsilon_3 y^3 - n_l y - F_0)^2 \tag{B.3}$$

The minimum value of the squared error is found by calculating the partial derivative with respect to n_l and setting the result to zero,

$$\frac{\partial \epsilon^2}{\partial n_l} = -2y(\varepsilon_{2s}y^2 + \varepsilon_3 y^3 - n_l y - F_0) = 0. \tag{B.4}$$

The ensemble average of the above expression is then taken such as,

$$E[2y(\varepsilon_{2s}y^2 + \varepsilon_3 y^3 - n_l y - F_0)] = 0 \;\rightarrow\; \varepsilon_{2s}E[y^3] + \varepsilon_3 E[y^4] - n_l E[y^2] - F_0 E[y] = 0. \tag{B.5}$$

Assuming Gaussian approximation for the response and taking the statistical moments[1] for a non-zero mean process, the above expression results in a new relationship for optimal value of n_l in terms of the mean μ_y and variance σ_y,

$$\varepsilon_{2s}(\mu_y^3 + 3\mu_y\sigma_y^2) + \varepsilon_3(\mu_y^4 + 6\mu_y^2\sigma_y^2 + 3\sigma_y^4) - n_l(\mu_y^2 + \sigma_y^2) - F_0\mu_y = 0. \tag{B.6}$$

Also, from linearisation we expect that,

$$F_0 = E[\varepsilon_{2s}y^2 + \varepsilon_3 y^3 - n_l y] \tag{B.7}$$

which results in a second equation for F_0,

$$F_0 = \varepsilon_{2s}(\mu_y^2 + \sigma_y^2) + \varepsilon_3(\mu_y^3 + 3\mu_y\sigma_y^2) - n_l\mu_y. \tag{B.8}$$

To get n_l, we substitute Eq.(B.8) into Eq.(B.6) and rearrange, such as,

$$n_l = 2\varepsilon_{2s}\mu_y + 3\varepsilon_3(\mu_y^2 + \sigma_y^2). \tag{B.9}$$

Finally, in order to calculate μ_y and σ_y, the system of equations,

$$2\beta\sigma_y^2(1 + 2\varepsilon_{2s}\mu_y + 3\varepsilon_3(\mu_y^2 + \sigma_y^2)) - \pi S_{gg} = 0 \tag{B.10a}$$

$$\mu_y + \varepsilon_{2s}(\sigma_y^2 + \mu_y^2) + \varepsilon_3(\mu_y^3 + 3\mu_y\sigma_y^2) = 0 \tag{B.10b}$$

needs to be solved. The first equation, Eq.(B.10a), is obtained by the fact that $\sigma_y^2 = \pi S_{ff}/2\beta(1+n_l)$ from the standard properties of the linearised system. The second one, Eq.(B.10b), arises from the expectation of the unforced version of Eq.(B.1).

[1] Chapter 4, Julius S. Bendat and Allan G. Piersol., Random Data: Analysis and Measurement Procedures. John Wiley & Sons, 2nd edition, 1986; [5]

Appendix C

Single-pole fitting method parameters

SDOF system parameters

The equation used for the figures in Chapter 3 has the form,

$$G(\omega) = c + \frac{-2\alpha\omega_p}{-\omega^2 + \omega_p^2 + \gamma^2 + 2i\gamma\omega} \tag{C.1}$$

Nonlinear stiffness

Table C1 Parameters figure 3.2a

α	ω_p	γ	c
-0.13	2.55	1.00	0.50

Table C2 Parameters figure 3.3a

α	ω_p	γ	c
-0.11	3.60	2.30	1.35

Nonlinear stiffness and nonlinear damping

Table C3 Parameters figure 3.6a

α	ω_p	γ	c
-0.09	2.85	1.2	0.32

2DOF system parameters

The general form of equation used in figures in Chapter 4 has the form,

$$G(\omega) = c + \frac{-2\alpha\omega_p}{-\omega^2 + \omega_p^2 + \gamma^2 + 2i\gamma\omega} + \frac{-2\alpha_1\omega_{p1}}{-\omega^2 + \omega_{p1}^2 + {\gamma_1}^2 + 2i\gamma_1\omega} + \frac{-2\alpha_2\omega_{p2}}{-\omega^2 + \omega_{p2}^2 + {\gamma_2}^2 + 2i\gamma_2\omega} \tag{C.2}$$

If a table does not include some of the parameters, automatically, this means that they are equal to zero for the particular case.

Case 1 - 2DOF / $\varepsilon_{nl1} = 0.1$

Table C4 Parameters figure 4.4

α	ω_p	γ	c
-30.00	2.50	1.50	70.00

Table C5 Parameters figure 4.6

α	ω_p	γ	c
-3.50	0.90	0.45	67.00
α_1	ω_{p1}	γ_1	
-14.50	2.50	0.8	

A double-pole fit is required for the first case of the 2DOF system.

Case 2 - 2DOF / $\varepsilon_{nlc} = 0.01$

Table C6 Parameters figure 4.10

α	ω_p	γ	c
-14.00	1.40	0.16	115

Table C7 Parameters figure 4.12

α	ω_p	γ	c
-14.00	1.40	0.16	117.00
α_1	ω_{p1}	γ_1	
-20.00	4.65	0.28	

Table C8 Parameters figure 4.14

α	ω_p	γ	c
-13.00	1.36	0.16	117.00
α_1	ω_{p1}	γ_1	
-1.10	1.70	0.035	
α_1	ω_{p1}	γ_1	
-14.50	2.50	0.8	

A triple-pole fit is required for the second case of the 2DOF system.